INFORMATION TO USERS

GIAMPAPA, MARK STEVEN

THE CHROMOSPHERES OF M DWARF STARS

The University of Arizona   PH.D.   1980

University Microfilms International   300 N. Zeeb Road, Ann Arbor, MI 48106

THE CHROMOSPHERES OF M DWARF STARS

by

Mark Steven Giampapa

_____

A Dissertation Submitted to the Faculty of the

DEPARTMENT OF ASTRONOMY

In Partial Fulfillment of the Requirements
For the Degree of

DOCTOR OF PHILOSOPHY

In the Graduate College

THE UNIVERSITY OF ARIZONA

1 9 8 0

THE UNIVERSITY OF ARIZONA
GRADUATE COLLEGE

As members of the Final Examination Committee, we certify that we have read

the dissertation prepared by _____ MARK STEVEN GIAMPAPA _____

entitled _____ THE CHROMOSPHERES OF M DWARF STARS _____

_____

_____

_____

_____

and recommend that it be accepted as fulfilling the dissertation requirement

for the Degree of _____ DOCTOR OF PHILOSOPHY _____.

P R Shirts	_8/8/80_
	Date
T. L. Swihart	_8/8/80_
	Date
Jeffrey L. Linsky	_8/08/80_
	Date
J. W. Becher	_8/08/80_
	Date
James W. Liebert	_8-08-80_
	Date

Final approval and acceptance of this dissertation is contingent upon the
candidate's submission of the final copy of the dissertation to the Graduate
College.

I hereby certify that I have read this dissertation prepared under my
direction and recommend that it be accepted as fulfilling the dissertation
requirement.

_____   _August 8, 1980_____
Dissertation Director   Date

STATEMENT BY AUTHOR

This dissertation has been submitted in partial fulfillment of requirements for an advanced degree at The University of Arizona and is deposited in the University Library to be made available to borrowers under rules of the Library.

Brief quotations from this dissertation are allowable without special permission, provided that accurate acknowledgment of source is made. Requests for permission for extended quotation from or reproduction of this manuscript in whole or in part may be granted by the copyright holder.

SIGNED: _____

ACKNOWLEDGMENTS

The essence of the pursuit of graduate study is well illustrated
by the experience of an apprentice, such as the experience of a student
of art during the Italian Renaissance. According to the Encyclopaedia
Britannica, an apprenticeship is "the learning of an art, trade, or
other calling by practical experience under the guidance of a master,
perhaps also with some classroom study." I was indeed fortunate to be
an apprentice to a true master of the art of contemporary astrophysics,
Dr. Simon P. Worden. The qualities characterizing the scientific
research conducted by Pete Worden, namely, competence, dedication, and
creative insight, were a continual source of inspiration and encourage-
ment for me. His steadfast loyalty and friendship, even in the most
uncertain of times, were invaluable to me. Pete Worden is foremost
among those who receive my deepest gratitude.

I am also indebted to the other members of my dissertation com-
mittee. In particular, I thank Jeff Linsky for his support and en-
couragement during my visit to the Joint Institute for Laboratory
Astrophysics. In addition, I am grateful to Pete Worden, Jeff Linsky,
Jim Liebert, Jacques Beckers, Tom Swihart, and Peter Strittmatter for
their perceptive comments which served to enhance the quality of this
dissertation. I also thank Bob Stencel and Gibor Basri for their patient
assistance in the implementation of the model atmosphere computer codes,
and I am grateful to Tim Schneeberger for his assistance in the aquisi-
tion of the observational data utilized in this investigation.

Furthermore, many illuminating and interesting discussions with Tom Ayres and Lawrence Cram materially contributed to this investigation.

I am also grateful to other members of Steward Observatory and Sacramento Peak Observatory for the productive scientific investigations we have conducted and the parties they have given. These individuals include (in random order): Ray White, Andrzej Pacholczyk, Bill Tifft, Cathy Imhoff, John Cocke, George Coyne, and Dave Dearborn among others (Steward Observatory); George Simon, Jacques Beckers, Dick Altrock, Jack Zirker, Rich Robinson, Don Neidig, Alan Nye, and Steve Keil (Sacramento Peak Observatory). In addition, I maintained a mutually beneficial relationship with past and present Steward graduate students which resulted in the fine tuning of our extensive skills in a wide range of debauchery. These individuals include (in random order): Bill Romanishin, Susan Wilkerson, Del Lindley, Pete Gural, Mark Adams, Rich More, Karen Huyser, Mike Gresham, Allen Schiano, Dave and Diane Turnshek, Eric Jensen, Steve Grandi, Paul Hintzen, John Scott, Joe Davila, and, of course, Pete Worden. To all these people, thanks for so well illustrating aspects of the art of wild and dissipated living! I particularly thank Pete Worden for his advice on the art of high living and fine wine.

I also wish to thank Don Barry, Gibson Reaves, John Russell, and Gerhard Weissler for their support and encouragement during my under-graduate days at the University of Southern California. In addition, I extend my heartfelt gratitude to my parents for their love and support during the arduous years of graduate school. Unlike many of my acquant-ances, I could always go home.

TABLE OF CONTENTS

TABLE OF CONTENTS--<u>Continued</u>

LIST OF ILLUSTRATIONS--<u>Continued</u>

LIST OF ILLUSTRATIONS--<u>Continued</u>

LIST OF ILLUSTRATIONS--<u>Continued</u>

LIST OF TABLES

ABSTRACT

I construct single-component, homogeneous, quiescent semi-empirical model chromospheres based upon high resolution, well-calibrated profiles of the Ca II K line in 3 dMe and 2 dM stars.

The results of the atmospheric models inferred from the observed Ca II K line profiles reveal several systematic trends which characterize the chromospheres of M dwarf stars. In particular, I deduce high values of T_{min}/T_{eff} for the stars considered in this investigation thus indicating an unusually large degree of nonradiative heating present in the upper photospheres of M dwarf stars. Hence dissipation of mechanical energy is an important parameter in the control of the energy balance in the upper photospheres of M dwarf stars. I also find that the value of the lower chromospheric temperature gradient, dT/d log m, is similar for the M dwarf stars considered in this dissertation. I therefore conclude that the chromospheric K-line emission strength is most sensitive to the total amount of chromospheric material present within the approximate temperature range T_{min} - 6000K. Thus increased emission strength is not simply due to an increased temperature gradient. I also find that the electron density and electron temperature at a thermalization length below the top of the chromospheres are each greater for the dMe stars than for the dM stars. Hence the chromospheric line emission in collisionally controlled lines is enhanced in dMe stars relative to the non-dMe stars. In addition, a steep chromospheric temperature rise is present over the region of formation of the K-line emission core

thus implying that the chromospheric temperature gradient is signifi-cant, regardless of the chromospheric emission flux.

I develop dMe and dM semi-empirical model chromospheres which incorporate microturbulent velocity fields. I find that a solar-like microturbulent velocity distribution fails to reproduce the observed Ca II K-line profiles. Microvelocity models with a distribution of 1 to 2 km-s^{-1} are the most appropriate microturbulent velocity models. I therefore conclude that the microturbulent velocities in the chromos-pheres of M dwarf stars are small as compared to solar-like chromospheric microvelocity fields. I suggest that chromospheric mass motions are inhibited by magnetic fields which pervade the stellar chromosphere. If this is true then the actual microturbulent velocities present in dMe and dM chromospheres are smaller than the values I infer since I ignore the effects of magnetic line broadening in this investigation.

I also explore the formation of other chromospheric spectral line diagnostics in dM and dMe stars, namely, the Hα line and the Mg II h and k lines. I find that Hα is strictly an upper chromospheric (T > 6000K) diagnostic while the K-line is a lower chromospheric diag-nostic which is insensitive to the upper chromospheric thermal structure. Thus it is possible to construct single-component, semi-empirical model chromospheres for M dwarf stars which simultaneously satisfy both the Ca II K-line and the Hα line. However, I find that single-component, homogeneous model chromospheres fail to reconcile overlapping chromos-pheric spectral diagnostics such as Ca II and Mg II.

Finally, I estimate relative active-region filling factors for dMe and dM stars on the basis of the observed Ca II (H+K) and Mg II

(h+k) line fluxes. I estimate values in the range of 5% to 34% for the

dMe stars, with the filling factors based on Mg II greater than those

based on Ca II. The apparently discrepant active region filling factors

derived from the Ca II H and K and the Mg h and k lines combined with

the failure of model chromospheres to reconcile two overlapping

chromospheric spectral features suggest that single-component,

homogeneous model atmospheres are not physically realistic representa-

tions of M dwarf stars. In conclusion, I suggest that multi-component

model atmospheres are more realistic physical representations of stellar

chromospheres. In particular, I hypothesize that a detailed considera-

tion of the line spectrum arising from magnetic flux tubes with di-

verging magnetic field lines is required in order to reconcile various

chromospheric spectral line diagnostics.

CHAPTER 1

INTRODUCTION

The lower end of the main sequence is comprised of the majority
of the stars in the Galaxy. However, the M dwarf stars have only re-
cently become the objects of systematic and detailed observational and
theoretical investigation. These investigations have been primarily
motivated by the apparent similarity of physical processes and charac-
teristics, exhibited by the M dwarf stars, to analogous aspects of the
Sun. Both the Sun and the M dwarf stars possess a geometrically thin,
hot region immediately above their respective photospheres. This region
is commonly referred to as a chromosphere and I devote this dissertation
to the study of the physical structure of the quiescent (non-flare)
chromospheric regions in the M dwarf stars. In the following I enumer-
ate the basic astrophysical properties of the M dwarf stars in order to
provide the proper context in which to approach the study of the
chromospheres of the M dwarf stars.

The mass of an M dwarf star generally lies within the range 0.06
$\leq M/M_\odot \leq 0.7$ (Mullan 1976) and the luminosities are typically $L/L_\odot \leq 0.2$,
following Kunkel (1975). The effective temperatures are characterized
by $T_{eff} \leq 3950K$ (Hoxie 1973, Mullan 1976) while the radii are $0.18 \leq$
$R/R_\odot \leq 0.61$ (Mullan 1976). These physical quantities imply a stellar
gravity which is similar to, or a few times larger than the solar
gravity. For the specific case of the dM 4.5e flare star YZ CMi, I have

1

that $M/M_\odot \simeq 0.2$ and $R/R_\odot \simeq 0.3$ (following Allen 1976). Thus the mean density of YZ CMi is ~ 10 times the mean density of the Sun. Since the pressure scale height, H_p, is proportional to T/g, I have that $H_p \simeq 0.2$ $H_p^\odot$ in the case of YZ CMi. Thus the gas pressure and density rise more steeply beneath the photosphere of YZ CMi than they do beneath the solar photosphere. Stellar interior models for the lower main sequence show surface convection zones which extend deeper into the star as the mass of the star decreases (Kumar 1963; Hayashi, Hoshi, and Sugimoto 1962; Ezer and Cameron 1967; Straka 1971; Grossman and Graboski 1971). Eventually the star becomes completely convective at a critical mass $0.2 \le M_c/M_\odot \le 0.3$, corresponding to spectral type M5.5 (Mullan 1976). How-ever, Shaviv (1980) finds that an interior model of the dM4.5e star Kruger 60B ($M/M_\odot \simeq 0.15$; Mullan 1976) yields a very small value of ℓ/H_p, where ℓ is the local mixing length. Shaviv (1980) suggests that strong interior magnetic fields inhibit convective mass motions in this particular M dwarf star.

The main sequence lifetime, τ, of an M dwarf star is given approximately by

$$\tau \sim 0.007 \frac{M_* c^2}{L_*} \times 13\%, \qquad (1.1)$$

or $\tau \sim 10^{11}$ years for $M_*/M_\odot = 0.2$ and $L_*/L_\odot - 0.01$. The first constant in Eq. (1.1) is the H $\rightarrow$ He mass defect while the final constant is the H $\rightarrow$ He conversion efficiency for the Zero Age Main Sequence (Schwarzschild 1958).

The dwarf M stars are divided into subclasses according to the appearance of certain spectral features. The appearance of Hα in

emission distinguishes dMe stars from the non-emission (dM) dwarf M stars. Joy and Abt (1974) have shown that the dMe and dM stars do not differ statistically in absolute magnitude, implying that the Hα emission is not a consequence of dMe stars being spectroscopic binaries. This result strongly implies that the dMe and dM stars have similar photospheric properties but differ in their outer layers, presumably analogs of the solar chromosphere. Since essentially all M dwarfs exhibit Ca II H and K line emission indicative of chromospheres, the difference between dMe and dM stars may be analogous to the difference beteween solar plages and quiet regions, which is a consequence of enhanced and closed magnetic field structures in solar plages.

Moreover, the fraction of M dwarf stars which are classified as dMe stars increases from 8% at M_V = 9 mag to 45% at M_V = 12 mag to 80% at M_V = 14 mag (Petit 1961). In fact, Joy and Abt (1974) conclude that all M dwarfs of spectral type M5.5 or later are classified as dMe. However, recent observations by Liebert et al. (1979), Giampapa and Worden (1980), and Liebert and Green (1980) demonstrate the existence of non-emission M dwarf stars of spectral types later than M6. If the aforementioned conventional stellar interior models are correct then the existnce of Balmer line emission is not solely dependent upon the depth of the stellar convection zone. In addition, dMe stars appear among both the kinematic old disc and young disc populations (Greenstein and Arp 1969, Veeder 1974, Evans 1975). Thus the line emission is not necessarily a _function_ of age for a given M dwarf star, although the decline in line emission strength may be _statistically correlated_ with

age over an evolutionary time-scale (Skumanich 1972; Barry, Schoolman, and Hege 1980).

A distinctive feature of M dwarf stars, especially the dMe stars, is the occurrence of stellar flares. In particular, the UV Ceti-type flare stars form a subgroup of the dM stars which have been observed to flare; that is they exhibit transient brightenings on time-scales of second to minutes. While the better known flare stars like UV Ceti, YZ CMi, and AD Leo have been observed to flare repeatedly, the majority of this subclass have been observed to flare only once (Kunkel 1973). In an extended study of CM Dra, Lacy (1977) concluded that this star could have a flare rate as low as 0.02 per hour. It is possible, therefore, that all dM stars would be identified as flare stars if observers had the time to monitor them sufficiently long.

The flare spectra of flare stars have been studied by Kunkel (1970), Moffett and Bopp (1976), and more recently by Schneeberger and associates (1979, 1980) and Worden et al. (1979). These investigators typically find that both during and after flare events the hydrogen Balmer lines, Ca II resonance lines, and the He I lines appear in emission at levels greater than the quiescent (non-flare) chromospheric emission line flux levels. Also, the continuum can be enhanced as much as 6 mag in the U band. In more detail, Schneeberger and associates (1979, 1980) and Worden et al. (1979) generally find that a dMe stellar flare is characterized by a rapid rise ($\leq 5^m$) to maximum line and con-tinuum emission. The continuum emission then declines as do the central intensities of the line emission. However, the line emission remains at enhanced levels for hours following U band flares. I show in Figures

1 to 5 the temporal evolution of a flare event observed in September, 1979, on UV Ceti with the Steward Observatory 2.3 m telescope and the Reticon scanner. The spectral resolution is 6Å and the temporal resolution is approximately 5^m. This flare event caused a 4.7 mag increase in the U band. The flare energies are typically greater than solar flare energies (Schneeberger et al. 1980, Worden et al. 1979) and the total energy output of the brightest dMe stellar flares is estimated by Kunkel (1970) to be 100 times that of the brightest solar class 3^+ flares ($\geq 1.6 \times 10^{31}$ ergs; Allen 1976). In addition to the optical observations of flares, Lovell (1971) has detected radio fluxes during the dMe stellar flare as large as 10^{24} Jy while Haisch et al. (1980) report L_x (0.2 – 4.0 keV) = 4.6×10^{27} ergs-s^{-1} for a major X-ray flare event on Proxima Centauri. These authors also report that no ultraviolet, optical, or radio emission corresponding to this flare event was detected. Thus Haisch et al. (1980) conclude that the flare plasma cools predominantly by X-ray radiation. Another unique property of M dwarf flares is that, unlike solar flares, the optical emission lines do not broaden during flare events although the line center intensity may increase by over a factor of two during some flare events (Worden et al. 1979; Schneeberger and associates 1979, 1980; Svestka 1972).

Besides the transient brightenings due to flare events, the dMe stars also exhibit quasi-periodic variability as seen in broad-band photometric observations (Krzeminski 1969). These variations have periods of several days and the amplitude of the variations are ≤ 0.3 mag. Furthermore, the amplitude and phase of the quasi-periodic light variations are irregular over time-scales of weeks (Krzeminski 1969).
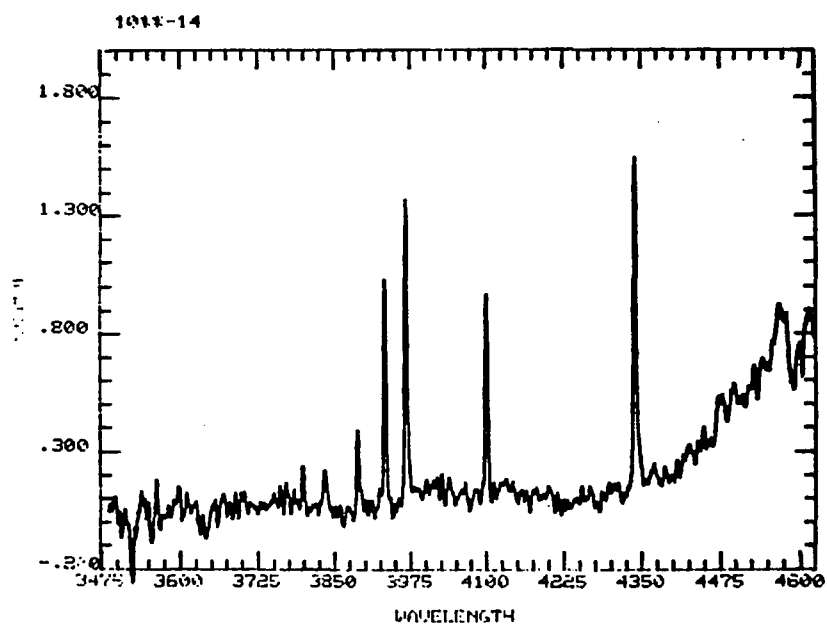
Figure 1. Temporal evolution of a flare event on UV Ceti: the quiescent spectrum.
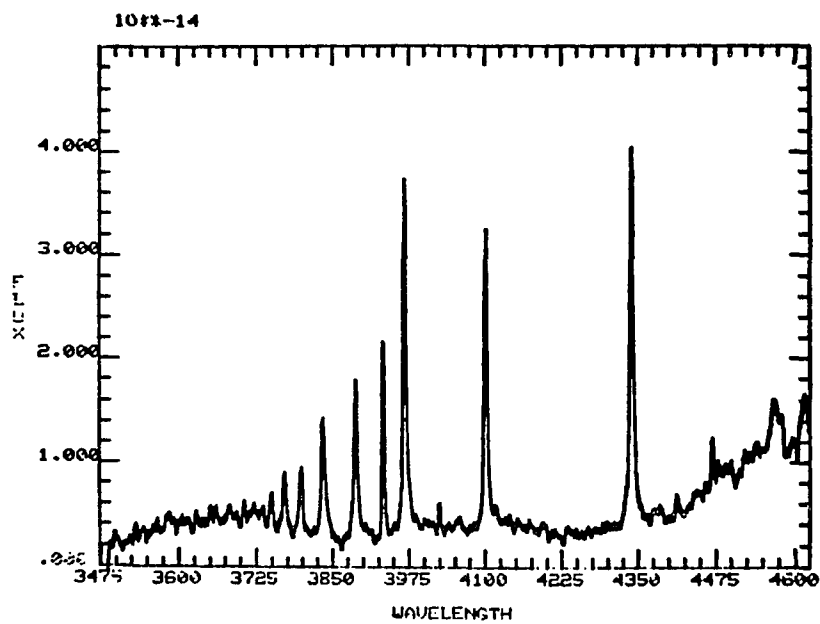
Figure 2. Rise to flare maximum: UV Ceti.
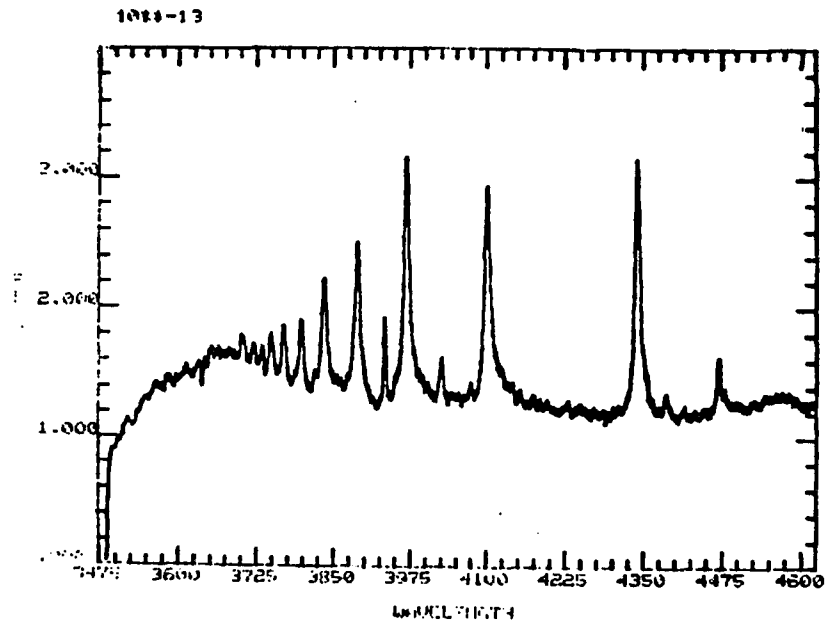
Figure 3. Maximum flare emission: UV Ceti.
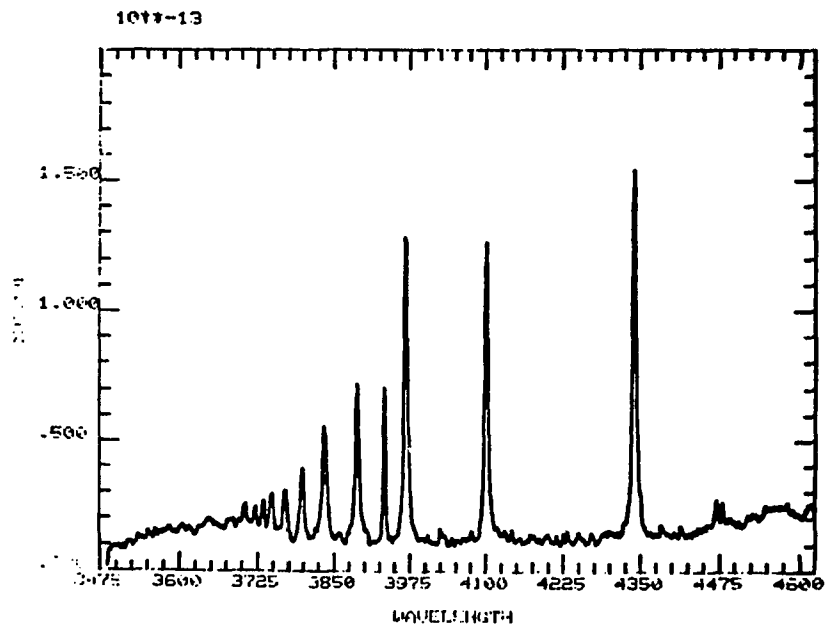
Figure 4. Decline from flare maximum: UV Ceti.
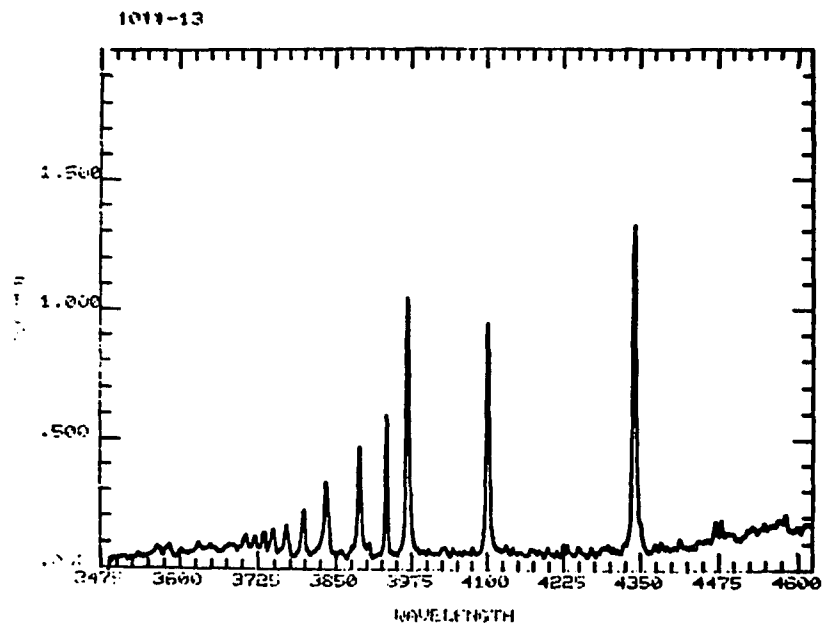
Figure 5.   Lingering enhanced line emission after flare maximum: UV Ceti.

These observations are extended by Torres and Mello (1973), Anderson and Bopp (1975), Bopp (1974), and Worden (1975). Through the application of narrow-band photometry, Worden (1975) finds that <u>decreases</u> in intensity in upper photospheric-temperature minimum region spectral diagnostics correspond to <u>increases</u> in intensity in upper chromospheric region spectral diagnostics. Hence this compelling observational evidence allows Worden (1975) to conclude that the quasi-periodic variability exhibited by dMe stars can be attributed to the rotational modulation of extensive starspot (analogous to sunspots) and active (plage) regions which exist in the stellar photosphere. Corroborative evidence for this conclusion is offered by Torres and Mello (1973), Bopp (1974), and Anderson and Bopp (1975). In addition, high resolution spectroscopic observations reveal that line flux changes occur in active chromosphere stars. In particular, Hα spectra of EQ Vir (dK5e) presented in Kelch, Linsky, and Worden (1979) and Hartmann and Anderson (1977) show a definite Hα emission feature. However, Hα spectra of the same star by Worden, Schneeberger, and Giampapa (1980) show a weak or no Hα line. Thus Worden et al. (1980) conclude that the Hα feature in EQ Vir is variable. Additional evidence for profile variations is given by Bopp (1974) who finds profile variations in the dM3.5e star AD Leonis on time scales as short as 4 hours. The dM0e flare star BY Draconis is an extreme example of the tendency of dMe stars to exhibit quasi-periodic photometric variability in addition to flaring (Kunkel 1975). In summary, the variable photometric behavior exhibited by dMe stars is generally attributed to the probable presence of magnetic surface

activity that is similar in character to such solar phenomena as sunspots and plages.

The previously discussed quasi-periodic variations observed in M dwarf stars offer the unique opportunity to accurately determine rotational velocities independent of uncertainties in the inclinations. Thus Bopp (1980) and Carrasco, Franco, and Roth (1980) find that as a class the dMe stars rotate more rapidly than the dM stars. More specifically, Carrasco et al. (1980) find that the dMe stars have values of angular momentum per unit mass, J/M, which exceed by several orders of magnitude the values expected from any extrapolation of the observed J/M values for the intermediate (A0 to G2) main sequence. Interestingly, I find that the dMe stars have larger chromospheric radiative loss rates and therefore larger nonradiative heating rates than the dM stars (Chapter 2). Thus the level of nonradiative heating in the stellar atmosphere must be intimately related to the stellar angular momentum per unit mass. This result is anticipated by Mullan (1974) and Worden (1974) who attribute both quiescent chromospheric line emission and flare activity to stellar-surface magnetic-field effects resulting from an interaction between convective motions, rotation, and subsurface magnetic fields. The assumed battery mechanism which is suggested by Biermann (1950), discussed by Mestel and Roxburgh (1962), and applied to the dMe stars by Worden (1974) yields an equilibrium toroidal magnetic field produced after a time t which is of order

$$H \sim \frac{4\pi\sigma}{c} \frac{m_H}{2e} \frac{(J/M)^2}{R^2} \qquad (1.2)$$

following Worden (1974). In this expression σ is the electrical

conductivity and R is the stellar radius. Mullan (1974) finds a similar

expression assuming a dynamo mechanism. Worden (1974) finds that

magnetic fields 10-100 times the strength of solar magnetic fields can

be produced in this manner. The relationship between chromospheric

activity and angular momentum (per unit mass) is further emphasized by

Kunkel (1975) who finds that duplicity prolongs the duration of the

flare active phase of evolution in M dwarf stars. Finally, I may write

Eq. (1.2) as

$$\log \tilde{H} \propto 2 \log [\tilde{J}/M] + 4 \log \tilde{T}_{eff} - \log \tilde{L}, \qquad (1.3)$$

where I have used $L_* = 4\pi R_*^2 \sigma T_{eff}^4$ and all values in Eq. (1.3) are

normalized to the respective solar value. I show in Figure 6 the

derived magnetic field strengths using stellar parameters from Allen

(1976) and assumed values of $\log [\tilde{J}/M]$. I conclude on the basis of

Figure 6 that the M dwarfs produce higher magnetic field strengths for a

given angular momentum per unit mass than do earlier type main sequence

stars. Alternatively, the earlier type dwarf stars must have higher

values of (J/M) to produce the equivalent magnetic field strength

inferred for an M dwarf star.

Besides the various solar-type magnetic surface activity

exhibited by the dMe stars, these stars also show evidence for the

existence of plasma in their outer atmospheres at temperatures T > 1 x

10^5K. Prominent in the non-flare spectra are lines of NV, C IV, Si IV,

He II, O III, Al III, C II, Si II, Mg II, Al II, Fe II, O I, and C I

(Carpenter et al. 1980, Hartmann et al. 1979). According to Carpenter et

al. (1980) the surface fluxes of the transition region lines
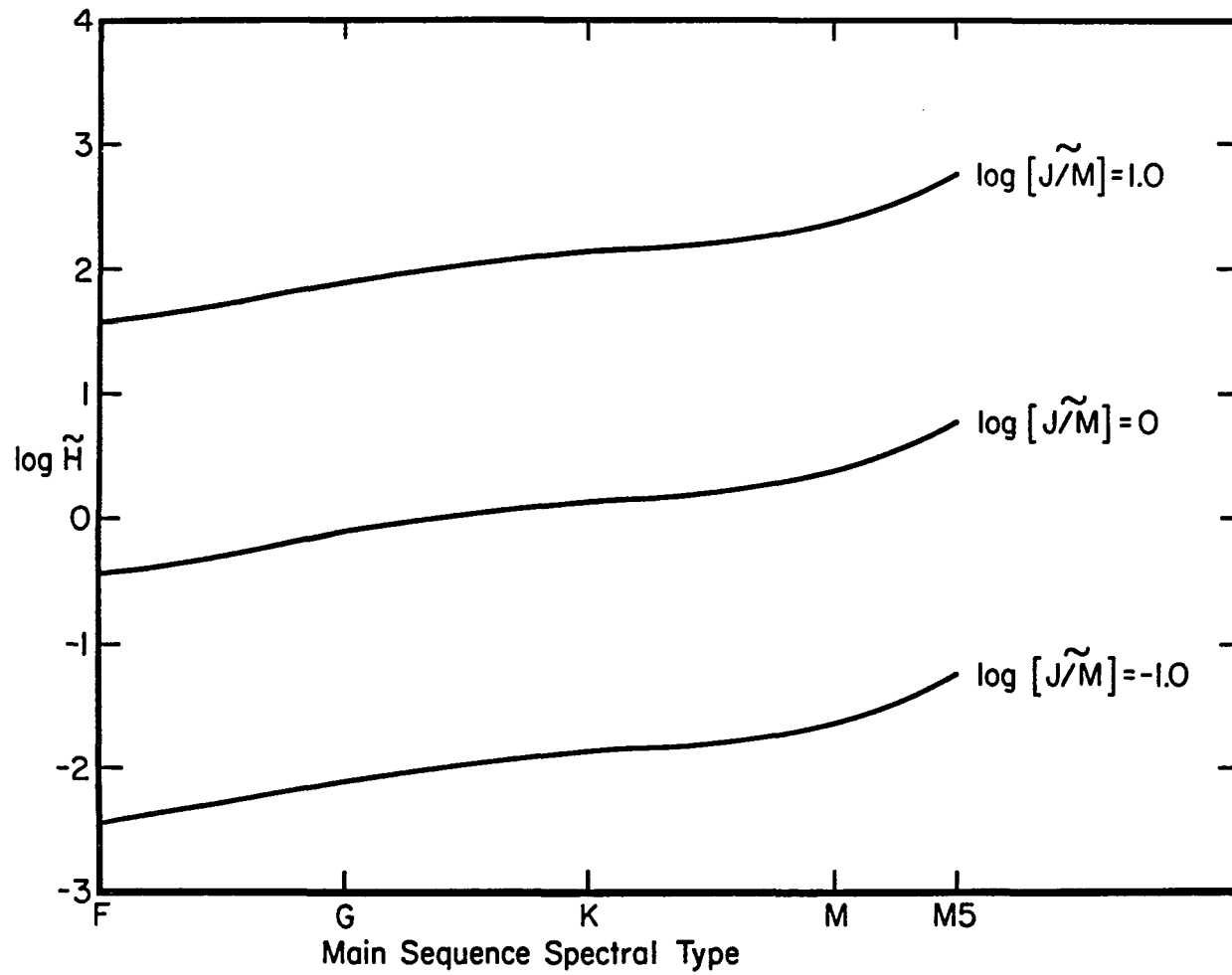
Figure 6. Magnetic field strength versus spectral type for various values of J/M.

(T = 2 x 10^4 - 2 x 10^5K) of the dM stars are similar to the quiet Sun

whereas the transition region lines in the dMe stars are typically

10-100 times larger than the quiet Sun. The ultraviolet lines of

neutral species are prominent in the dM stellar spectra, whereas they

are extremely weak or absent in the dMe stellar spectra. I display in

Figures 7 to 9 low-dispersion spectra of Proxima Centauri and YZ CMi

obtained by Carpenter and Wing (1979) with the IUE satellite. Further-

more, Haisch et al. (1980) observe quiescent soft X-ray emission outside

of flares in Proxima Centauri characterized by L_x = 1.5 x 10^{27} ergs-s^{-1},

L_x/L_{bol} = 2.2 x 10^{-4}, and a coronal temperature of $T_c \simeq$ 3.5 x 10^6K. By

comparison, the ratio L_x/L_{bol} for Proxima Centauri is 170 times greater

than the same value for the quiet Sun while the coronal temperature for

Proxima Centauri is 2.3 times larger than the solar coronal temperature.

In general, the values of log L_x/L_{bol} for the dMe and dM stars, as

deduced from recent HEAO-B observations, lie in the range -4 to -1,

which is larger than for any other stellar type (Linsky 1980a, Vaiana

1980).

The aforementioned physical characteristics of dMe and dM stars

are of general astrophysical importance. Their large mass-to-luminosity

ratios, high flare activity, and large space density (Luyten 1968)

suggest that these stars could play an important role in galactic

dynamics. The sheer numbers of M dwarf stars (80-90% of the total

number of stars in the Galaxy; Mullan 1976) implies that the process of

star formation favors the production of low mass stars. In fact, a

preliminary determination indicates that the maximum of the luminosity

function lies at M = +15.4, or later than spectral type dM5 (Luyten
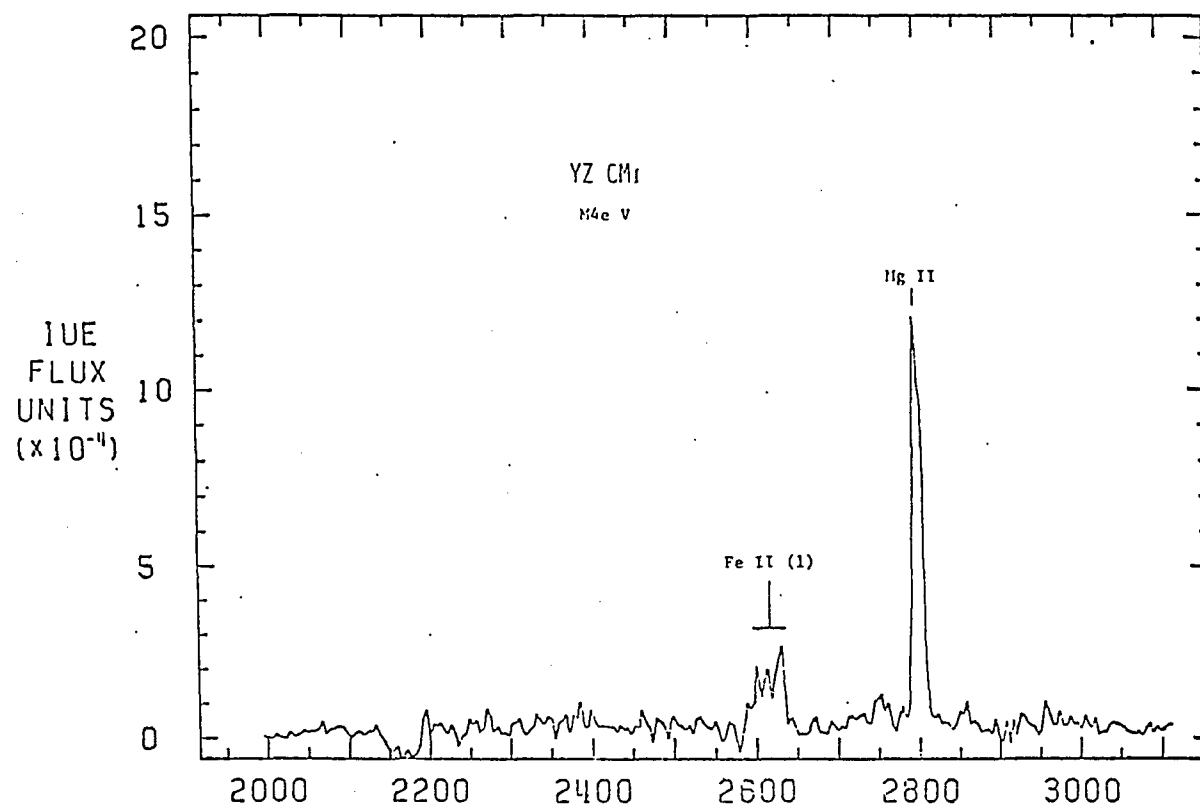
Figure 7. Low-resolution spectrum of YZ CMi in the ultraviolet -- Here the most prominent emis-
sion features are due to relatively low-temperature lines: UV multiplet (1) of Fe II
and the resonance doublet of Mg II. A 70-min exposure on February 18, 1979.
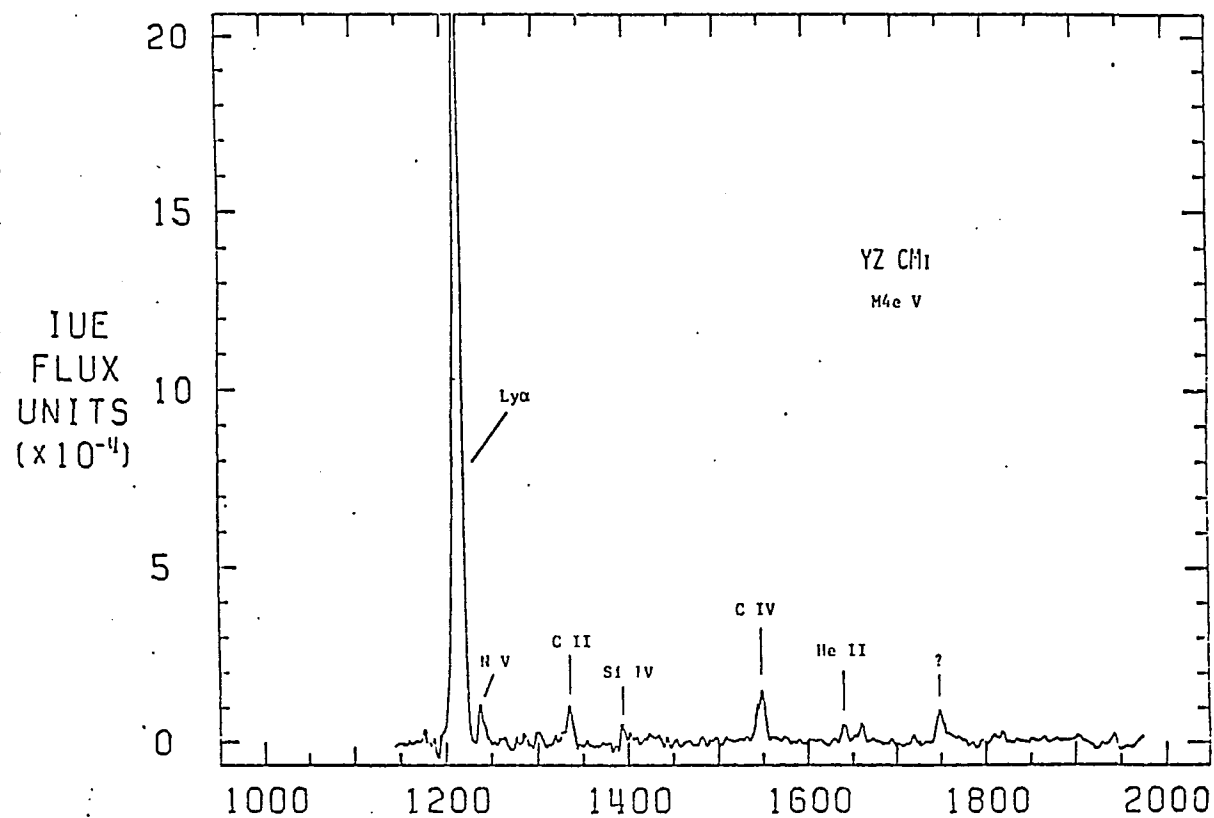
Figure 8. Low-resolution transition region line spectrum of YZ CMi -- Several of the high-temperature lines are identified. A 110-min exposure on February 18, 1979.
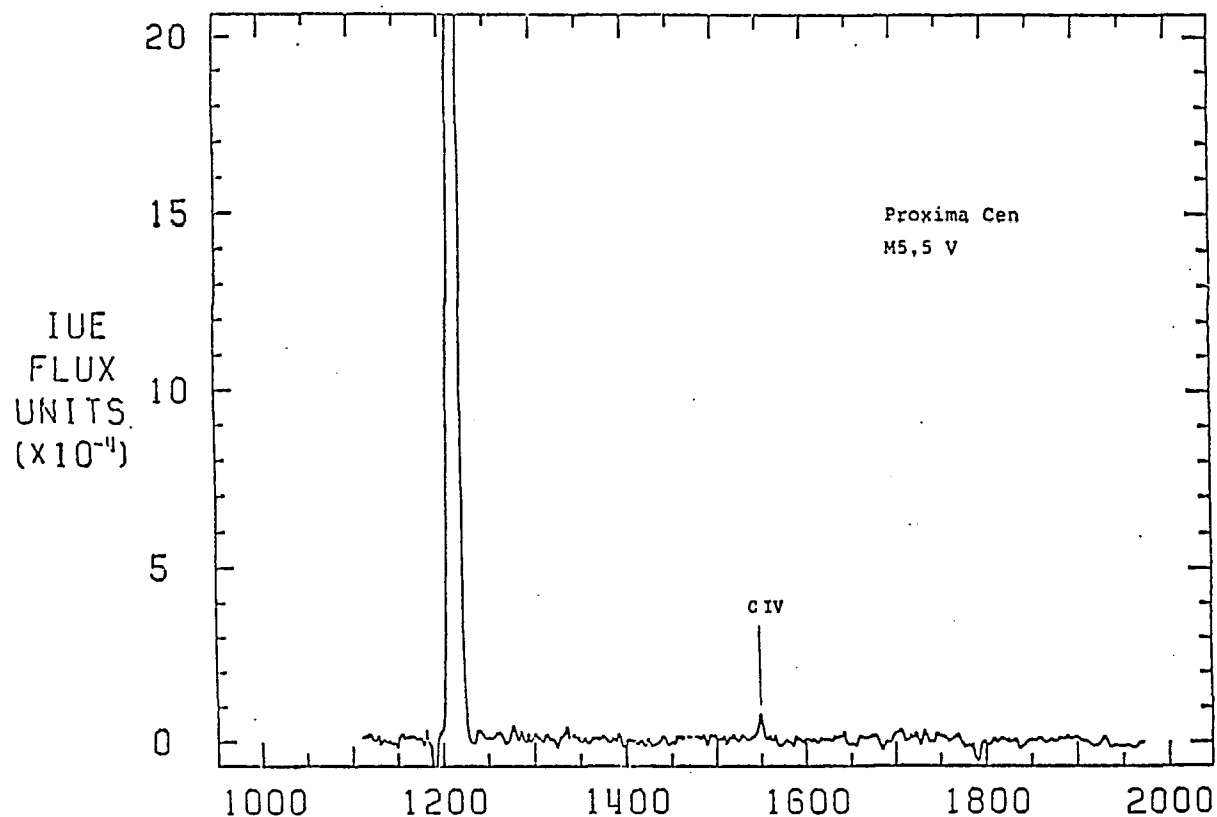
Figure 9. Low-resolution transition region line spectrum of Proxima Cen -- The detection of the C IV line at 1549 Å in this four-hour exposure on V645 Cen (Proxima Centauri) demonstrates the existence of hot transition-region material in the outer atmosphere of this M5.5 dwarf. The structure of the outer atmosphere of lower main-sequence stars appears not to differ greatly from that of solar-type dwarfs.

1974). The high fractional abundance of dMe and dM stars combined with the observed quiescent X-ray emission suggests that the M dwarf stars may significantly contribute to the diffuse X-ray background. Furthermore, Coleman and Worden (1976) show that mass loss from M dwarf stars arising from stellar winds and flaring could provide a substantial mass and energy input into the interstellar medium. In addition, flares on these stars may be producing many light element isotopes such as deuterium and lithium through spallation (Coleman and Worden 1976). The similarity between solar activity and M dwarf star activity suggests that these stars can be used as tests for theoretical models describing observed solar/stellar surface phenomena. Moreover, the chromospheric physical conditions in these cool dwarfs may differ significantly from those existing in the solar chromosphere. Thus the M dwarfs provide an important laboratory to test theories of nonradiative heating of stellar atmospheres. I therefore devote this dissertation to an exploration of the physical structures of the quiescent (non-flare) chromospheres of M dwarf stars. I defer detailed consideration of flare mechanisms and stellar flares in M dwarf stars to a future investigation.

The study of chromospheres was originally motivated by a desire to understand (1) the existence of a temperature inversion in the solar atmosphere in apparent violation of the second law of thermodynamics, (2) the effect of this region on the emergent solar spectrum, (3) the detailed nature of the coupling of the chromosphere to the underlying photosphere, and (4) the origin of the Wilson-Bappu effect (Wilson and Bappu 1957).

The solar chromosphere is a geometrically thin region ($\Delta R/R_\theta$ ~ 2×10^{-3}) which is observationally distinguishable as a bright pink flash which occurs a few seconds before and a few seconds after totality during an eclipse. Alternatively, Gibson (1973, p. 20) states that the "chromosphere can be viewed as the froth on top of the turbulent and relatively dense photosphere, a froth that is closely coupled by magnetic fields to the underlying dynamics." Finally, Linsky (1980b) operationally defines a chromosphere as that region of a stellar atmosphere where there exists a degree of nonradiative heating such that dT/dh > 0 (or dT/dm < 0, where m is the mass column density).[1] In recent years models of the chromospheres of stars other than the Sun have been developed through the use of modern model atmospheres techniques as applied to specific chromospheric spectral line diagnostics, such as the Ca II H and K resonance lines (see Linsky 1980b for a review). The model chromospheres developed for dwarf stars are similar to the general structural characteristics of solar chromospheric models. This apparent similarity suggests that there is a common physical basis governing the formation of late-type stellar chromospheres. The energetics of chromospheres are generally regarded as dominated by the dissipation of mechanical energy in the stellar atmosphere (Linsky 1977, 1980b). Following the initial suggestions of Biermann (1946) and Schwarzschild (1948), a general consensus developed

---

1. The implied restriction in this definition, namely that non-radiative heating dominates the chromospheric energy balance, is necessary since positive temperature gradients can occur in a stellar atmosphere in pure radiative equilibrium via the Cayrel mechanism.

that the chromospheres and coronae of the Sun and stars are heated by

acoustic waves generated by turbulent motions in the hydrogen convection

zone immediately below the visible photosphere. A review of this theory

as applied to the Sun is presented by Ulmschneider (1979). Stein and

Leibacher (1980) show theoretically that the acoustic flux is propor-

tional to $g^{-1}T_{eff}^{17}$, while Renzini et al. (1977) and Ulmschneider et al.

(1977) also find a g^{-1} dependence for models which include losses due

to photospheric radiative damping. These severe dependencies on gravity

and effective temperature immediately demand verification (or refuta-

tion) by the observational investigation of stellar chromospheres as

they occur throughout the Hertzsprung-Russell diagram. Recently,

Stencel et al. (1980), Linsky et al. (1979), and Basri and Linsky (1979)

show that the chromospheric radiative loss rates (and thus nonradiative

heating rates) estimated from Mg II and Ca II for a large stellar sample

including high luminosity stars, radically disagree with the afore-

mentioned predictions of the acoustic wave theory. I also find that the

acoustic wave theory fails to account for the observed chromospheric

line emission in dMe and dM stars (Chapter 2). A variety of empirical

evidence suggests that magnetic heating processes control the energy

balance in stellar chromospheres. The compelling circumstantial evi-

dence includes: (1) the correlation of photospheric magnetic field

strength and chromospheric emission line flux in the solar supergranula-

tion network (Skumanich, Smythe, and Frazier 1975), (2) the correlation

of solar magnetic field flux with X-ray emission (Golub, Maxson, et al.

1980; Golub, Rosner, et al. 1980), (3) the detection of both high

magnetic field strength and flux in stars with intense chromospheric

line emission (Robinson, Worden, and Harvey 1980), and (4) the
empirical evidence presented in this chapter in the case of the M dwarf
stars. The details according to which the magnetic heating occurs·are
uncertain. Thus the investigation of stellar chromospheres proceeds
through the deduction of the spatially averaged chromospheric thermal
structure (as inferred from chromospheric line diagnostics), with the
understanding that any future theory for the nonradiative heating of
stellar atmospheres must account for these structural details.

The resonance lines of Ca II, known as the H and K lines, are
notable as diagnostics of stellar chromospheric properties as well as
for their accessibility to earth-based observation. The occurrence of
chromospheric H and K emission in spectral types later than F5V (Wilson
1973) provides a valuable tool with which to study analogues of the
solar chromosophere and the chromospheres of cool stars. The Balmer
lines also become useful chromospheric diagnostics in the specific case
of the dMe and dM stars. Fosbury (1974) finds that $H\alpha$ line emission
observed in the dMe stars arises from a chromospheric temperature rise
coupled with a collisionally controlled $H\alpha$ source function in a region
characterized by electron densities $n_e \sim 10^{11} cm^{-3}$. Worden and Peterson
(1976) conclude that the dMe, centrally reversed, $H\alpha$ profile is asso-
ciated with an optically thick emitting region with an electron density
$n_e \lesssim 10^{13} cm^{-3}$. Worden et al. (1980) show that centrally reversed $H\alpha$
emission profiles are a general feature of dMe stellar spectra, with
the exception of those dMe stars which are members of close binary
systems. In these instances, Worden et al. (1980) attribute the lack of
a central reversal in the observed $H\alpha$ emission profile to the effects of

rotational line broadening. Giampapa et al. (1978) extend the study of

dMe chromospheric properties through the investigation of the He I

triplet (λ5876Å) and singlet (λ6678Å) lines which appear in emission in

the optical spectrum of the dM3.5e star AD Leonis. Giampapa et al.

(1978) find that these lines are collisionally excited and that they are

formed in a geometrically thin chromospheric layer at 20,000-50,000K

with a column density of $n_e\ell \simeq 6 \times 10^{18}\,cm^{-2}$. The most recent models of

the chromospheres of dMe and dM stars are those by Cram and Mullan

(1979). These investigators find that Hα absorption, as well as Hα

emission, is indicative of the presence of a chromosphere in M dwarf

stars (see Chapter 5). However, Cram and Mullan (1979) develop only

nonspecific chromospheric models which simply consist of an ad hoc

temperature rise beginning at the very top of an M dwarf photospheric

model taken from Mould (1976). Cram and Mullan (1979) do not include

microturbulence in their models and they address only a single M dwarf

chromospheric diagnostic, namely, the Balmer lines.

In this dissertation, I develop semi-empirical stellar model

chromospheres on the basis of the observed Ca II H and K line profiles

for a sample of dMe and dM stars. In particular, I find a single-

component, homogeneous model chromospheric thermal structure that

yields a theoretical Ca II K-line profile which most closely resembles

the observed K-line profile for a specific M dwarf star. In Chapter 2 I

present the observational data-set upon which this dissertation is

principally based. I discuss the spectral synthesis formalism that is

utilized in the construction of model stellar chromospheres in Chapter 3.

I present the inferred semi-empirical model chromospheres for a sample.

of 3 dMe and 2 dM stars in Chapter 4. In addition, I discuss the salient features of these models and delineate the similarities and differences between the chromospheres of the dMe and dM stars. In Chapter 5 I discuss additional chromospheric line diagnostics within the context of the model chromospheres given in Chapter 4. In Chapter 6 I discuss the applicability of single-component model chromospheres as a description of the chromospheres of M dwarf stars. In particular, I present estimates of active (plage) region filling factors for dMe and dM stars, and I offer a hypothesis which may explain discrepancies between model chromospheres based upon overlapping chromospheric line diagnostics. I summarize the principal results of this dissertation and I offer suggestions for future research in Chapter 7.

The combination of this dissertation with similar observational and theoretical investigations for stars throughout the HR diagram will allow astronomers to begin to address the fundamental questions of how the origin, structure, and evolution of stellar chromospheres depends upon the dynamic and thermal properties of stars.

CHAPTER 2

OBSERVATIONAL DATA

In this chapter I present 142 mÅ resolution spectra of the cores
and wings of the Ca II H and K lines in 3 dMe and 4 comparison M dwarf
stars, obtained with the Kitt Peak National Observatory 4m echelle
spectrograph and blue image tube. The data I present in this chapter
serve the need for high resolution, well calibrated spectra which I will
use in Chapter 4 to compute chromospheric models for M dwarf stars.
The data presented here will also be a useful supplement to currently
existing high resolution data on the Balmer lines in M dwarfs (Worden
et al. 1980). The primary purpose of this chapter is to present a set
of high resolution spectra of dMe and dM stars which will serve the
needs just described. In addition, I will qualitatively assess the
data and discuss any trends that may be present.

Observations and Reduction of the Data

The Ca II spectra were obtained with the Kitt Peak National
Observatory 4-meter echelle spectrograph and the blue image tube camera
with a dispersion of 1.95 Å mm^{-1} at 3950Å on the nights of 1979 February
11 and 12. The spectra were taken with baked III a-J plates. For one
star, GL 526, I obtained two plates in one night with different exposure
times in order to check the consistency of the reduction methods and
the flux in the stellar emission lines.

The data were reduced using the Kitt Peak National Observatory PDS microdensitometer. The scanning aperture was 40μm square with digitization steps every 20μm. I calibrated the III a-J plates by using a spot sensitometer plate with 16 calibrated spots. The spot sensitometer plate was also scanned and the stellar spectra calibrated by linear interpolations between spot calibration points. The "S" distortion inherent in echelle/image tube configurations was removed in the following manner. I scanned each order along reference lines perpendicular to the dispersion direction. These perpendicular cuts were then cross-correlated to determine the shift perpendicular to the dispersion as a function of position along the order. I then used this information to straighten out the echelle order. I then summed the data points perpendicular to the dispersion at each location (i.e., wavelength) along each order and subtracted the mean background, as determined from the clear plate between the orders, to produce a one-dimensional spectrum for each order. The standard star Hiltner 600 was used to remove the wavelength-dependent sensitivity profile of the echelle grating by dividing each observed spectral order by the identical (in terms of wavelength) order appearing in the echelle spectrum of Hiltner 600. This entire process yielded relative flux calibrations along each order. The data reduction method just described is identical to the methods used by Linsky et al. (1979). Thus these consistent data reduction schemes insure that data obtained during different observing sessions can be confidently intercompared. I used an entrance slit width of 100μm, which corresponds to 43.3μm in the exit plane with the 2.31 projection factor of the long camera. I estimate the spectral

resolution of the data by assuming that the instrumental profile for each optical component is Gaussian, following Linsky et al. (1979). Thus the spectral resolution is the square root of the sum of the squares of the FWHM for each optical component. Taking 43.3 μm in the exit plane for the projected slit width, 40 μm for the image tube resolution, 15 μm for the plate resolution,[2] and 40 μm for the PDS resolution yields an instrumental resolution of 73 μm at the plate. This corresponds to 142 m$\overset{\circ}{A}$ with the dispersion of 1.95 $\overset{\circ}{A}$ mm^{-1}. I find that unblended comparison lines have FWHM values which lie within 10 m$\overset{\circ}{A}$ of the calculated resolution, and conclude that the resolution of the data is 142 m$\overset{\circ}{A}$ $\pm$ 10 m$\overset{\circ}{A}$.

Both the Ca II H line and the K line appear in two orders in our echelle plates. Thus to reduce the noise I derived mean H and K line profiles using the profiles in both orders. Since the dispersion differs slightly between orders it was necessary to artificially expand the dispersion in one order to make it equal to the dispersion in the next order so that the line profiles could be properly added. This was accomplished by Fourier interpolation. An echelle order containing an H (or K) line was Fourier transformed using the Cooley-Tukey Fast Fourier Transform for an arbitrary number of data points. An appropriate number of zeroes were added to the order in transform space to yield, upon application of the inverse transform, a spectral order of the required dispersion in real space.

---

2. See Photobulletin: Kodak Pamphlet No. 14 (1979).

I convert the observed relative fluxes to absolute stellar surface fluxes according to the method described by Linsky et al. (1979). The stellar surface flux in a specific bandpass $F(\Delta\lambda)$ is

$$F(\Delta\lambda) = f(\Delta\lambda) \left(\frac{d}{R}\right)^2 = f(\Delta\lambda)(4.125 \times 10^8/\phi')^2, \qquad (2.1)$$

where $f(\Delta\lambda)$ is the flux observed at the Earth, d is the stellar distance, R is the stellar radius, and ϕ' is the stellar angular diameter in milliarcsec (Mihalas 1970, Linsky et al. 1979). Barnes and Evans (1976) and Barnes, Evans, and Parsons (1976) have shown that measured angular diameters including limb darkening of 27 late-type stars and 25 early-type stars lead to a tight correlation between the stellar surface brightness in the visual bandpass and the (V-R) color over a very wide range of spectral type. Their relations are, in terms of the stellar angular diameter, as follows (Linsky et al. 1979):

$$\log \phi' = 0.4874 - 0.2 \, V_o + 0.858(V-R) \qquad (2.2)$$

for $0.00 \leq V-R \leq 1.26$,

$$\log \phi' = 0.7674 - 0.2 \, V_o + 0.640(V-R) \qquad (2.3)$$

for $1.26 \leq V-R \leq 4.2$, where V_o is the apparent visual magnitude corrected for interstellar absorption. Differences in metal abundance are not considered in the calibration of the relations since the effect of metallicity on stellar radius is small. In particular I have that, following Iben (1967), $dR/R \alpha d\mu/\mu$, where μ is the mean molecular weight.

Willstrop (1964, 1972) has obtained absolute photometry of 215 stars of spectral types 05-M9 in the 3925Å-3975Å bandpass with a stated absolute accuracy of 10% (Willstrop 1972). The data set includes at least 14 stars with spectral types between M0 and M9 (Willstrop 1964).

Utilizing the Barnes-Evans angular diameter relations of Eq. (2.2) and
(2.3), the (V-R) photometry of Johnson et al. (1966), and the absolute
photometry of Willstrop (1964, 1972) yields the following piecewise
linear least squares fit to these data (cf. Linsky et al. 1979):

$$\log F(\Delta\lambda) = 8.264 - 3.076(V-R) \qquad (2.4)$$

for (V-R) < 1.30,

$$\log F(\Delta\lambda) = 5.500 - 0.944(V-R) \qquad (2.5)$$

for (V-R) > 1.30, where $F(\Delta\lambda)$ is the stellar surface flux per angstrom
in the 3925Å-3975Å bandpass. The errors in the flux calibration depend
on the systematic errors in the data obtained by Willstrop (1964, 1972),
the accuracy of the (V-R) photometry for the stars considered here and
in the Barnes-Evans relation, the random noise in my data, and on the
intrinsic scatter of $F(\Delta\lambda)$ about the mean curves. The intrinsic scatter
may be due, in part, to differences in metal abundance and, therefore,
in line blanketing. The first source of error is $\pm$ 10% (Willstrop 1972)
and the second and third quantities should in general be small (Linsky
et al. 1979). I estimate the random errors of measurement by comparing
monochromatic fluxes derived from two plates of GL 526 with very dif-
ferent exposure times. The monochromatic H_2 fluxes differed by 5.9%
between the two plates and the K_2 fluxes differed by 11.0%. Since the
exposure times for the two plates were greatly different, the latter
number should be representative of the upper limit of the random measure-
ment errors in my data. The intrinsic scatter of $F(\Delta\lambda)$ about the mean
curves is 1.4% (Linsky et al. 1979). The combination of the afore-
mentioned errors yields an estimated uncertainty in the flux scale of

± 15% for the stars discussed in this chapter. I equate the total relative flux in the 3925Å–3975Å bandpass to the surface flux computed using Eq. (2.4) or (2.5) to yield the conversion factor between relative and absolute surface flux for each spectrum.

In Table 1 I list the stars observed, the dates observed, number of observations, best exposure times, and adopted (V–R) colors. Spectra for stars observed more than once during a night were averaged. The (V–R) colors for the stars in this sample are taken from Veeder (1974). The effective temperatures are taken from the (V–R) – T_{eff} relation of Johnson (1966), linearly interpolated to the nearest 50 K. The dK5e star GL 517 (EQ Vir) does not have a published (V–R) value. Therefore, I assumed a (V–R) value (and hence a value of effective temperature) identical to that of a dK5 star as given by Johnson (1966). I also list, if available, the kinematic population in which the given star is a member (Veeder 1974). The population given for EQ Vir is inferred from data given by Gliese (1969).

In columns 8 and 9 of Table 1 I list the K_1 and H_1 indices, $F(K_1)$ and $F(H_1)$, defined (as in Linsky et al. 1979) as the total surface flux above the zero flux level between the K_1 or H_1 minima. In some cases the locations of these minima are uncertain. However this is not a serious problem since the H_2 and K_2 central emissions dominate the flux in the H and K lines for this sample of stars.

Chromospheric Radiative Loss Rates

The calibrated spectra are displayed in Figures 10–13 in order of decreasing effective temperature. The vertical axes are scaled so

Table 1. Summary of Observations and Integrated Line Surface Fluxes

Sequence Number	Star	Spectral Type	Pop.[a]	Day Obs.[b]	Number Obs.	Exp. Time (min)	V-R	$F(K_1)$[c]	$F(H_1)$[c]	$F'(K_1)$[c]	$F'(H_1)$[c]
1	GL 517 (EQ Vir)	dK5e	YD	2	1	21.6	(0.99)	8.7(+5)	1.0(+6)	8.5(+5)	1.0(+6)
2	GL 380	dM0	YD	1	1	1.6	1.23	6.5(+4)	7.2(+4)	6.1(+4)	6.9(+4)
3	GL 526	dM4	OD	1	2	39.4	1.40	1.8(+5)	1.9(+4)	1.7(+4)	1.8(+4)
4	GL 616.2(BD+55½1823)	dM1.5e	OD	2	1	32.3	1.46	1.3(+5)	1.5(+5)	1.3(+5)	1.4(+5)
5	GL 411(BD+36½2147)	dM2	Halo	1	1	15.7	1.51	5.7(+3)	6.6(+3)	5.0(+3)	5.9(+3)
6	GL 393	dM2	YD	1	1	31.8	1.50	2.3(+4)	1.9(+4)	2.2(+4)	1.9(+4)
7	GL 285 (YZ CMi)	dM4.5e	YD	2	1	122.0	1.81	6.6(+4)	7.3(+4)	6.6(+4)	7.3(+4)

[a]YD = young disk; OD = old disk.

[b]The day observed refers to the UT day at the beginning of the night: day 1 = 1979 February 11, day 2 = 1979 February 12.

[c]Units: ergs $cm^{-2}s^{-1}$.
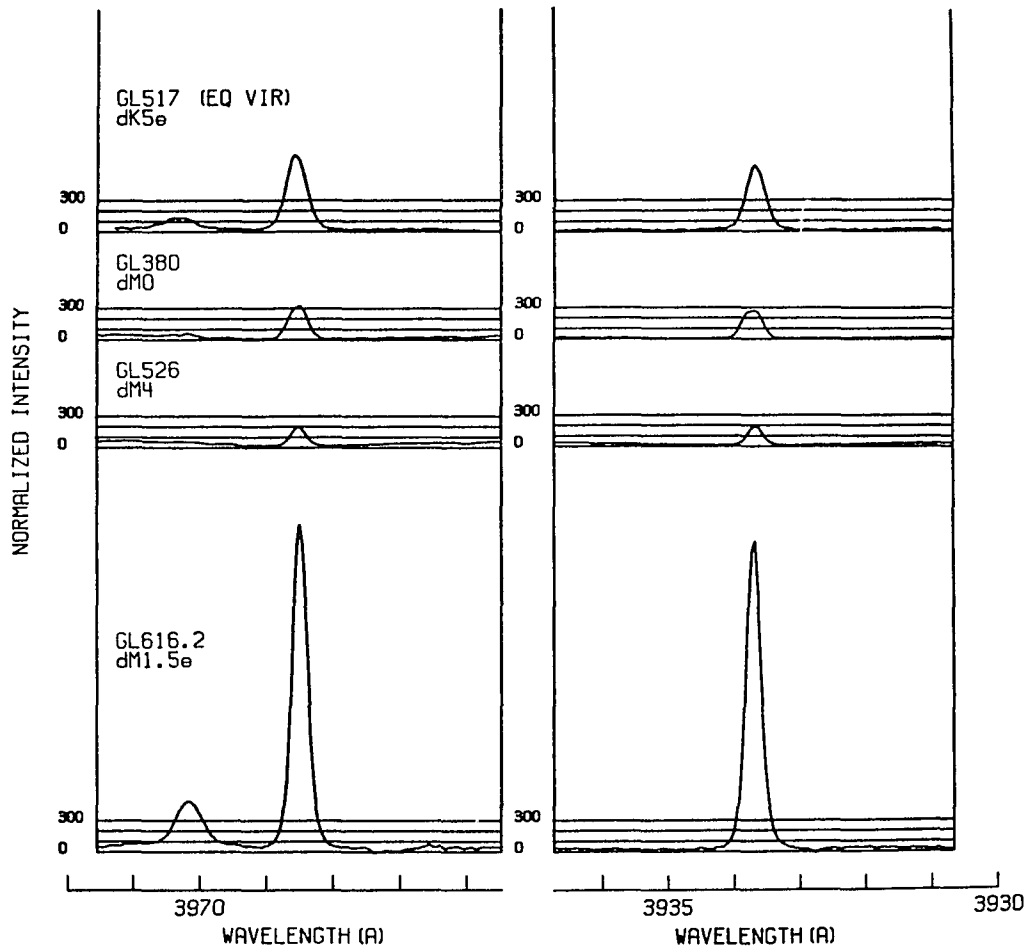
Figure 10. The Ca II H and K lines for selected dMe and dM stars.
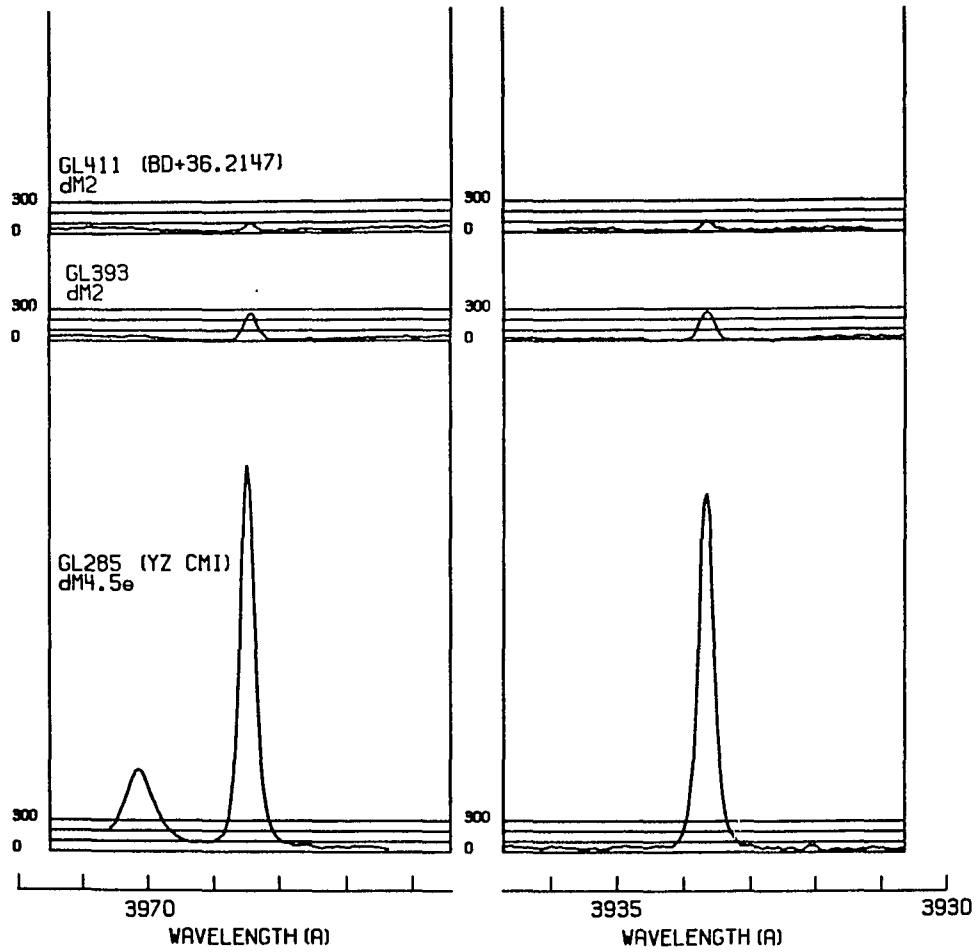
Figure 11.   The Ca II H and K lines in GL 411, GL 393, and YZ CMi.
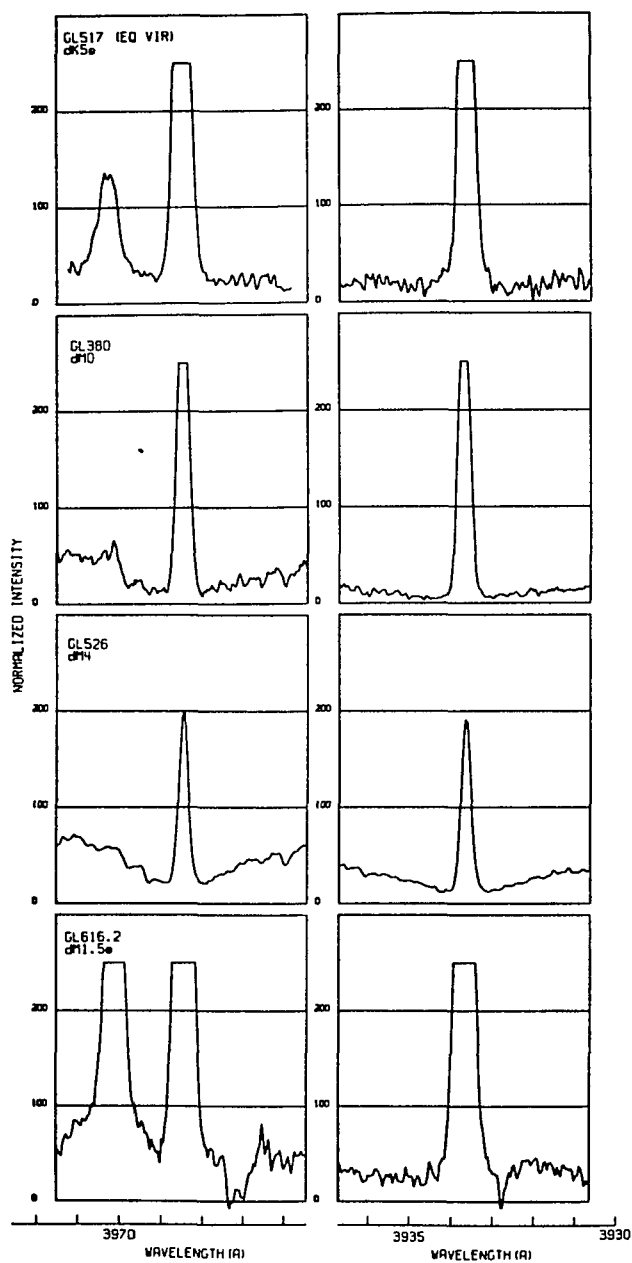
Figure 12.   The cores and wings of the Ca II H and K lines for selected
             M dwarf stars.
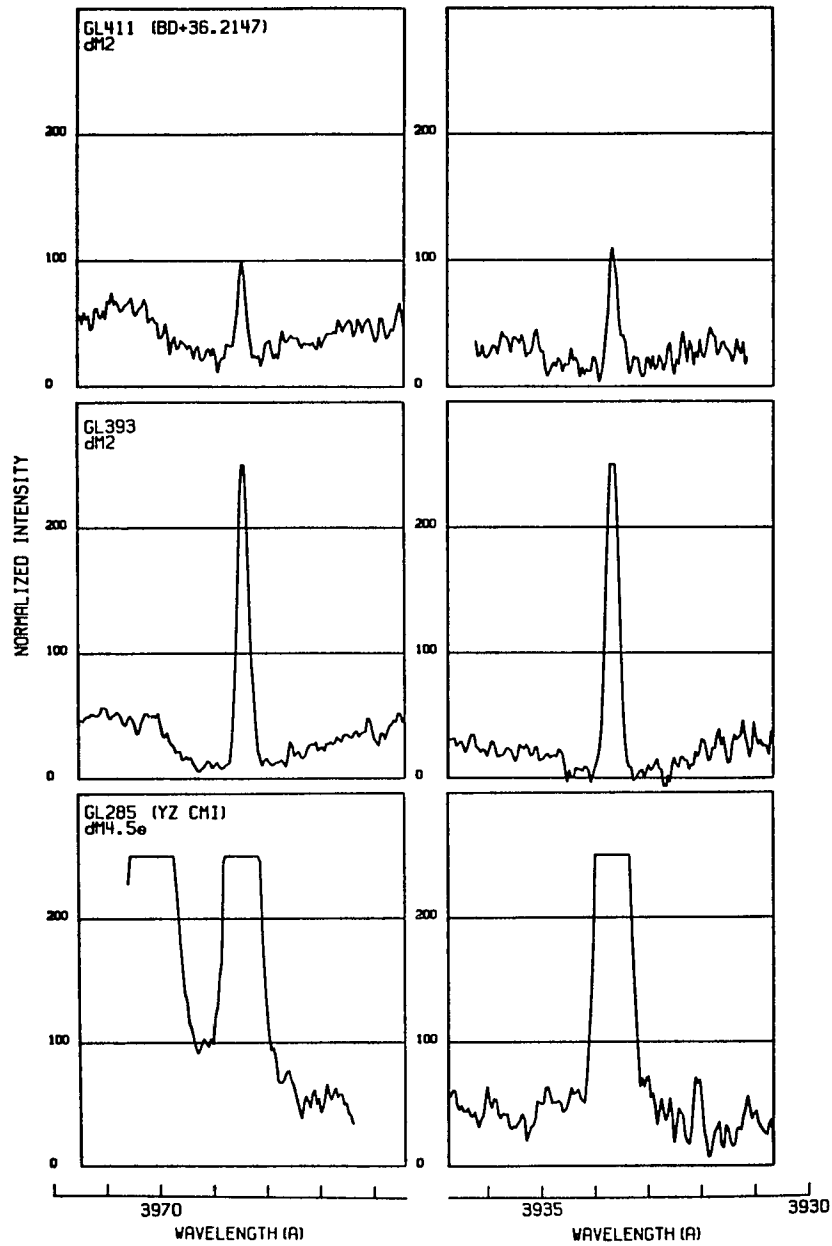
Figure 13. The cores and wings of the Ca II H and K lines in GL 411, GL 393, and YZ CMi.

that 100 corresponds to the observed maximum surface flux between the H and K lines. The peaks[3] of the H_2, K_2, and $H\epsilon$ emission lines have been adopted as absolute wavelength standards with H_2, K_2, and $H\epsilon$ at the laboratory wavelengths 3968.47Å, 3933.66Å, and 3970.07Å, respectively. Emission in the H and K lines is prominent in each of the spectra. The $H\epsilon$ line appears in emission in the active dwarf stars GL 517 (dK5e), GL 616.2 (dM1.5e), and GL 395 (dM4.5e) but is absent in all of the dM stellar spectra.

As demonstrated by Linsky and Ayres (1978), the net chromospheric radiative losses due to the H and K lines can be determined by measuring the excess flux in these lines over the expected H and K line flux for a stellar atmosphere in radiative equilibrium. Thus the net cooling rate in the chromosphere due to these lines expressed in terms of the corrected H_1 and K_1 indices, $F'(H_1)$ and $F'(K_1)$, is given by Linsky et al. (1979)

$$F'(H_1) = F(H_1) - F_{RE}(H_1) , \qquad (2.6)$$

$$F'(K_1) = F(K_1) - F_{RE}(K_1) , \qquad (2.7)$$

where $F_{RE}(H_1)$ and $F_{RE}(K_1)$ are the computed H_1 and K_1 indices for an atmosphere in radiative equilibrium (that is, a model atmosphere with no chromosphere). Values of $F_{RE}(K_1)$ and $F_{RE}(H_1)$ as a function of (V-R) have been computed for 13 main sequence stars by Kelch et al. (1979). Their relation was linearly exptrapolated to include the stars in my sample which have larger (V-R) indices than those originally considered

---

3. Since I do not see any central minima in the H and K line profiles, I call the peak intensities H_2 and K_2.

by Kelch et al. (1979). The resulting radiative equilibrium correction terms are found to be generally less than 10% and sometimes less than 1% of $F(H_1)$ and $F(K_1)$. Thus I conclude that even large errors in $F_{RE}(K_1)$ and $F_{RE}(H_1)$ would be unimportant for my purposes.

The importance of chromospheric nonradiative heating present in this sample of M dwarf stars can be readily intercompared through the ratio·

$$R_{HK} = \frac{F'(H_1) + F'(K_1)}{\sigma T^4_{eff}} \, , \qquad (2.8)$$

where the index R_{HK} represents the chromospheric radiative loss in the H and K lines normalized to the total stellar surface flux. The values of R_{HK} are listed in the third column of Table 2. A plot of R_{HK} versus T_{eff} is presented in Figure 14. I note that the value of R_{HK} for GL 517 (EQ Vir) is 8.8(-5) as compared with 7.1(-5) for the same star in Linsky et al. (1979) and the value of R_{HK} for GL 411 (BD +36°2147) is 1.4(-6) compared with 1.2(-6) in Linsky et al. (1979). I can attribute these differences to both measurement error and to intrinsic variations in the stellar chromospheres but note that the differences are small ($\lesssim$ 20%). Furthermore, I find that the values of R_{HK} for the dMe stars GL 616.2 and GL 285 in Figure 14 are larger than for the dM stars by a factor of 2.5 or more. The quiet dwarfs have values of R_{HK} comparable to that of the mean Sun, $R_{HK} = 7.7(-6)$ (Linsky et al. 1979). Thus nonradiative heating is systematically larger in the dMe than dM stars as is expected in analogy with the relative nonradiative heating rate in solar plages and quiet regions (see also Chapters 4, 5, and 6).

Table 2. Summary of R_{HK} Values and Line Flux Ratios

Sequence Number	Star	$R_{HK} = \dfrac{F'(H_1)+F'(K_1)}{\sigma T_{eff}^4}$	$\dfrac{F(K_1)}{F(H_1)}$	$\dfrac{F'(K_1)}{F'(H_1)}$	$\dfrac{F_\nu(K_2)}{F_\nu(H_2)}$
1	GL 517 (EQ Vir)	8.8(-5)	0.84	0.83	0.84
2	GL 380	1.0(-5)	0.90	0.89	0.81
3	GL 526	3.6(-6)	0.95	0.95	0.95
4	GL 616.2	3.2(-5)	0.92	0.92	0.92
5	GL 411(BD+36°2147)	1.4(-6)	0.86	0.85	1.03
5	GL 393	5.4(-6)	1.18	1.19	1.03
7	GL 285 (YZ CMi)	2.7(-5)	0.90	0.90	0.93
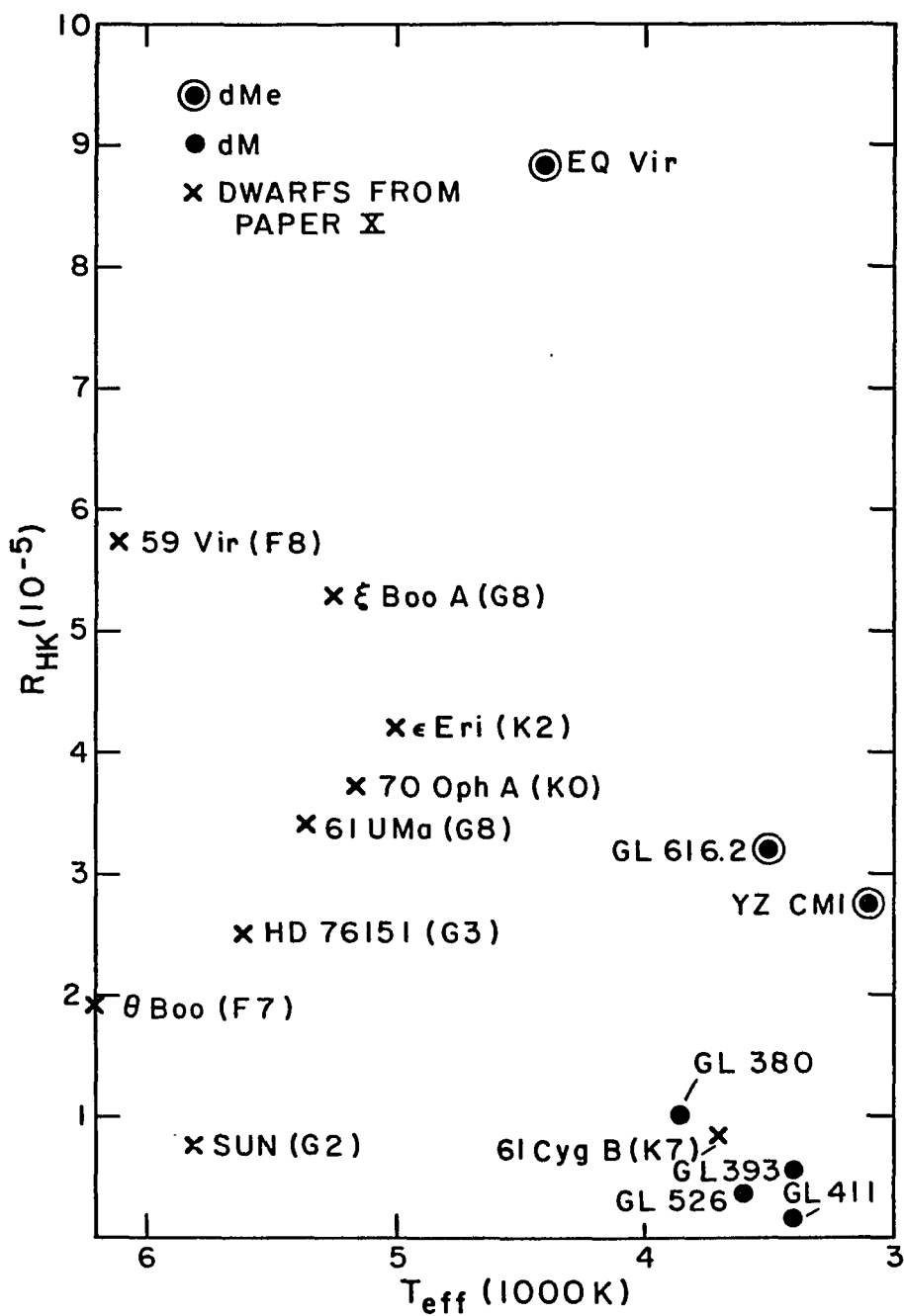
Figure 14. The degree of non-radiative heating present versus effective temperature -- Linsky et al. (1979) is Paper X in the stellar model chromospheres series.

In addition, the active dwarfs (and to a lesser extent, the quiet dwarfs) may show a trend of decreasing R_{HK} with <u>decreasing</u> effective temperature, thus implying that the proportion of the stellar luminosity converted into nonradiative heating in the chromosphere decreases with decreasing effective temperature for this particular selection of stars. Finally, it is interesting to note that Stein and Leibacher (1980) and Renzini et al. (1977) predict that the acoustic energy generation decreases directly with effective temperature to a high power. However, the importance of the role of acoustic energy flux as a chromospheric heating mechanism is not well determined, even for the Sun (Cram 1977; Athay and White 1978). Moreover, Figure 14 shows that M dwarf stars with similar effective temperatures and gravity may exhibit very different degrees of nonradiative heating, contrary to the predictions of the acoustic wave theory (see Chapter 1).

Doublet Ratios

The relative flux in the H and K lines may be indicative of chromospheric optical depths and temperature gradients. The ratio $F(K_1)/F(H_1)$ is listed in column four of Table 2 and plotted with respect to the total fluxes, $F(K_1) + F(H_1)$, in Figure 15. As in Linsky et al. (1979) the data are widely scattered with no apparent physical relationship between the two parameters. However, the dwarfs in this sample tend to lie below the dwarfs considered by Linsky et al. (1979). The mean value of $F(K_1)/F(H_1)$ in this work is 0.94. The ratios of chromospheric radiative losses in the two lines $F'(K_1)/F'(H_1)$ are given in column five of Table 2. These ratios are essentially identical to the
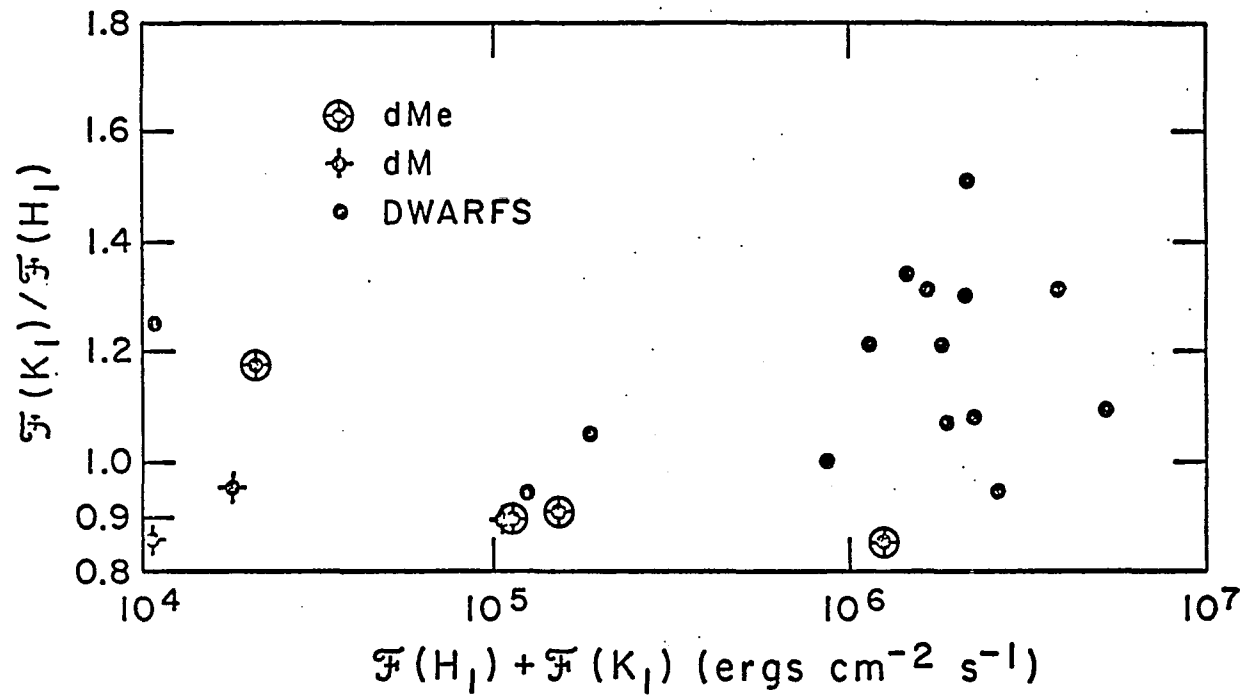
Figure 15. Relative flux in the H and K lines versus the total H and K line flux.

values of $F(K_1)/F(H_1)$ for each star. This is understandable given the relatively small radiative equilibrium correction terms applied to $F(K_1)$ and $F(H_1)$ to derive $F'(K_1)$ and $F'(H_1)$, respectively. The mean value of $F'(K_1)/F'(H_1)$ is 0.93, indicating that the H and K lines are optically thick in these stars. This mean value is lower than the mean ratio of 1.25 found for dwarfs by Linsky et al. (1979); however, I estimate the uncertainty in the mean value of $F'(K_1)/F'(H_1)$ I deduce for the sample of dwarf stars considered here to be $\pm$ 0.20.

As discussed in Linsky et al. (1979) uncertainty in the locations of the H_1 and K_1 features may be an additional source of error which can add to the scatter in Figure 15. However, for the stars considered in the present work this potential source of error is small since the H_2 and K_2 emission features greatly dominate the emitted flux in the H and K lines. Nevertheless, to minimize this possible source of error I include the ratio of monochromatic fluxes at the line peaks $F_\nu(K_2)/F_\nu(H_2)$ in column six of Table 2 and plot these ratios in Figure 16. The scatter is slightly reduced but there are still no apparent trends with respect to $F(H_1) + F(K_1)$.

Monochromatic Surface Fluxes

We list in Table 3 monochromatic surface fluxes for those features in the observed H and K line profiles which are important for comparison with computed line profiles. As usual, H_1 and K_1 refer to the minima outside the line cores and H_2 and K_2 refer to the peak emission in the line cores. The central reversals, H_3 and K_3, do not appear in our data but might be present in higher resolution data. However,
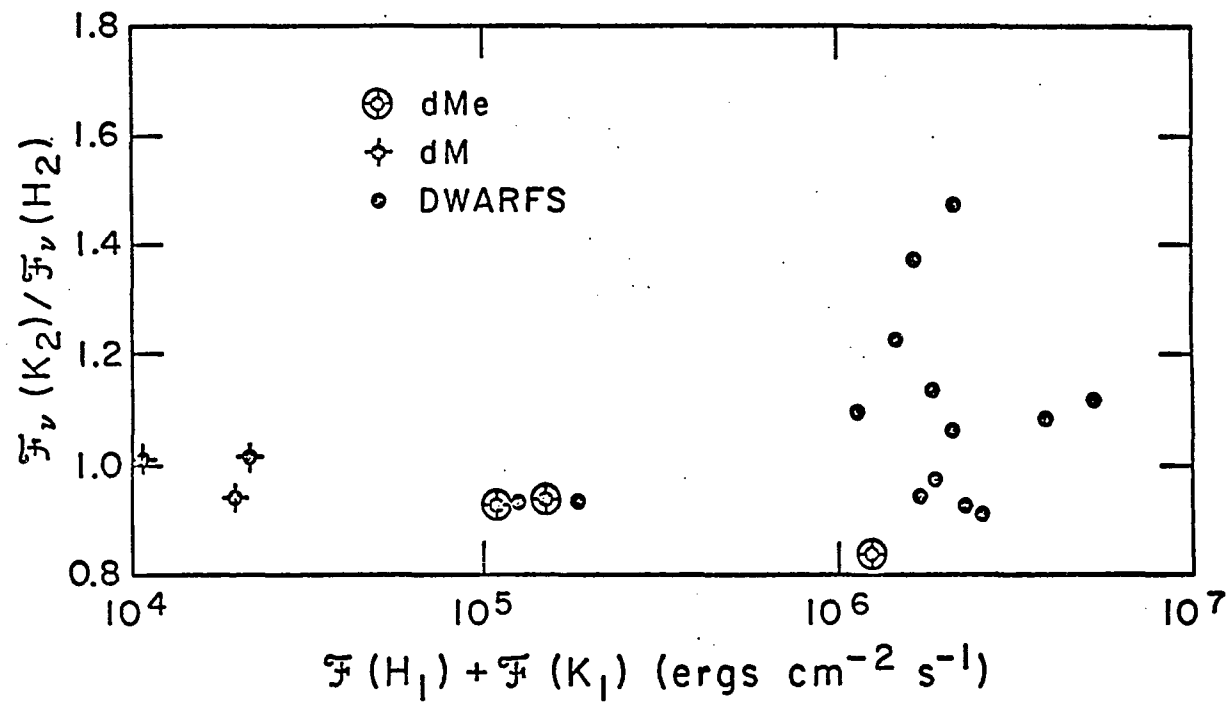
Figure 16.   Peak relative H and K line flux versus the total H and K line flux.

Table 3. Monochromatic Surface Fluxes[a]

Sequence Number	Star	$F_\nu(K_{1_V})$	$F_\nu(K_{1_R})$	$\overline{F_\nu(K_1)}$	$F_\nu(H_{1_V})$	$F_\nu(H_{1_R})$	$\overline{F_\nu(H_1)}$	$F_\nu(K_2)$	$F_\nu(H_2)$	$T_R(K_1)$	$T_R(H_1)$
1	GL 517 (EQ Vir)	2.0(-7)	2.0(-7)	2.0(-7)	1.0(-6)	1.2(-6)	1.1(-6)	3.2(-5)	3.8(-5)	3174	3714
2	GL 380	3.2(-8)	3.2(-8)	3.2(-8)	6.5(-8)	1.3(-7)	9.8(-8)	2.5(-6)	3.1(-6)	2737	2968
3	GL 526	5.2(-8)	4.9(-8)	5.1(-8)	8.9(-8)	9.1(-8)	9.0(-8)	8.3(-7)	8.7(-7)	2836	2948
4	GL 616.2	2.8(-8)	4.6(-8)	3.7(-8)	5.7(-8)	9.5(-8)	7.6(-8)	6.7(-6)	7.2(-6)	2768	2908
5	GL 411(BD+36½2147)	3.3(-8)	1.1(-8)	2.2(-8)	5.2(-8)	3.5(-8)	4.3(-8)	3.2(-7)	3.1(-7)	2663	2783
6	GL 393	2.7(-8)	--	2.7(-8)	4.1(-8)	4.1(-8)	4.1(-8)	1.2(-6)	1.1(-6)	2569	2771
7	GL 285 (YZ CMi)	3.1(-8)	4.9(-8)	4.0(-8)	6.6(-8)	8.8(-8)	7.7(-8)	3.3(-6)	3.6(-6)	2783	2911

[a]Units are ergs cm^2 s^1 Hz^{-1}.

Kelch et al. (1979) warn that observations acquired at a higher spectral resolution may still not reveal the central reversal because of the effects of rotational line broadening (see also Chapters 4 and 7), whereas Baliunas et al. (1979) claim that the absence of a central reversal is due to the existence of a high pressure transition region. The subscripts V and R refer to the violet and red sides of the line profiles, while $\overline{F_V(K_1)}$ and $\overline{F_V(H_1)}$ are the mean K_1 or H_1 monochromatic surface fluxes. The determination of $F_V(H_1)$ for some stars in my sample may be influenced by the presence of the Hε line.

Columns ten and eleven of Table 3 are radiation temperatures derived by setting the mean K_1 or H_1 monochromatic surface fluxes equal to the flux from a blackbody. For all of the stars presented here, $T_R(H_1) > T_R(K_1)$ as predicted by Shine, Milkey, and Mihalas (1975a) on the basis of partial redistribution (PRD) diagnostics, to be discussed later. In Figure 17 I plot $T_R(K_1)/T_{eff}$ versus log T_{eff}. The dwarf stars of our sample lie above the giants presented in Figure 8 of Linsky et al. (1979), as predicted by PRD theory (Shine, Milkey, and Mihalas 1975b). In brief summary, complete redistribution (CRD) requires that both the H_1 and K_1 line source functions saturate to the Planck function at the depths where these spectral features are formed. In contrast, the PRD solutions allow the two line source functions to thermalize independently at these frequencies. Since the H line is more trans-parent, thermalization occurs deeper, and therefore at a higher value of the local Planck function. Hence $T_R(H_1) > T_R(K_1)$. In the case of the giant stars, the effects of PRD are enhanced in a low density atmosphere. An effect of PRD is to inhibit the diffusion of core
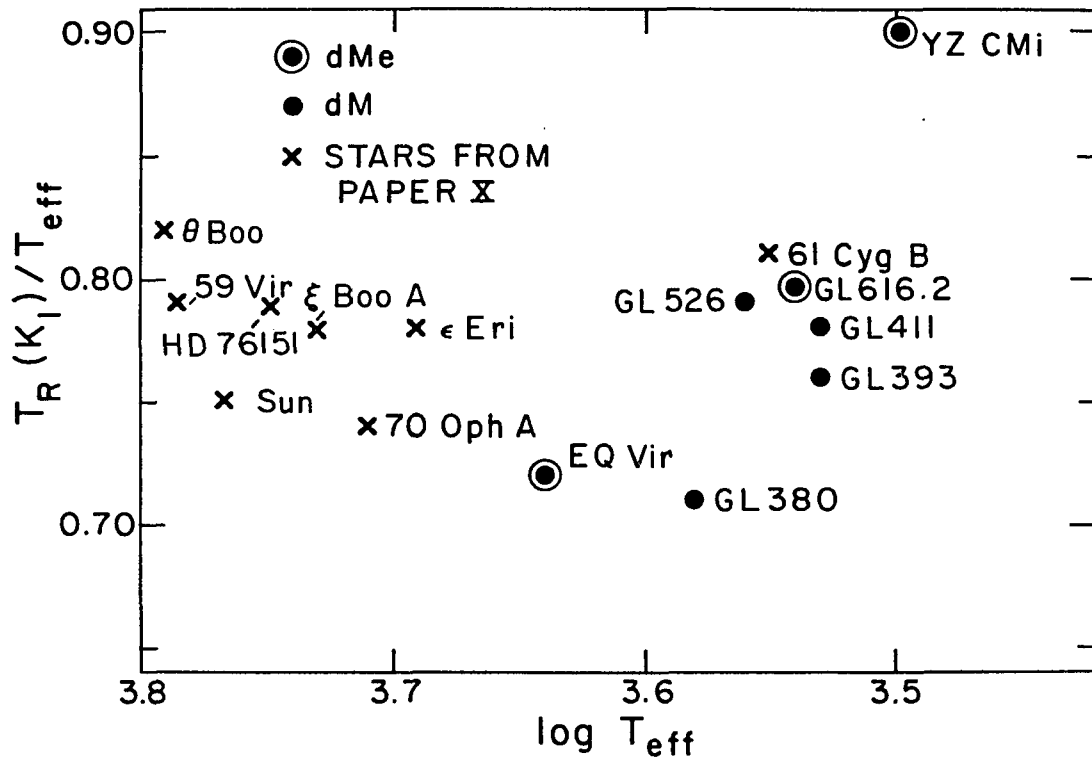
Figure 17.   Relative brightness temperature at K_1 versus effective
temperature.

photons to the line wings (see Chapter 4). Since this PRD effect is enhanced in the low density atmospheres of the giant stars, I have that $T_R(K_1)/T_{eff}$ is smaller in the giants than for the dwarf stars. Kelch et al. (1979) show that among the dwarfs $T_R(K_1)/T_{eff}$ may be an empirical age indicator. In Figure 17 I see that the dwarfs have values of $T_R(K_1)T_{eff}$ similar to the active dwarfs studied by Linsky et al. (1979). The flare star GL 285 (YZ CMi) has an anomalously large value of $T_R(K_1)/T_{eff}$ which may be indicative of the relatively young ages usually ascribed to active flare stars. The dM0 star GL 380 has a $T_R(K_1)T_{eff}$ ratio similar to the solar value of 0.75 (Linsky et al. 1979) as does the flare star GL 517 (EQ Vir). The latter case is inconsistent with the two other dMe stars and could be due to errors in the assumed effective temperature for EQ Vir. As mentioned previously there is no published (V-R) value for this star and I used instead the value for a star of the same spectral type (Johnson 1966), which implies an effective temperature of 4400K. Nevertheless, Figure 17 shows no apparent correlation between kinematic population (see Table 1), which may be indicative of age, and the observed values of $T_R(K_1)/T_{eff}$. However, membership in a certain kinematic population is not an accurate indicator of age for a given field star. Moreover, the M dwarfs considered in this chapter are all within ~ 21 pc of the Sun, which is much less than a galactic scale height (Chiu 1978, Wielen 1974).

Line Widths

I list in Table 4 the line widths $\Delta\lambda_{K_1}$, $\Delta\lambda_{H_1}$, FWHM(K), and FWHM(H). The definitions of these quantities are the same as in Linsky et al. (1979).

These line widths are important tests of theories of Ca II line formation. In particular, Ayres (1979) has derived the following scaling law for the $\Delta\lambda_{K_1}$ width:

$$\log \Delta\lambda_{K_1} = 1/4 \log \tilde{A}_{Fe} + 1/4 \log \tilde{F} - 1/4 \log \tilde{g} + 7/4 \log \tilde{T}_{eff} + \text{constant}$$

(2.9)

In this expression $\tilde{g}$ is the gravity, $\tilde{T}_{eff}$ the effective temperature, and $\tilde{A}_{Fe}$ is the iron abundance, each normalized to the solar value. In this study I assume $\tilde{A}_{Fe}$ to be unity since (1) the stars considered here are in the solar neighborhood, and (2) accurate metallicity measurements for the M dwarfs discussed in this chapter are unavailable. $\tilde{F}$ is a scale factor which is proportional to the chromospheric heating rate. The quiet Sun would be characterized by $\tilde{F} \sim 1$ while $\tilde{F} \sim 10$ would represent the so-called active chromosphere stars (Linsky 1977) or solar plage regions. The index $\tilde{F}$ is given by (Ayres 1979, eq. [4]):

$$\tilde{F} \simeq F_*^{tot}/7 \times 10^6 \, \tilde{T}_{eff}^6,$$

(2.10)

where F_*^{tot} is the total heating above the temperature minimum estimated for this sample of stars by scaling from the measured total solar chromospheric losses. Hence,

$$F_*^{tot} = F_*^{H'+L'} F_\odot^{tot}/F_\odot^{H'+K'},$$

(2.11)

where $F_*^{H'+K'}$ is the measured chromospheric loss rate in the H and K

Table 4. Line Widths and Atmospheric Parameters

Sequence Number	Star	$\Delta\lambda_{K_1}$ (Å)	$\Delta\lambda_{H_1}$ (Å)	FWHM(K) (Å)	FWHM(H) (Å)	T_{eff} (K)	$\tilde{F}$
1	GL 517 (EQ Vir)	0.93	0.72	0.32	0.34	4400	16.2
2	GL 380	0.67	0.42	0.33	0.33	3850	2.3
3	GL 526	0.47	0.50	0.27	0.26	3600	1.0
4	GL 616.2	0.72	0.82	0.25	0.25	3500	8.8
5	GL 411(BD+36°2147)	0.29	0.39	0.21	0.18	3400	0.4
6	GL 393	0.86	0.27	0.23	0.22	3400	1.6
7	GL 285 (YZ CMi)	0.52	0.77	0.23	0.25	3100	9.5

lines and $F_\theta^{H'+K'}$ is the same quantity for the Sun. F_θ^{tot} is the total

chromospheric loss rate in H^- and important spectral lines (Ayres 1979).

The chromospheric heating dependence in the scaling law for $\Delta\lambda_{K_1}$ is

tested by plotting $\log \Delta\lambda_{K_1}$ versus $1/4 \log \tilde{F}$ in Figure 18. The metal-

licity term has been assumed to be zero according to the previously

stated reasons. The gravity and effective temperature dependences have

been deleted since the logarithmic values of these terms are all

similar for the stars considered here. The data for this sample exhibit

a trend of increasing $\Delta\lambda_{K_1}$ with increasing $\tilde{F}$ which is consistent with

the results of Kelch et al. (1979) for a sample of solar type stars.

Uncertainty in the location of the K_1 minima and omission of the

temperature and gravity terms contribute to the scatter in Figure 18.

Nevertheless the results for the dwarfs presented here are generally

consistent with the scaling law proposed by Ayres (1979).

Emission Lines in the Wings of H and K

I now consider the prominent $H\varepsilon$ line at 3970.07Å which appears

in emission in three of the objects: the dMe stars GL 517 (EQ Vir),

GL 616.2, and GL 285 (YZ CMi). I list in Table 5 the measured FWHM and

corrected $H\varepsilon$ indices, $F'(H\varepsilon)$, defined as the total surface flux in the

$H\varepsilon$ line above the wing of the Ca II H line. The corrected $H\varepsilon$ indices

are analogous to the corrected H_1 and K_1 indices and, therefore, are

measures of the chromospheric radiative loss rates in the $H\varepsilon$ line. The

relative importance of the $H\varepsilon$ line as a mechanism for chromospheric

cooling is reflected in the ratio $F'(H\varepsilon)/[F'(H_1)+F'(K_1)]$. The ratio is

listed in Table 5 and plotted with respect to effective temperature in
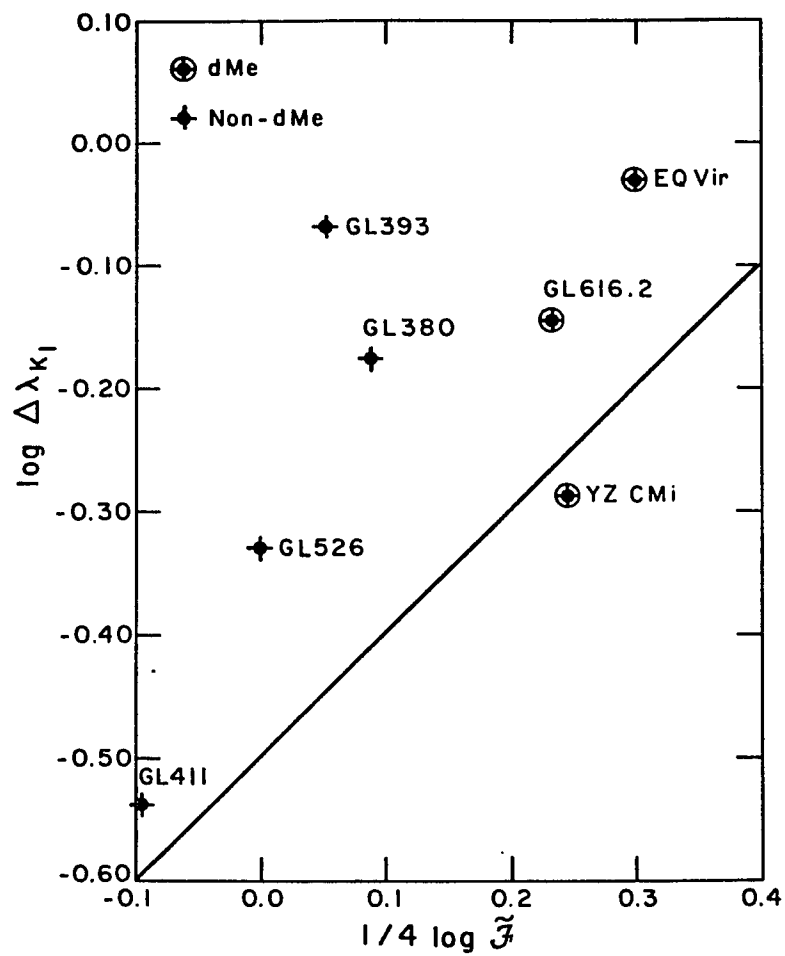
Figure 18. A test of the chromospheric scaling laws.

Table 5. The Hε Emission Line

Sequence Number	Star	Hε FWHM (Å)	F'(Hε)[a]	$\dfrac{F'(H\epsilon)}{F'(H_1)+F'(K_1)}$
1	GL 517 (EQ Vir)	0.51	3.6(+5)	0.19
4	GL 616.2	0.45	4.6(+4)	0.17
7	GL 285 (YZ CMi)	0.50	3.5(+4)	0.25

[a]Units: ergs $cm^{-2}s^{-1}$.

Figure 19. I note that the ratio $F'(H\varepsilon)/[F'(H_1) + F'(K_1)]$ for GL 517

is identical to the value measured for this object by Linsky et al.

(1979). Moreover, the ratios for the dwarfs in Table 5 lie far above

the dwarfs given in Figure 14 of Linsky et al. (1979) as well as above

the giants. This anomaly may be due to high electron densities in the

chromospheres of dMe stars thus leading to collisionally dominated

Balmer lines, as suggested by Fosbury (1974), and corroborated, in the

case of the dMe star AD Leo, by Giampapa et al. (1978; see Chapter 1).

Wilson–Bappu Widths

Finally I list in Table 6 the FWHM(K) after application of a

quadratic correction for instrumental broadening as suggested by Lutz

(1970). Also listed are the corresponding values of $\log W_0$ along with

the values of $\log W_0$ which would be predicted by the $M_v - \log W_0$ least

squares relation of Lutz (1970) which takes into account the error of

measurement in the values of M_v and W_0. The values of M_v are taken from

Gliese (1969). I plot in Figure 20 the measured values of $\log W_0$ for

these stars. The line represents the Wilson–Bappu widths as predicted

by Lutz (1970). I see that the dwarfs generally follow the Wilson–

Bappu relation with some scatter. The error bars in Figure 20 are

derived from the uncertainty in the resolution and the parallax. The

dMe flare star YZ CMi is the most deviant point. However the scatter

of points in Figure 20 is similar to the scatter in Figure 9 of Lutz

(1970) in which the two least-squares solutions for the M_v versus $\log W_0$

relationship are presented.
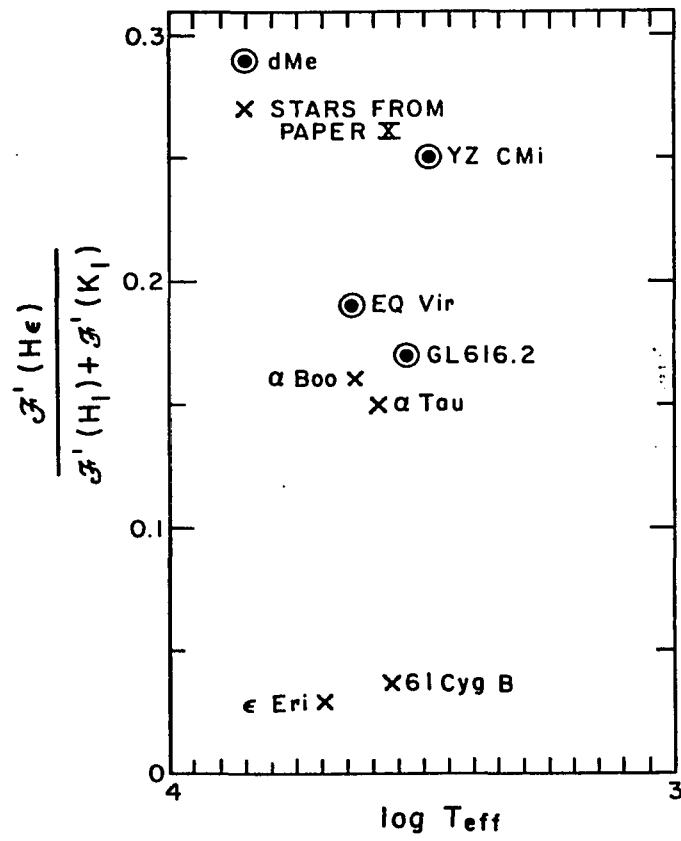
Figure 19. The importance of Hε to net chromospheric radiative cooling.

Table 6. Corrected FWHM(K) and Wilson-Bappu Widths

Sequence Number	Star	FWHM(K) (Å)	log W_0	Predicted log W_0
1	GL 517 (EQ Vir)	0.29	1.34 ± 0.02	1.32
2	GL 380	0.30	1.36 ± 0.02	1.30
3	GL 526	0.23	1.24 ± 0.02	1.19
4	GL 616.2	0.21	1.20 ± 0.02	1.26
5	GL 411	0.11	0.93 ± 0.03	1.16
6	GL 393	0.17	1.11 ± 0.03	1.18
7	GL 285 (YZ CMi)	0.21	1.20 ± 0.02	1.04
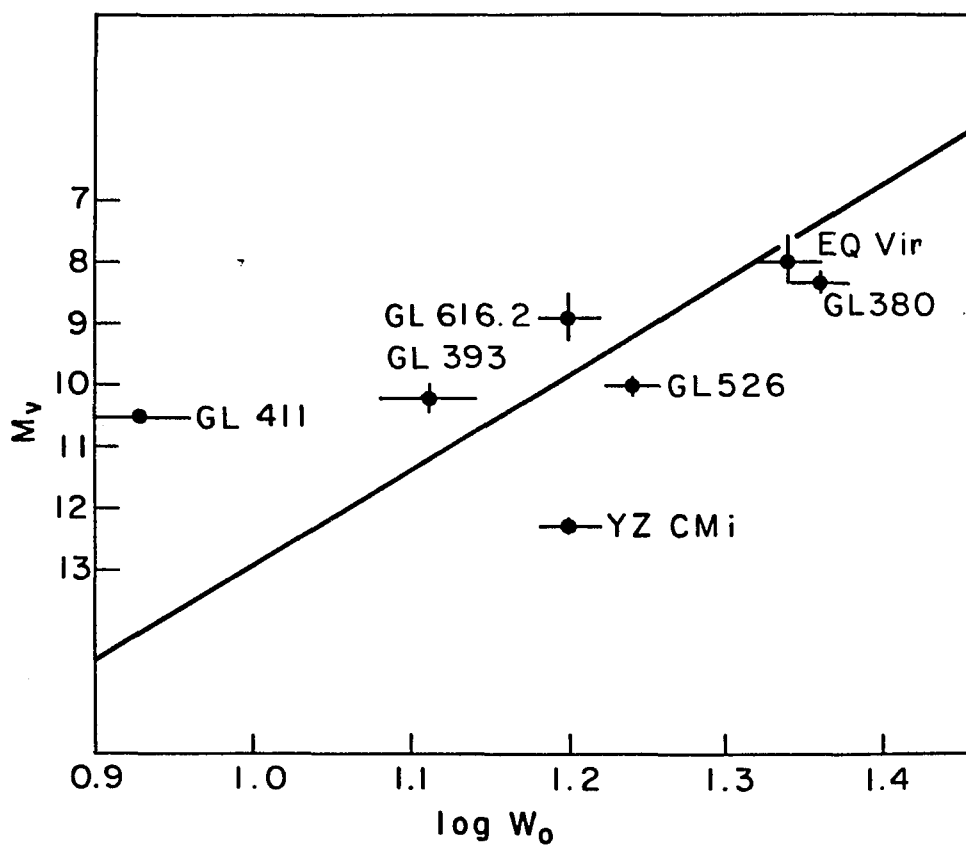
Figure 20. The Wilson-Bappu relation and its applicability to M dwarf stars.

In the following chapter I discuss the model atmospheres formalism which I utilize in order to construct semi-empirical model chromospheres for dMe and dM stars on the basis of the observational data just presented.

CHAPTER 3

SEMI-EMPIRICAL MODEL ATMOSPHERES

The widespread occurrence of Ca II and Mg II resonance-line emission in dwarf M stars (Chapter 2; Giampapa et al. 1980), the presence of Balmer line emission in the dMe stars (Worden et al. 1980) and the recent detections of high excitation transition region lines (Carpenter et al. 1980, Hartmann et al. 1979), as well as the high X-ray luminosities (Linsky 1980a, Vaiana 1980) imply the existence of a non-radiatively heated region above the cool stellar photosphere. Hence the emergent spectrum of an M dwarf star cannot be properly understood solely in the context of a pure radiative-convective equilibrium model atmosphere. We must include a hot chromospheric layer above the stellar photosphere to account for the aforementioned spectral features. The thermal structure of the chromosphere itself is dependent upon the nature of the source of mechanical heating which is present in the chromosphere. Thus the energy equation which describes the emergent flux is

$$F_r + F_c + F_m = \sigma T^4_{eff},\qquad (3.1)$$

where F_r is the radiative flux, F_c is the convective flux, and F_m is the mechanical flux. However, the detailed nature of the mechanical flux is unknown at this time (Chapter 1). Therefore it is impossible to use an energy equation, such as Eq. (3.1), to construct chromo-spheric models from first principles. Thus I adopt the semi-empirical

approach to stellar chromospheric modeling developed by J. L. Linsky and collaborators, and A. K. Dupree and collaborators, during the course of their systematic study of the chromospheric phenomena throughout a large region of the H-R diagram (see Linsky 1980b and references therein). In this approach I specify the atmospheric structure at the onset of the model calculation. The input thermal structure is $T(m), \xi_t(m)$, where m is the mass column density in the atmosphere measured in $g\text{-}cm^{-2}$, ξ_t is the microturbulent velocity measured in $cm\text{-}s^{-1}$, and T is the temperature in degrees Kelvin. The actual chromospheric structure consists of segments within each of which $dT/d \log m$ is constant. The preliminary model chromosphere is adjoined to an appropriate M dwarf photospheric model given by Mould (1976). The line profile derived theoretically is then compared to an observed Ca II K line profile given in Chapter 2. I adjust the chromospheric structure until the best possible correspondence between the observed line profile and the line profile resulting from the stellar atmospheric model calculation is achieved.

The method of solution for the coupled equations of radiative transfer and statistical equilibrium relies upon several simplifying assumptions. I assume (1) plane parallel approximation, (2) hydrostatic equilibrium, (3) the ionization equilibrium for all metals is given by the Saha ionization equation for local thermodynamic equilibrium (LTE), and (4) the atmosphere is laterally homogeneous. Hence the run of physical variables can be expressed as functions of geometrical height alone or, alternatively, mass column density alone. The validity of the LTE approximation for the metals is discussed by Linsky (1968) and Vernazza, Avrett, and Loeser (1973).

These investigators adopt an LTE approximation for the metals in the interest of numerical simplicity and expediency. The complex model atmospheric programs which are required for a completely general, simultaneous solution of the equations of radiative transfer and statistical equilibrium for all of the important line transitions in all of the metals are currently unavailable. In a more recent study, Vernazza, Avrett, and Loeser (1976) nevertheless conclude that neglect of non-LTE effects in the metals may cause an overestimate of the contribution to the opacity due to the metals. The validity of the fourth assumption of lateral homogeneity is less certain for the M dwarfs. I defer a more detailed discussion of this assumption to Chapter 6.

In the following I describe the procedure utilized in the construction of semi-empirical model chromospheres. The steps I follow are:

1. Choose a photospheric model for a given effective temperature, T_{eff}, and stellar surface gravity, g.

2. Include the important sources of line and continuous opacities. This can be done through the use of analytical and empirical expressions which may exist for a particular opacity source, or through the construction of opacity tables.

3. Specify the particular line and continuum transitions in the adopted model <u>hydrogen</u> atom which are to be studied.

4. Adjoin an arbitrary (or the result of step 13) chromospheric temperature rise to the adopted photospheric model. The chromospheric temperature rise is specified by the functions $T_e(m)$, $\xi_t(m)$, where T_e is the electron temperature, m is the mass

column density, and ξ_t is the microturbulent velocity for each depth point in the chromosphere.

5. Beginning from an LTE estimate of the level populations, compute the radiation fields in the explicitly treated line and/or continuum transitions and the hydrostatic and ionization equilibrium.

6. Use this solution for the radiation fields to recompute the level populations in hydrogen.

7. With the new hydrogen populations recompute the radiation fields.

8. Repeat steps 6-7 for a number of iterations specified at the outset of the computation.

9. The end result of step 8 is a model atmosphere which specifies the non-LTE hydrogen populations and the electron density at each depth point in the atmosphere. This model, along with the computed departure coefficients, is then used as the new starting estimate of the solution and steps 6-8 are repeated to finally yield a new model atmosphere.

10. If the electron densities of the new model agree at each depth point to within a few per cent of the starting model (step 9), then I have a fully self-consistent ionization balanced atmosphere model and I may proceed to the next step. If not, then I repeat steps 6-9 until I obtain self-consistent electron densities.

11. I use the model atmosphere obtained by step 10 as the input model to solve the chromospheric spectrum synthesis problem of the "trace" elements, such as Ca II. In particular, I run a

multilevel complete redistribution (CRD; to be discussed later)

code for Ca II to obtain non-LTE level populations and radia-

tion fields in the allowed transitions.

12. I now use the output of step 11 as the input for the two-level

partial redistribution (PRD; to be discussed later) refinement

of the CRD calculation. A result is the theoretical Ca II K-

line profile.

13. I convolve the theoretical K-line profile (obtained in step 12)

with the instrumental profile and compare the result to the

observed profile. If necessary, I adjust the chromospheric

thermal structure and repeat the PRD computation (step 12) unitl

agreement between the theoretical and the observed line profile

is achieved.

14. I now repeat the entire procedure (steps 4-13) with the new

thermal structure found in step 13 in order to obtain a fully

self-consistent model atmosphere.

The computational method I have just outlined is the procedure

used to develop semi-empirical model chromospheres. There are a variety

of formal details which constitute the foundation of the procedure I

have just described. These details include the actual numerical method

used to solve the coupled equations of radiative transfer and statis-

tical equilibrium, as well as the treatment of the hydrostatic and

ionization equilibrium. In addition, the appropriate atomic parameters,

photoionization and collisional cross cross-sections, boundary

conditions, and rate equations must be included. I will discuss these formal details for the remainder of this chapter.

Radiative Transfer and Statistical Equilibrium

The state of a stellar atmosphere is determined when the distribution of the composite particles over all available bound and free states is known. In local thermodynamic equilibrium (LTE) these occupation numbers are functions of the local density and temperature. However, in the relatively low density and high temperature conditions of a stellar chromosphere, non-local thermodynamic equilibrium (non-LTE) prevails (Jeffries and Thomas 1959). Thus the occupation numbers, n_i, are described by n_i (N,T,J_ν) where T is the kinetic temperature and J_ν represents the frequency dependence of the radiation field over the entire spectrum. The radiation field is in turn a function of the state of the gas, as evident from the line source function (Böhm 1960)

$$S_\nu = \frac{2h\nu^3}{c^2} \left(\frac{g_j}{g_i}\frac{n_i}{n_j} - 1\right)^{-1} \frac{\psi_\nu}{\phi_\nu} , \qquad (3.2)$$

where ψ_ν and ϕ_ν are the emission and absorption profiles, respectively. In addition, the equation of transfer will couple all points in the atmosphere to, in effect, cause global responses to local changes in physical quantities. Thus to properly solve for the ionization equilibrium (discussed in a later section) I must solve, simultaneously, the equations of radiative transfer and statistical equilibrium. This approach accounts for the global response of the gas to the radiation field simultaneously with the reciprocal response of the radiation field to material properties. I apply this method, initially, to hydrogen.

Hydrogen is the most abundant element (by several orders of magnitude, neglecting helium). Also, for a given kinetic tempertature, the velocity and therefore the flux of hydrogen atoms through a given point in the atmosphere is greater than for any other ion. Hence electron-hydrogen collisions leading to collisional excitations and ionizations (or radiative and three-body recombinations) are very probable. As mentioned previously, I treat the ionization equilibrium for the metals in an LTE approximation. However, for accurate electron densities to be obtained it is necessary to account for departures from LTE in hydrogen. Thus I solve the coupled equations of radiative transfer and statistical equilibrium simultaneously for a given model hydrogen atom. The ionization equilibrium solution can then be obtained according to a scheme described later in this chapter. Once a self-consistent atmosphere model is constructed, I then proceed to the spectral synthesis of the chromospheric lines.

The Complete Rate Equations

The number density of particles in a bound or free state i for some element is a function of the net flux of particles through the given volume and the net rate at which particles are arriving at state i from other states j, due to a variety of radiative and collisional processes. Thus the following "continuity equation" can be written for a given state i (Mihalas 1978):

$$\frac{\partial n_i}{\partial t} = - \vec{\nabla} \cdot (n_i \vec{v}) + \sum_{j \neq 1} (n_j P_{ji} - n_i P_{ij}), \tag{3.3}$$

where P_{ij} (P_{ji}) is a total rate containing both radiative and

collisional terms. In this investigation I assume a static, steady state atmosphere. Hence $\partial n_i / \partial t = 0$ and $- \vec{\nabla} \cdot (n_i \vec{V}) = 0$. Therefore,

$$n_i \sum_{j \neq 1} P_{ij} - \sum_{j \neq 1} n_j P_{ji} = 0. \tag{3.4}$$

In this expression the first term represents the number of atoms lost from state i while the second term represents the number of atoms arriving into state i from state j, due to radiative and collisional processes (Gray 1976). The first term in Eq. (3.4) is

$$n_i \sum_{j \neq i} P_{ij} = n_i \sum_{j < i} (R'_{ij} + C_{ij}) + n_i \sum_{j > i}^{k} (R_{ij} + C_{ij}), \tag{3.5}$$

where k represents the continuum, the R_{ij} are the radiative rates, and the C_{ij} are collisional rates. Now $R'_{ij} \equiv (n_j/n_i)^* R_{ij}$ (see Eq. [3.49]) and $C_{ij} = (n_j^*/n_i^*) C_{ji}$ (see Eq. [3.59]), for $j < i$. Therefore

$$n_i \sum_{j \neq i} P_{ij} = n_i \{ \sum_{j < i} (n_j^*/n_i^*) [R_{ij} + C_{ji}] + \sum_{j > i}^{k} (R_{ij} + C_{ij}) \}. \tag{3.6}$$

The second term in Eq. (3.4) is

$$\Sigma n_j P_{ji} = \sum_{j < i} n_j (R_{ji} + C_{ji}) + \sum_{j > i} n_j (R'_{ji} + C_{ji}). \tag{3.7}$$

As before, I can write $R'_{ji} = (n_i^*/n_j^*) R_{ji}$ and $C_{ji} = (n_i^*/n_j^*) C_{ij}$, each for $j > i$. Hence

$$-\Sigma n_j P_{ji} = -\sum_{j < i} n_j (R_{ji} + C_{ji}) - \sum_{j > i}^{k} n_j (n_i^*/n_j^*) (R_{ji} + C_{ij}). \tag{3.8}$$

Substituting Eqs. (3.6) and (3.8) into Eq. (3.4) yields the complete rate equation for level i:

$$-\sum_{j < i}^{j=i-1} n_j (R_{ji} + C_{ji}) + n_i \{ \sum_{j < i} (n_j^*/n_i^*) [R_{ij} + C_{ji}] + \sum_{j > i}^{k} (R_{ij} + C_{ij}) \}$$

$$- \sum_{j > i}^{k} n_j (n_i^*/n_j^*) (R_{ji} + C_{ij}) = 0. \tag{3.9}$$

One such equation can be written for each bound state. The system is
completed by invoking an additional physical constraint. The total
number of atoms and ions of the element considered must equal the
correct fraction of the total hydrogen number density (for hydrogen in
all forms). Thus

$$\sum_{i,j} n_{ij,k} - (n_k/n_H) \, n_H = 0. \tag{3.10}$$

where $\sum_{i,j} n_{ij,k}$ is the total number density of element k summed over all
excitation and ionization states considered for element k. The final
system for all levels of all ions of all species is

$$\underline{A} \, \underline{n} = \underline{B}, \tag{3.11}$$

where $\underline{n}$ is the vector of all occupation numbers, $\underline{A}$ is the rate equation
matrix, and $\underline{B}$ is a vector with elements given by the number conservation
Eq. (3.10). The simultaneous solution of the equation of radiative
transfer and the equation of statistical equilibrium (Eq. [3.11]) is
discussed in the following.

The Complete Linearization Method

The _simultaneous_ solution of the coupled equations of radiative
transfer and statistical equilibrium is the mathematical realization of
the physical concept of non-local thermodynamic equilibrium. The
complete linearization method is a numerical procedure by which the
solution is obtained. The result is a model atmosphere which specifies
the state of the gas through the determination of the occupation numbers
as a function of depth in the atmosphere. The distribution of particles
over bound and free states, given by the vector $\underline{n}$ in the rate equation

(Eq. [3.11]), can be determined if n_e, T_e, and J_ν are specified. However, during a model atmosphere computation only current estimates of these variables are available in an overall iterative process. During the iterative process the variables n_e, T_e, and J_ν change by amounts δn_e, δT_e, and δJ_ν to better satisfy the constraints of energy and pressure balance. By the condition of non-LTE, $\underline{n}$ will change accordingly. The change in $\underline{n}$ is given by (Auer and Mihalas 1969):

$$\delta \underline{n} = \frac{\partial n}{\partial T_e} \delta T_e + \frac{\partial n}{\partial n_e} \delta n_e + \sum_{i=1}^{NJ} \frac{\partial n}{\partial J_i} \delta J_i, \qquad (3.12)$$

where NJ is the number of angle-frequency quadrature points. For any variable X we have (Mihalas 1978):

$$\frac{\partial n}{\partial X} = \underline{A}^{-1} [\frac{\partial \underline{B}}{\partial X} - (\frac{\partial \underline{A}}{\partial X} \cdot \underline{n})]. \qquad (3.13)$$

In this investigation I specify the atmospheric structure, $T_e(m)$, $\xi_t(m)$, at the onset of the calculation. Hence $\delta T_e = 0$ in Eq. (3.13) and I have that

$$\delta \underline{n} = \frac{\partial \underline{n}}{\partial n_e} \delta n_e + \sum_{i=1}^{NJ} \frac{\partial \underline{n}}{\partial J_i} \delta J_i. \qquad (3.14)$$

I also have from Eq. (3.13) that

$$\frac{\partial n}{\partial J_i} = \underline{A}^{-1} [\frac{\partial \underline{n}_e}{\partial J_i} - (\frac{\partial \underline{A}}{\partial J_i}) \underline{n}]. \qquad (3.15)$$

Auer (1973) has shown that this kind of formulation of the complete linearization method combined with an already specified atmospheric structure will result in a system of coupled linear equations which contain only the δJ_i explicitly. According to Auer (1973) the solution of the system yields δJ_i which satisfies both the equation of transfer

and the linearized form of the rate equation. I will briefly sketch the basic formalism underlying the complete linearization method.

The equation of transfer in a plane parallel atmosphere at frequency ν is

$$\mu \frac{dI_\nu}{d\tau_\nu} = I_\nu - S_\nu,$$ (3.16)

where the source function can be written as

$$S_\nu = \frac{\int J_\nu \phi_\nu d\nu + \varepsilon B_\nu(T_e) + \eta B^*}{1 + \varepsilon + \eta}$$ (3.17)

following Jefferies and Thomas (1958). A detailed discussion of the meaning of this expression is deferred to Chapter 4. The method of solution requires the transfer equation to be cast as a second order differential equation. The equation and the boundary conditions are then written as finite-difference equations. Finally the inter-dependence among the transitions is linearized and solutions for the corrections in the radiation fields are determined in an iterative fashion. The remainder of this description of the complete linearization method follows the discussion by Lites (1972). Two variables are defined

$$P_\nu \equiv 1/2 \, [I_\nu(+\mu) + I_\nu(-\mu)],$$ (3.18)

$$R_\nu \equiv 1/2 \, [I_\nu(+\mu) - I_\nu(-\mu)],$$ (3.19)

where P_ν is similar to the mean intensity, J_ν, and R_ν is similar to the flux. The transfer equations for the $+\mu$ and $-\mu$ directions are

$$+\mu \frac{dI_\nu(+\mu)}{d\tau_\nu} = I_\nu(+\mu) - S_\nu$$ (3.20)

$$-\mu \frac{dI_\nu(-\mu)}{d\tau_\nu} = I_\nu(-\mu) - S_\nu.$$ (3.21)

Addition and subtraction of these equations yields the first-order
differential equations

$$\mu \frac{dP_\nu}{d\tau_\nu} = R_\nu \tag{3.22}$$

$$\mu \frac{dR_\nu}{d\tau_\nu} = P_\nu - S_\nu, \tag{3.23}$$

from which it follows that

$$\mu^2 \frac{d}{d\tau_\nu} [\frac{dP_\nu}{d\tau_\nu}] = P_\nu - S_\nu. \tag{3.24}$$

The actual mean intensity, J, is given by a weighted sum of
P_ν's where the weighting coefficients depend upon the angle quadrature.
The upper boundary condition for this problem is $I_\nu(-\mu) = 0$. Thus

$$P_\nu|_{\tau=0} = R_\nu|_{\tau=0} , \tag{3.25}$$

and

$$\mu \frac{dP_\nu}{d\tau_\nu} \Big|_{\tau=0} = P_\nu|_{\tau=0} , \tag{3.26}$$

following Eq. (3.22). The lower boundary condition is given by the
diffusion approximation

$$I_\nu(+\mu) = B_\nu + \mu \frac{dB_\nu}{d\tau_\nu} , \tag{3.27}$$

where B_ν is the Planck function of the last depth point. This boundary
condition can be specified as

$$\mu \frac{dP_\nu}{d\tau_\nu} \Big|_{\tau=\tau_{max}} = [I_\nu(+\mu) - P_\nu] \Big|_{\tau=\tau_{max}} , \tag{3.28}$$

where I have used the equality $R_\nu = I_\nu(+\mu) - P_\nu$ which follows from the
definitions of P_ν and R_ν, and $I_\nu(+\mu)$ is given by Eq. (3.27). The

difference equation for the transfer equation at depth point d is

(following Auer and Mihalas 1969)

$$\mu^2 \frac{P_{d-1}}{\Delta\tau_{d-1/2}\Delta\tau_d} - \mu^2 \frac{P_d}{\Delta\tau_d}[\frac{1}{\Delta\tau_{d-1/2}} + \frac{1}{\Delta\tau_{d+1/2}}] + \mu^2 \frac{P_{d+1}}{\Delta\tau_d\Delta\tau_{d+1/2}} =$$

$$P_d - \frac{\eta_d}{\chi_d}, \quad\quad\quad (3.29)$$

where

$$\Delta\tau_{d-1/2} = 1/2(W_{d-1} + W_d)(m_d - m_{d-1}) \quad\quad (3.30)$$

$$\Delta\tau_{d+1/2} = 1/2(W_d + W_{d+1})(m_{d+1} - m_d) \quad\quad (3.31)$$

$$\Delta\tau_d = 1/2 (\Delta\tau_{d+1/2} + \Delta\tau_{d-1/2}), \quad\quad (3.32)$$

where $W_d = \chi_d/\rho_d$ and ρ_d is the mass density, χ_d is the absorptivity

and m_d is the mass column density, each at depth d. Note that these

equations are tridiagonal in depth. Each depth point d is related to

the surrounding depth points d+1 and d-1. Hence changes in the state

of the atmosphere at any depth point d will affect all other points in

the atmosphere, as prescribed by the non-LTE condition. The boundary

conditions can be similarly expressed as difference equations. I need

to solve the system of equations (i.e., radiative transport and

statistical equilibrium) for the mean intensities in each line

$$\bar{J} = \int J_\nu \phi_\nu d\nu \simeq \sum_i w_i J_{\nu_i} \quad\quad (3.33)$$

and the level populations. This set of variables is represented by a

vector, ψ which is N_d X (number of variables) in length and N_d is the

number of discrete depth points. The equations are represented by an

operator f such that

$$f(\underline{\psi}) = 0. \qquad (3.34)$$

The linearization process begins with an estimate of the solution, $\underline{\psi}_o$. I begin by assuming an LTE solution. The actual solution $\underline{\psi}$ is

$$\underline{\psi} = \underline{\psi}_o + \delta\underline{\psi}, \qquad (3.35)$$

where $\delta\psi$ is a correction. Thus

$$f(\underline{\psi}) = f(\underline{\psi}_o + \delta\underline{\psi}), \qquad (3.36)$$

and to first order

$$f(\underline{\psi}_o) + \frac{\partial f}{\partial \underline{\psi}} \delta\underline{\psi} = 0. \qquad (3.37)$$

Equation (3.37) yields $\delta\underline{\psi}$ which is added to $\underline{\psi}_o$. The process is repeated until convergence. I calculate the $\frac{\partial f}{\partial \underline{\psi}}$ for the discretized transfer equations and their boundary conditions. The $\delta\underline{\psi}$ consists of the $\delta P_\nu(\mu)$, and δn_i and δn_j for the lower and upper levels of each transition. A linear matrix equation can be written for each transition, or (Mihalas 1978)

$$\underline{f}_k \, \delta \underline{P}_k + \underline{A}_k \, \delta \underline{n}_i + \underline{B}_k \, \delta \underline{n}_j = \underline{L}_k, \qquad (3.38)$$

for each frequency-angle point k. The resulting matrix is an $N_d \times N_d$ array. The corrections to the mean radiation field in a transition are obtained from a weighted sum of the $\delta \underline{P}_k$ at each angle-frequency point or,

$$\delta\overline{J} = \sum_i \sum_j W_{\mu,i} \, W_{\nu,j} \, \delta\underline{P}_{i,j} \, . \qquad (3.39)$$

Equation (3.38) is multiplied by $\underline{f}_k^{-1}$ and each of the equations for each transition are summed according to Eq. (3.39):

$$\delta\overline{J} + \underline{G} \, \delta\underline{n}_i + \underline{H} \, \delta\underline{n}_j = \overline{D}, \qquad (3.40)$$

where, for example

$$\underline{G} = \sum_i \sum_j W_{\mu,i} \; W_{\nu_{ik}} \; \underline{f}_{k,i,j}^{-1} \; \underline{A}_{k,i,j} \; . \tag{3.41}$$

In practice the statistical equilibrium equations are used to express the $\underline{\delta n}$ in terms of the $\overline{\delta J}$ of all other transitions, as suggested by Auer (1973). Thus the iterative scheme proceeds by finding the δJ_i by solving the linearized transfer equations in the explicitly treated bound-bound and bound-free transitions. The new J_i are used to revise the radiative rates and to find the new populations (populations treated in LTE are also revised in order to be consistent with the current ionization equilibrium). The new populations are used in a solution of the transfer equation which in turn yields new values of J_i. The rates and populations are again revised, thus completing an iteration. I continue this iterative scheme until I obtain electron densities accurate to within a few per cent. The program computes depth-dependent Doppler profiles, including the non-thermal microturbulent broadening, for the explicitly treated transitions. At this stage the line transfer is computed in the complete redistribution (CRD) approximation. This assumption states that there is no correlation between the frequencies of incoming and scattered photons (Mihalas 1978). This assumption is also referred to as complete noncoherence. In CRD the emission and absorption profiles are identical ($\psi_\nu = \phi_\nu$). Also, Thomas (1957) has shown that CRD leads to a frequency independent source function. Thus frequency shifts are due to Doppler redistribution.

In summary, the advantage of the complete linearization method is that corrections applied to a variable at some depth point in the

model atmosphere will properly affect all other parameters describing the state of the gas at all other points in the atmosphere. Hence convergence is global and the rate of convergence is quadratic (Auer and Mihalas 1969).

Atomic Models, Radiative and Collisional Rate Equations

I adopt a five-level plus continuum representation of the hydrogen atom. I explicitly solve the coupled equations of radiative transfer and statistical equilibrium in the Lyman continuum and in the Hα line. The Lyman continuum is represented by nine equally spaced frequency points extending from the ionization edge at $\nu_o = 3.29 \times 10^{15}$ Hz to $\nu = 4.89 \times 10^{15}$ Hz. The Lyman lines, Ly α and Ly β, are assumed to be in detailed balance. The remaining bound-bound and bound-free transitions are specified by fixed rates according to the radiation temperature assigned to a particular transition at the outset of the calculation (Auer, Heasley, and Milkey 1972). Noyes and Kalkofen (1970), Ayres (1975), and Ayres and Linsky (1975) find that adequate self-consistency in the electron density can be achieved with this representation of the hydrogen atom. Furthermore, Auer and Mihalas (1969) find that the assumption of detailed balance in Ly α and Ly β is generally valid for Lyman continuum optical depths larger than 0.1. The model atom and transitions are summarized in Figure 21 and Table 7.

Fixed Rates

Radiative Transition Rates. The upward rate for a bound-bound transition from level i to level j is
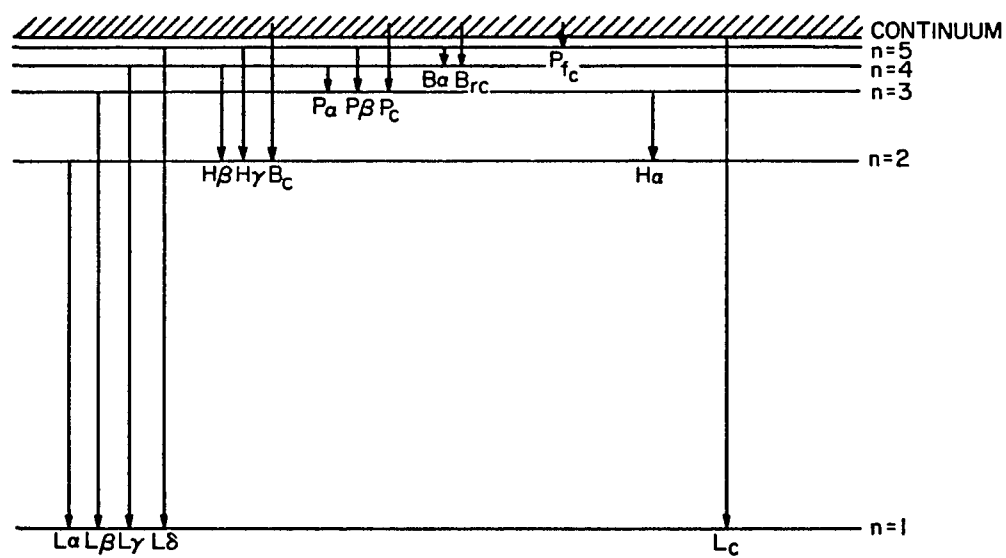
Figure 21. Model hydrogen atom utilized in the development of M dwarf model chromospheres.

Table 7. Hydrogen Model Atom Representation

Radiative Transitions with Fixed Rates		Radiative Transitions in Detailed Balance		Explicitly Solved Transitions	
Lγ	λ 972.537 Å	Lα	λ 1215 Å	Hα	λ 6562 Å
Lδ	λ 949.743	Lβ	λ 1025	Lc	λ 912
Hβ	λ 4862.685				
Hγ	λ 4341.684				
Bc	λ 3646				
Pα	λ 18756.061				
Pβ	λ 12821.532				
Pc	λ 8206				
Brα	λ 40522.415				
Brc	λ 1458.8				
PFc	λ 22794				

$$n_i R_{ij} = n_i B_{ij} \int \phi_\nu J_\nu d\nu. \tag{3.42}$$

Since the absorption profile is a sharply peaked function of ν, I have that

$$n_i R_{ij} = n_i B_{ij} \overline{J}_\nu, \tag{3.43}$$

where the total cross-section for absorption is

$$\alpha_{ij} = B_{ij} h\nu_{ij}/4\pi, \tag{3.44}$$

and $\alpha_{ij} = \frac{\pi e^2}{mc} f_{ij}$, where the oscillator strength, f_{ij}, includes the appropriate Gaunt factor. Following Auer et al. (1972) I set $\overline{J}_\nu = B_\nu$ (T_{rad}) for a fixed transition. Hence for a line transition with a fixed radiation temperature, T_{rad}, the upward rate per atom is

$$R_{ij} = \frac{4\pi}{h\nu_{ij}} \frac{\pi e^2}{mc} f_{ij} B_\nu(T_{rad}). \tag{3.45}$$

The number of downward emissions is composed of the sum of spontaneous and stimulated emissions in the line transition. The total downward rate from level j to level i is (Mihalas 1978)

$$n_j R'_{ji} = n_j (A_{ji} + B_{ji} \overline{J}_{ij}), \text{ or} \tag{3.46}$$

$$n_j R'_{ji} = n_j (4\pi/h\nu_{ij})(g_i \alpha_{ij}/g_j)[2h\nu_{ij}^3/c^2 + \overline{J}_{ij}]. \tag{3.47}$$

The total upward and downward rates can be related by multiplying Eq. (3.46) by $n_j \frac{g_i}{g_j}$ and multiplying Eq. (3.47) by n_i. This eventually leads to

$$R'_{ji} = \frac{g_i}{g_j} R_{ij} [1 + \frac{2h\nu_{ij}^3}{c^2} \frac{1}{\overline{J}_{ij}}]. \tag{3.48}$$

For a fixed transition I again have $\overline{J}_{ij} \equiv B_\nu(T_{rad})$, following Auer et al. (1972). Substituting this expression into Eq. (3.48) yields

$$R'_{ji} = R_{ij}\, g_i/g_j\, e^{h\nu_{ij}/k\,T_{rad}} .$$

From the Boltzmann equation this can be rewritten as

$$R'_{ji} = R_{ij}\, \frac{n_i^*}{n_j^*}\Big|_{T_{rad}} , \qquad (3.49)$$

where n_i^* and n_j^* denote the LTE populations for levels i and j

evaluated at the radiation temperature, T_{rad}.

Photoionizations and Radiative Recombinations. The rate for

direct photoionizations from bound level i to the continuum level k is

$$n_k R_{ik} = 4\pi n_i \int_{\nu_o}^{\infty} \alpha_{ik}(\nu)\, \frac{J_\nu}{h\nu}\, d\nu , \qquad (3.50)$$

where, as before, $J_\nu \equiv B_\nu\,(T_{rad})$ for fixed transitions. The rates are

explicitly solved for the Lyman continuum in this investigation. The

total downward rate is composed of spontaneous and stimulated recom-

binations. The spontaneous recombinations represent a coupling of the

given bound-free transition to the local thermal pool. Hence the

spontaneous captures are in LTE (Mihalas 1970). By detailed-balancing

arguments (Mihalas 1970), the LTE rate of photoionizations must equal

the number of spontaneous recombinations corrected for stimulated

emissions. Thus

$$n_k^* R_{ki} = 4\pi n_i^* \int_{\nu_o}^{\infty} \frac{\alpha_{ik}(\nu)B_\nu}{h\nu}\, (1-e^{-h\nu/kT})d\nu, \qquad (3.51)$$

or,

$$R_{ki} = 4\pi \frac{n_i^*}{n_k^*} \int_{\nu_o}^{\infty} d\nu\, (h\nu)^{-1}\alpha_{ik}(\nu)B_\nu(1-e^{-h\nu/kT}). \qquad (3.52)$$

The calculated rate must apply per ion in non-LTE as well (Mihalas 1978). This is fundamentally due to the fact that recombination is a collisional process which is proportional to $n_k \cdot n_e$ and to the electron temperature, T_e. Therefore the non-LTE rate for spontaneous recombination is

$$n_k R_{ki} = n_k (n_i^* / n_k^*) \ 4\pi \int_\nu^\infty \frac{\alpha_{ik}(\nu)}{h\nu} \frac{2h\nu^3}{c^2} e^{-h\nu/kT} \, d\nu. \qquad (3.53)$$

The Saha equation can be expressed as

$$n_i^* / n_k^* = n_e \phi_{ik}(T_e), \qquad (3.54)$$

where $\phi_{ik}(T_e)$ is the temperature dependence of the Saha equation. So $n_k R_{ki} \propto n_k n_e \phi_{ik}(T_e)$ which shows the explicit dependence of the spontaneous recombination rate on the product of the electron and ion densities and a function of temperature.

The stimulated recombination rate follows from similar arguments to those given for the spontaneous recombination case. For the general non-LTE case the actual ion density is used, as before, but now B_ν is replaced by the actual J_ν. The stimulated recombination rate is now given by Mihalas (1978)

$$n_k R_{ki}^{stim} = n_k \frac{n_i^*}{n_k^*} \ 4\pi \int_\nu^\infty \frac{\alpha_{ik}(\nu)}{h\nu} J_\nu \, e^{-h\nu/kT} d\nu. \qquad (3.55)$$

The total number of recombinations is given by

$$n_k R_{ki}^{spon} + n_k R_{ki}^{stim} = 4\pi n_k (n_i^* / n_k^*) \int_\nu^\infty (h\nu)^{-1} \alpha_{ik}(\nu) [\frac{2h\nu^3}{c^2} + J_\nu] e^{-h\nu/kT} d\nu. \qquad (3.56)$$

The reader may note the similarity of the expression in the integrand

to the description of the total downward rate for a <u>line</u> transition
given by Eq. (3.48). The only physical difference is due to the fact
that there is a continuum of possible frequencies for the case of
recombination.

Following Auer et al. (1972) I compute the fixed radiative rates
by setting $\bar{J}_\nu = B_\nu (T_{rad})$. As long as the relevant transitions remain
optically thin the radiative rates can be fixed at the outset of the
radiative transfer calculation (Ayres 1975). This is physically due to
control of the rates by the background stellar spectral energy distribu-
tion (Auer 1973). When $\bar{J}_\nu$ thermalizes to the local Planck value of the
Planck function, $T_{rad} = T_e$. Near the top of the atmosphere T_{rad} assumes
a value consistent with the surface value of $\bar{J}_\nu$. In the actual computa-
tion I set $T_{rad} = T_e$ below the optical depth at which $\bar{J}_\nu$ begins to
thermalize to B_ν. Above this level I adopt a T_{rad} corresponding to the
surface value of $\bar{J}_\nu$. The radiation temperatures for the fixed line
transitions are taken from Ayres (1975). The same approach is used in
the case of the bound-free transitions (except for the Lyman continuum
which is explicitly calculated). The photoionization rate, given by
Eq. (3.50), is written as (Auer et al. 1972)

$$R_{ik} = 4\pi \int_0^\infty (h\nu)^{-1} \alpha_\nu B_\nu (T_{rad}) d\nu. \tag{3.57}$$

Following Basri (1979), Eq. (3.57) is numerically integrated using
estimates of J_ν and then Eq. (3.57) is inverted to obtain T_{rad}.

Collisional Rates

As the temperature in the chromosphere (or photosphere)
rises and the material becomes more ionized then collisions

with electrons predominate. This is due to the long-range nature of Coulomb forces and to the flux of impinging electrons at a given point in the atmosphere. The collision frequency is proportional to the particle flux which in turn is proportional to the particle velocity. In thermal equilibrium the electron velocities are of order $(m_H A/m_e)^{1/2} =$ 43 $A^{1/2}$ larger than those of ions of atomic weight A.

The total number of transitions due to collisions with electrons of velocity V for a transition $i \rightarrow j$ (where $i \rightarrow j$ may be a bound-bound or bound-free transition) is

$$n_i C_{ij} = \int_{V_o}^{\infty} \sigma_{ij}(V) f(V) \, V dV, \qquad (3.58)$$

where $\sigma_{ij}(V)$ is the cross-section, $f(V)$ is the electron velocity distribution, and V_o corresponds to the threshold energy of the transition. Since the velocity distribution is the Maxwell distribution the collisional processes are in detailed balance. Therefore

$$n_i^* C_{ij} = n_j^* C_{ji} , \qquad (3.59)$$

where n_i^* and n_j^* are the LTE populations for the lower and upper levels of the transition. The total number of downward transitions are then given by

$$n_j C_{ji} = n_j \, (n_i^*/n_j^*) \, C_{ij}. \qquad (3.60)$$

In the case of collisional recombination $n_j^* = n_p$ for hydrogen, where n_p is the proton density. For each depth in the atmosphere the collision rate matrix C is calculated. The elements C_{ij} of the matrix are related by the condition of detailed balance, Eq. (3.59), while the diagonal elements C_{ii} are by definition zero.

The collisional excitation and ionization rates can be expressed as

$$C_{ij} = \Omega_{ij} (T_e) n_e , \qquad (3.61)$$

where n_e is the electron density and Ω_{ij} is the rate coefficient which is of the form (Mihalas 1970)

$$\Omega_{ij} \; \alpha \; T_e^{1/2} \; e^{-h\nu_{ij}/kT_e} . \qquad (3.62)$$

The collisional rates for hydrogen ionization are taken from Mihalas (1967b). For the $i \rightarrow i + 1$ excitations the rate coefficients of Golden and Sampson (1971) are used, with the exception of the Ly α transition. For this case the experimental results of Crandall et al. (1974) are used. The remaining collisional excitation rates are based upon the semi-empirical estimates of Sampson and Golden (1970).

Background Opacities and Emissivities. The opacity at each frequency can be generall expressed as

$$\chi_\nu = \chi_\nu^{\ell} + \chi_\nu^{b} , \qquad (3.63)$$

where χ_ν^{ℓ} is the line opacity and χ_ν^{b} is the background opacity. In the model atmosphere calculation performed in this investigation I compute background opacities and emissivities for the transitions considered, at each frequency point in the line, at each depth point in the atmosphere. The first five bound-free continua of hydrogen are included in the opacity calculation, allowing for departures from LTE in the Lyman continuum (Mihalas 1967a). The hydrogen free-free opacity is treated in LTE.

The bound-free absorption cross-sections from level n are (Mihalas 1978)

$$\alpha_{\nu n} = 2.815 \times 10^{29} \frac{g_n(\nu)}{n^5 \nu^3} , \qquad (3.64)$$

where $g_n(\nu)$ is the appropriate Gaunt factor at frequency ν. The hydrogen opacity per gram due to photoionizations is (Mihalas 1967a)

$$k_\nu = \frac{1}{\rho} \alpha_{1\nu} n_{H_1} (1 - \frac{1}{b_1} e^{-h\nu/kT_e}) + \frac{1}{\rho} \sum_{i=2}^{5} \alpha_{i\nu} n_{H_i} (1 - e^{-h\nu/kT_e}), \qquad (3.65)$$

where n_{H_i} is the density of hydrogen in state i and ρ is the total mass density. Note that a correction for stimulated recombination is included as well as an allowance for non-LTE in the Lyman continuum through the ground state departure coefficient b_1 (Mihalas 1967a, 1978; Beebe and Milkey 1972). The corresponding emissivity per gram is assumed to be given by Kirchoff's Law:

$$\varepsilon_\nu = k_\nu B J_\nu \qquad (3.66)$$

These relations are depth dependent because n_{H_i} and ρ are depth dependent as dictated by the constraint of hydrostatic equilibrium. The hydrogen free-free opacity per gram is (Mihalas 1978)

$$k_{ff} = \frac{1}{\rho} \frac{3.69 \times 10^8}{\nu^3} g_{ff} (T_e, \nu) T_e^{-1/2} n_e n_p (1 - e^{-h\nu_{ff}/kT_e}). \qquad (3.67)$$

where $g_{ff} (T_e, \nu)$ is the free-free Gaunt factor (Mihalas 1967b), n_e is the electron density, n_p is the proton density, and T_e is the electron temperature. As before, the absorptivity and emissivity are related by

$$\varepsilon_{ff} = k_{ff} B_\nu (T_e). \qquad (3.68)$$

Finally, the opacity due to electron scattering, H^-, H_2^+, neutral carbon, magnesium, and silicon is included. The opacity calculations include corrections for stimulated emission. The free-free term in the H^- opacity is given by John (1964) and the bound-free term is given by Geltman (1962). The H_2^+ opacity is described by Gingerich (1964) and the bound-free CI opacity is given by Peach (1967). Finally, the opacity due to Si and Mg are calculated according to Gingerich and Rich (1968). These sources of opacity are computed in LTE and the opacities and emissivities are related by Kirchoff's Law.

The molecular opacities due to the oxide bands (TiO and H_2O) and CaH bands are implicitly included through the adoption of an M dwarf photospheric model computed by Mould (1976) who includes these opacity sources. The opacity due to CO is omitted since it is not included in the photospheric models developed by Mould (1976), and a detailed, numerically complex non-LTE analysis is required for CO because departures from LTE may be important in the CO line formation (Heasley et al. 1978). I note, however, that the results by Heasley et al. (1978) are for the specific case of Arcturus and therefore may not be applicable to the problem of CO line formation in the more dense atmospheres of M dwarf stars. In the following I describe the ionization and hydrostatic equilibrium. The method of the approach is similar to that adopted by Gray (1976) and Basri (1979).

The Hydrostatic and Ionization Equilibrium

The choice of mass column density, m, as the independent depth parameter is dictated by the lack of spatial resolution in stellar

observations. Thus a geometrical height scale is rendered irrelevant for comparisons between observational and theoretical results. Furthermore, a mass column density scale possesses the convenient property of essentially being proportional to the optical depth scale of any opacity which is proportional to n_H, the total hydrogen density (Ayres, Linsky and Shine 1974). Such opacity sources include Ca II H and K, Mg II h and k, the Lyman continuum, etc. Finally, the condition for hydrostatic equilibrium can be simply expressed by the algebraic relation

$$P_{total} = gm, \tag{3.69}$$

where g is the stellar surface gravity. Implicit in this expression is the assumption that radiation pressure is negligible in M dwarfs (Schwarzschild 1958). The total pressure is composed of the gas pressure, P_g, and the turbulent pressure, P_{ξ_t}, or

$$P_{total} = P_g + P_{\xi_t} . \tag{3.70}$$

The turbulent pressure is

$$P_{\xi_t} = 1/2 \, \rho \xi_t^2, \tag{3.71}$$

where ρ is the mass density and ξ_t is the microturbulent velocity. The gas pressure is given by the perfect gas law

$$P_g = n_{total} \, k \, T_e, \tag{3.72}$$

where n_{total} is the total particle density and T_e is the electron temperature. The electron temperature and the kinetic temperature of atoms and ions are essentially identical (Böhm 1960). The mass density is given by

$$\rho = n_e m_e + n_H m_H [\sum_j (n_j/n_H)(m_j/m_H)], \tag{3.73}$$

where m_e is the electron mass. The summation over j includes all important constituents of the atmosphere. The abundance and atomic weight of the jth element relative to hydrogen are n_j/n_H and m_j/m_H, respectively. The abundances are assumed to be solar and their values are taken from Lambert and Warner (1968). These values are summarized in Table 8. I assume solar abundances since (1) there are no metal abundance determinations for the M dwarf stars discussed in this dissertation; and (2) the stars considered here, including GL 411 which is classified as a member of the halo population (Veeder 1974), are within ~ 20 pc of the Sun. Thus the stars in the sample discussed in this investigation are in the solar neighborhood at distances from the Sun which are each much less than a galactic scale height (Chapter 2). I also note, parenthetically, that metal abundance determinations according to current methods can yield inaccurate results for stars which have chromospheres (Giampapa, Worden, and Gilliam (1979). The total particle density is

$$n_{total} = n_e + n_H \sum_j n_j/n_H. \tag{3.74}$$

Thus the total pressure is

$$P_{total} = gm = P_e + n_H A kT_e + 1/2\, n_H m_H \mu \xi_t^2 + 1/2\, n_e m_e \xi_t^2, \tag{3.75}$$

where $P_e = n_e kT_e$ is the electron pressure and I have defined $A \equiv \sum_j n_j/n_H$ and $\mu \equiv \sum_j (n_j/n_H)(m_j/m_H)$. Noting that $n_H A = n_{total} - n_e$ yields

$$gm = P_e - P_e(1 + \frac{m_H \mu}{A}\frac{\xi_t^2}{2kT_e}) + m_e P_e \frac{\xi_t^2}{2kT_e} + P_g (1 + \frac{m_H \mu}{A}\frac{\xi_t^2}{2kT_e}). \tag{3.76}$$

Table 8. Metal Abundances

Element	Abundance (relative to H)
H	1.0
He	0.08
C	4.17(−4)
N	8.71(−5)
O	6.92(−4)
Na	1.905(−6)
Mg	3.98(−5)
Al	3.3(−6)
Si	4.47(−5)
S	1.585(−5)
K	1.445(−7)
Ca	2.24(−6)
Cr	5.13(−7)
Fe	3.16(−5)
Ni	1.905(−6)

The gas pressure is then

$$
P_g = \frac{gm + P_e \frac{\xi_t^2}{2kT_e} (\frac{m_H \mu}{A} - m_e)}{1 + \frac{\xi_t^2}{2kT_e} \frac{m_H \mu}{A}} \tag{3.77}
$$

The solution for the gas pressure explicitly includes the electron pressure. An expression for the electron pressure can be derived through consideration of the ionization equilibrium.

In the treatment of the ionization balance I consider only the neutral and first ionization stages. Second ionizations of metals are neglected since the second ionization potentials are greater than the ionization potential for hydrogen (Allen 1976). Thus when second ionizations are important, the principal source of electrons will be hydrogen by virtue of its overwhelming abundance. By assumption (3) I can write the Saha equation

$$
n_{ij}/n_{oj} = \phi_j \, (T_e)/P_e, \tag{3.78}
$$

where n_{oj} is the number density of neutrals, n_{ij} is the number density of ions, and

$$
\phi(T_e) = 0.6665 \frac{U_1}{U_o} T_e^{5/2} 10^{-(5040\lambda_I/kT_e)}, \tag{3.79}
$$

where U_1/U_o is the ratio of ionic to neutral partition functions. By neglect of second ionizations I have that

$$
n_{ej} = n_{ij}, \tag{3.80}
$$

where n_{ej} represents the electrons contributed by the jth element. The total number density of species j is

$$n_j = n_{oj} + n_{ij} = n_{oj} + n_{ej}, \tag{3.81}$$

which leads to

$$n_{ej} = \frac{n_j \phi_j (T_e)/P_e}{1+\phi_j (T_e)/P_e} \tag{3.82}$$

by Eq. (3.77). The electron and gas pressures are $P_e = \sum_j n_{ej} kT_e$ and $P_g = \sum_j (n_j + n_{ej}) kT_e$, respectively. The electron pressure, in terms of the gas pressure, is

$$P_e = P_g \cdot \frac{\sum_j A_j \{\phi_j (T_e)/P_e [1+\phi_j (T_e)/P_e]\}}{\sum_j A_j (1+\{\phi_j (T_e)/P_e [1+\phi_j (T_e)/P_e]\})} \tag{3.83}$$

where $A_j \equiv n_j/n_H$. The expression is transcendental in P_e and a double-iterative scheme is employed to determine P_e and P_g from initial guesses for these quantities. Initial estimates of P_e and P_g are taken from either a previous model calculation or from

$$P_g \approx gm/(1 + \frac{\xi_t^2}{2kT_e} \frac{m_H \mu}{A}) , \tag{3.84}$$

and

$$P_e \approx \frac{P_g X}{1+X} , \tag{3.85}$$

where

$$X = \phi_H/[\phi_H + (P_g/100)]. \tag{3.86}$$

From an estimate of P_g a value for P_e is derived from Eq. (3.82). This value of P_e is then used in Eq. (3.76) to determine P_g. Stable convergence to within 1% is attained for P_e and P_g after a few iterations.

Summary

The previous sections essentially describe how non-LTE in hydrogen is taken into account. Once the departures from LTE are calculated, non-LTE values for the $\phi_j(T_e)$ terms in the Saha equation can be employed by the double-iterative scheme that is used to calculate the gas and electron pressures (see previous section). The total particle and electron number densities immediately follow from the gas and electron pressures via the perfect gas law. The total hydrogen density for hydrogen in all forms is

$$n_H = (n_{total} - n_e)/A. \qquad (3.87)$$

The abundances are relative to n_H. To find the number density of atomic hydrogen, I take into account the other forms of hydrogen; H^+, H_2, H_2^+, and H^-. The number densities of the molecules are determined according to Mihalas (1967b), assuming LTE. The entire scheme for the solution of the coupled equations of radiative transfer and statistical equilibrium described in this chapter yields a fully self-consistent ionization balanced model atmosphere. I can now proceed to the spectral synthesis of the Ca II K-line and other chromospheric lines.

CHAPTER 4

SPECTRAL SYNTHESIS OF THE Ca II K-LINE

In this chapter I describe the spectral synthesis formalism used
to construct model chromospheres for dMe and dM stars based upon the
observed Ca II K-line profiles presented in Chapter 2 and the input
model atmospheres derived in Chapter 3. Included in this discussion is
a description of the adopted Ca II atomic models along with the rele-
vant radiative and collisional rates. The coupled equations of radia-
tive transfer and statistical equilibrium are solved by the complete
linearization method (Chapter 3), initially in the complete redistribu-
tion (CRD) approximation. The resulting Ca II non-LTE level populations
are used as input for the more accurate partial redistribution (PRD)
formulation of the line transfer problem. I describe any systematic
trends present in the resulting chromospheric models and discuss the
underlying physical causes which give rise to the theoretically inferred
model properties.

Model Atom and Atomic Data

I use a three-level-plus-continuum representation for Ca II.
The levels considered are the $4s^2S_{1/2}$ ground state (level 1), $4p^2P_{3/2}$
excited state (level 3), the $3d^2D_{5/2}$ metastable level (level 2), and the
Ca III continuum (Figure 22). I treat the neutral fraction Ca I/Ca II
in LTE (Ayres and Linsky 1975) and explicitly solve the coupled
equations of radiative transfer and statistical equilibrium in the CRD
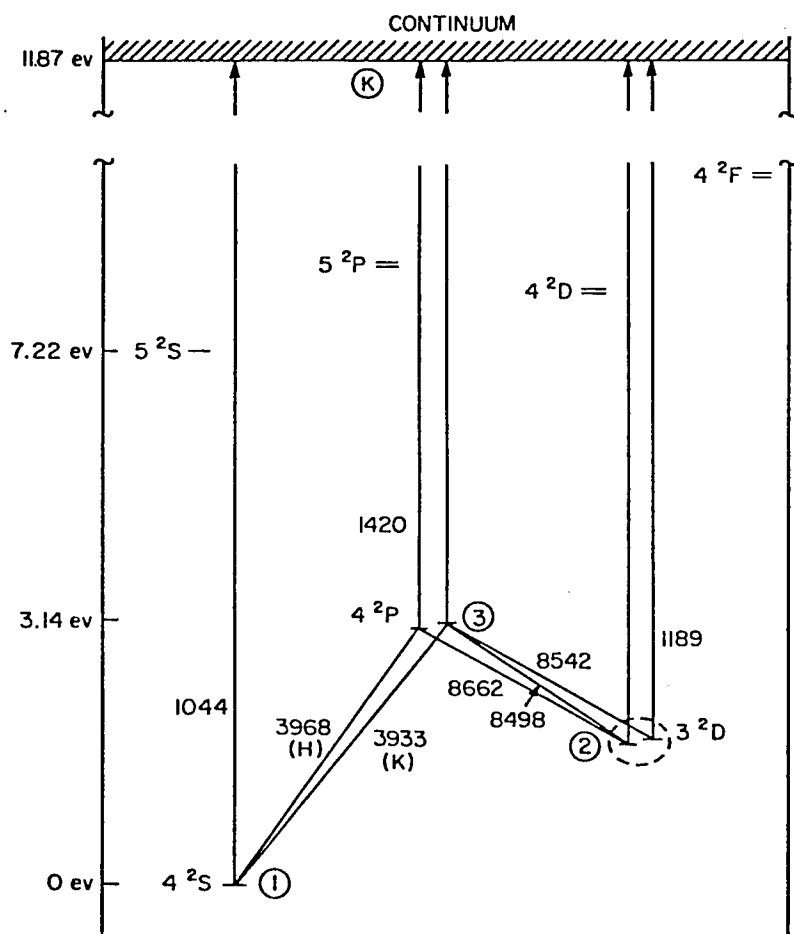
Figure 22. Model calcium atom showing important line transitions.

approximation for the permitted radiative transitions Ca II K (1-3, λ3934Å) and the subordinate infrared triplet line (2-3, λ8542Å). In the interest of numerical simplicity I avoid a full five-level treatment (i.e., calculating the H and K lines, and all three infrared triplet lines). According to Ayres et al. (1976) the differences in the K line profile between a five-level and a three-level treatment are found to be minimal in the specific cases of the dwarf stars α Cen A (G2V) and α Cen B (K1V). All levels are coupled by collisions and the collision rate coefficients are taken from Shine and Linsky (1974). Photo-ionizations from the three bound levels are treated as fixed rates by specifying a radiation temperature, T_{rad}, for the particular bound-free transition. The photoionization cross sections are given by Shine and Linsky (1974). The radiation temperatures are determined according to the method described in Chapter 3. In practice I find, as do Ayres et al. (1976), that large errors in T_{rad} have little effect on the emergent profiles of the collision dominated K-line. The radiative damping constants and van der Waals broadening constants for the K-line and the λ8542 line are taken from Shine and Linsky (1974). The assumed abundance is Ca/H = 2.141(-6) (Lambert and Warner 1968). The reasons for assuming solar abundances were given in Chapter 3. If solar abundance is an <u>overestimate</u> for a given M dwarf star then I may slightly underestimate the density of the chromosphere; if the assumption of solar abundances is an <u>underestimate</u> of the metallicity for a given M dwarf star then I may slightly overestimate chromospheric densities. In any event, the basic conclusions concerning the nature of the chromospheric thermal structure in dMe and dM stars will not be

changed. I adopt 2.6(-6) n_{e_d} for the Ca II Stark broadening parameter,

where n_{e_d} is the electron density at depth d (Raymer 1979). The com-

bined effect of these broadening mechanisms is described by a depth

dependent Voigt profile with damping constant $\underline{a}$ such that

$$a = \sum_i \gamma_i / \Delta\nu_D, \qquad (4.1)$$

where γ_i is the ith broadening mechanism and $\Delta\nu_D$ is the Doppler width

at depth d. In the following I describe the PRD refinement of the CRD

computation which finally yields the emergent Ca II K-line profile for

a given thermal structure.

<div align="center">

Line Formation with Complete and
Partial Redistribution

</div>

In the scattering process a redistribution function is employed

to describe the change in photon frequency and direction. The redistri-

bution function is given by (Mihalas 1978)

$$R(\nu', \underline{n}'; \nu,\underline{n}) \, d\nu' d\nu (d\omega'/4\pi) \, (d\omega/4\pi), \qquad (4.2)$$

which gives the joint probability that a photon will be scattered from

direction $\underline{n}'$ in solid angle $d\omega'$ and frequency range $(\nu', \nu' + d\nu')$ into

frequency range $(\nu, \nu + d\nu)$, direction $\underline{n}$ and solid angle $d\omega$. The two

extreme cases of the scattering process are complete redistribution

(CRD) and coherent scattering (i.e., $\nu' = \nu$). In CRD there is no

correlation between incoming and scattered photons. The assumption of

CRD is particularly applicable when the impact approximation strongly

prevails. In addition, Thomas (1957) has shown that CRD is a good

approximation in the line core ($|\Delta\lambda| \leq 3|\Delta\lambda_D|$) and it further provides

an excellent first approximation in line transfer problems. Finally, Thomas (1957) has shown that the assumption of CRD leads to a frequency independent source function and Doppler shifts redistribute the photons in frequency. However, the assumption of CRD fails to accurately predict the observed center-to-limb behavior of the solar Ca II H and K lines (Linsky and Avrett 1970) and the solar Lyman α profile (Vernazza 1972, Vernazza et al. 1973, Beebe and Milkey 1972). The discrepancy is removed when coherent scattering (in the rest frame of the atom) in the resonance line damping wings is taken into account (Milkey and Mihalas 1973). This method of approach to the line transfer problem which essentially incorporates elements of both CRD and coherent scattering is referred to as partial redistribution (PRD). The angle-averaged redistribution function is expressed as

$$R(\nu, \nu') = (1 - \gamma_\nu)R_{II}(\nu, \nu') + \gamma_\nu R_{III}(\nu, \nu'), \qquad (4.3)$$

where $\gamma \equiv \delta_c/(\delta_c + \delta_r)$ is the incoherence fraction. The factors δ_r and δ_c are the radiative and collisional damping widths, respectively. A fraction γ of the atoms in a particular upper state are expected to suffer collisions which completely redistribute the atoms among the substates of the upper state. The remaining fraction $(1 - \gamma)$ are expected to decay radiatively and emit coherently in the rest frame of the atom. The functions R_{II} and R_{III} are derived by Hummer (1962). The redistribution function R_{II} is applicable to the case where there is radiation damping in the upper state and coherence in the atomic rest frame. The redistribution function R_{III} represents complete redistribution in the rest frame of the atom. The incoherence fraction, γ, is

assumed to be frequency independent and R_{III} is assumed to be true

complete redistribution thus ignoring any residual Doppler coherency

(Mihalas 1978, Jefferies 1968). Therefore $R_{III}(\nu, \nu') \rightarrow \phi_\nu \phi_{\nu'}$. The

function R_{II} simulates nearly complete redistribution in the line core

and then becomes nearly coherent in the line wings. The physical basis

of this dichotomy is the following: within the line core most of the

emissions are from atoms absorbing at line center and moving with

velocities corresponding to $\Delta\nu/\Delta\nu_D \lesssim 2.5$ (Mihalas 1978). For incident

frequencies in the line wings the number of atoms with sufficiently

high velocity to absorb at line center declines exponentially (Jefferies

1968). Thus most emissions arise from atoms with low velocities and

absorbing in the line-wing. The resultant scattering is coherent in

the atomic rest frame and the atoms are nearly at rest in the frame of

the observer. Hence the scattering is nearly coherent in the laboratory

frame as well. In summary, there is Doppler redistribution and strong

noncoherence in the line-core. In the line wing the scattering is nearly

coherent. This particular case describes scattering by a resonance line

that is broadened by radiation damping. The function R_{II} is assumed to

be either a delta function or a combination of CRD and a delta

function. The redistribution functions $R_{II}(\nu, \nu')$ and $R_{III}(\nu, \nu')$ are

given in a tabulated form by Basri (1979) out to five Doppler widths,

in intervals of 0.2 Doppler widths across the Voigt profile at each

depth point. Beyond five Doppler widths of line center (i.e.,

arbitrarily far out into the line wings) analytical expressions are

available for R_{III} (Adams, Hummer, and Rybicki 1971). Evaluation of R_{II}

follows from the coherent nature of the scattering in the line wings and

the subsequent Doppler redistribution. Hnce the maximum of R_{II} is at $\Delta\nu'$ for each $\Delta\nu'$ in the wings. Furthermore the principal contribution to the function is within three Doppler widths of the particular $\Delta\nu'$. The PRD functions are delta functions convolved with a Maxwellian velocity distribution. The coupled equations of statistical equilibrium and radiative transfer are again solved by utilizing the complete linearization technique described in Chapter 3. The partial redistribution modifications involve splitting the upper state into substates, one for each frequency point in the line and solving the radiative transfer and statistical equilibrium for each substate to obtain the correct emission profile. The resulting frequency <u>dependent</u> line source function in the PRD approximation can be written as (Mihalas 1978)

$$S_\ell(\nu) = (1-\epsilon)\phi_\nu^{-1} \int R(\nu', \nu)\, J_\nu'\, d\nu' + \epsilon B_\nu, \qquad (4.4)$$

where $\epsilon \equiv \epsilon'(1+\epsilon)$ and ϵ' is basically a ratio of the collisional to the radiative rate. By contrast, the frequency <u>independent</u> line source function in the CRD approximation can be written as (Mihalas 1978)

$$S_\ell^{CRD} = (1-\epsilon) \int \phi_\nu J_\nu d\nu + \epsilon B_\nu. \qquad (4.5)$$

I use the populations and the mean intensities obtained from the complete redistribution solution to begin the partial redistribution calculation. In the PRD refinement of the CRD solution I use a two-level representation of Ca II, explicitly calculating the K-line profile. This approach is used in the interest of simplicity and numerical tractability. The code has been modified to account for the presence of the Ca II metastable states by including a fixed percentage (~6%) of

complete redistribution to mimic the fraction of noncoherence attributable to the infrared triplet (Ayres and Linsky 1975). This approximation is found by Ayres and Linsky to be in excellent agreement with the numerically more elaborate five-level calculations by Shine et al. (1975a) and Gingerich et al. (1971) for a solar model. I note, parenthetically, that an incoherence rate of ~3% is applicable in the case of supergiant chromospheres for which the infrared triplet lines are optically thin (Basri 1979). In summary, the diffusion of photons to the line wings is limited by the fact that Doppler shifting is produced by a Maxwellian velocity distribution and very little shifting occurs beyond approximately three Doppler widths (Jefferies 1968). The CRD approximation ignores this fact and allows photons to diffuse arbitrarily far into the line wings. Hence the line thermalizes when continuum thermalization begins to dominate in the far line wings (Basri 1979). The PRD treatment takes into account the coherent scattering in the line wings. The resultant PRD line source function thermalizes to the Planck function sooner than the CRD source function. This is due to the coherent nature of the scattering process in the line-wings which actually inhibits photon escape from the line-core. Thus the line core thermalizes more rapidly because the net escape probability for core photons to the line wings is reduced (Mihalas 1978).

The resulting frequency-dependent source function in the line-wings is substantially below the corresponding CRD source function since core photons cannot diffuse into the wings as efficiently (Milkey and Mihalas 1973).

Summary of Radiative Transfer Calculation

The procedure for calculating a semi-empirical model chromosphere based upon the Ca II K-line has been outlined in detail in Chapter 3 and in the previous sections of this chapter. In summary, I specify an input thermal structure (representing the chromosphere) as a run of temperature, T_e, with mass column density, m, and microturbulent velocity, ξ_t. I adjoin this thermal structure to a suitable M dwarf photospheric model given by Mould (1976). I then solve a multilevel CRD hydrogen problem to obtain the electron density and non-LTE hydrogen level populations at each depth. Once the fully self-consistent ionization balanced model atmosphere is obtained, I proceed to the multilevel CRD Ca II computation. The resulting non-LTE level populations for Ca II are then used as the input for the two-level PRD refinement of the CRD calculation. The PRD computation yields a theoretical K-line profile which I then convolve with the instrumental profile. I represent the instrumental profile by a Gaussian with a FWHM equal to the instrumental resolution. The actual convolution is accomplished with the Cooley-Tukey Fast Fourier Transform (FFT) routine for an arbitrary number of data points. I compare the resulting line profile to the observed profile and, if necessary, adjust the chromospheric thermal structure until the best possible agreement between the theoretical profile and the observations is achieved. Finally I repeat the aforementioned steps to obtain a fully self-consistent model atmosphere. I will now describe the results of this semi-empirical approach for a sample of dMe and dM stars.

<u>Results</u>

I adjoin a chromospheric temperature rise, $T_e(m)$, $\xi_t(m)$, to an M dwarf photospheric model given by Mould (1976). The model photospheres constructed by Mould (1976) represent a limited range in gravity (log g = 4.75 and log g = 5.75) and they have coarse resolution in effective temperature for the range of T_{eff} values considered (3000K to 4250K in increments of 250K). The two dM and three dMe stars I discuss in this section are single stars. Hence reliable measurements of the surface gravity for each star are unavailable. I obtain estimates of the surface gravity for each star from estimates of the stellar radii and masses. The radii are inferred from the angular diameter relations of Barnes and Evans (1976) and the distances based upon the parallaxes given by Gliese (1969). I estimate the masses by interpolating along the main sequence among the evolutionary tracks of Iben (1965) and Hayashi (1966) or taken from Allen (1976). I find that the log g = 4.75 photospheric models of Mould (1976) are more compatible with the surface gravity estimates for the stars in this investigation than are the log g = 5.75 photospheric models. The observational results given in Chapter 2 (see Figure 18) suggest that the chromospheric scaling laws developed by Ayres (1979) may be applicable to the M dwarf stars. These laws predict that the Ca II line widths, $\Delta\lambda_{K_1}$ and $\Delta\lambda_{K_2}$, and the mass column density at the temperature minimum, m_{min}, are only weakly dependent upon stellar gravity. In particular, Ayres (1979) finds that $\Delta\lambda_{K_1} \sim g^{-1/4}$. and $\Delta\lambda_{K_2} \sim g^{-1/4}$ and $m_{min} \sim g^{-1/2}$. Therefore I conclude that discrepancies between the adopted model stellar gravity and the actual stellar gravity are unimportant for this study. The inferred

T_{eff} values (Chapter 2, Table 4) for the dMe and dM stars discussed in this chapter are similar to the T_{eff} values for the adopted model photospheres. The differences are minor especially in view of the insignificant radiative equilibrium contribution to the total Ca II K-line flux (Chapter 2). The stars for which I present model chromospheres, their spectral types, and the adopted photospheric models (Mould 1976) are listed in order of decreasing R_{HK} value (Chapter 2) in Table 9. Rather than using the electron densities tabulated by Mould (1976), I re-solve for the photospheric structure in order to obtain a fully self-consistent model atmosphere. The computed photospheric electron densities differ from the tabulated values at given T_e, m, and P_g by less than 2%.

Table 9. Adopted Photospheric Models

Star	Sp Type	R_{HK}	T_{eff}	Log g
EQ Vir	dK5e	8.8(-5)	4250	4.75
GL 616.2	dM1.5e	3.2(-5)	3500	4.75
YZ CMi	dM4.5e	2.7(-5)	3250	4.75
GL 393	dM2	0.54(-5)	3500	4.75
GL 411	dM2	0.14(-5)	3500	4.75

The location of the temperature minimum is considered the boundary between the upper stellar photosphere and the stellar chromosphere thus dividing the stellar atmosphere into two distinct temperature regimes. More specifically,

$$dT/dh < 0, \quad m > m_{min}, \tag{4.6}$$

$$dT/dh > 0, \quad m < m_{min}. \tag{4.7}$$

The temperature distribution in a grey atmosphere will monotonically decrease outward to a limiting value $T_o/T_{eff} = 0.811$ (Mihalas 1978) if photospheric radiation dominates the local heating. However, if additional sources of heating are present, such as the dissipation of mechanical energy (nonradiative heating), then a temperature inversion may occur at a critical height m_{min}. In particular, if the nonradiative heating does not decrease outward at a rate proportional to m or faster then this additional heating will become comparable to the heating by photospheric radiation (Ayres 1979). As a result the radiative losses can no longer balance the nonradiative heating. Hence the temperature rises. This is the physical basis for the existence of a temperature minimum region followed by a chromospheric temperature rise. The relationship between an assumed mechanical energy flux, a radiative equilibrium temperature structure, and a chromospheric temperature rise is depicted schematically in Figure 23. I determine the location of the temperature minimum, m_{min}, by adjusting the thermal structure in m at an adopted constant value of T_{min} ($T_{min} > T_R(K_1)$; Chapter 2) until the base of the emission width of the theoretical profile agrees with that of the observed profile.
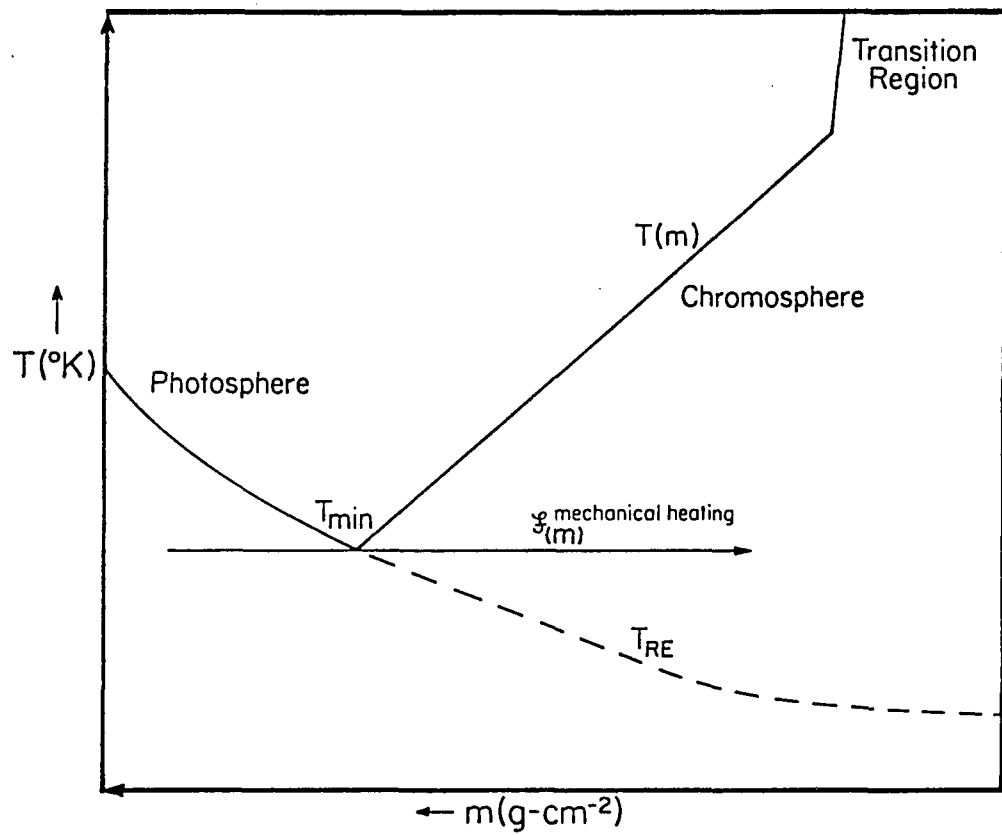
Figure 23. Schematic stellar atmosphere including non-radiative heating.

I identify the region between m_{min} and the transition region ($T_o \simeq$ 9000K) as the stellar <u>chromosphere</u>. This region is characterized by a temperature inversion and a radiative cooling function dominated by collisional excitation of effectively thin, strong resonance and subordinate lines such as Ca II H and K, Mg II h and k, and Hα. At low temperatures (T < 5000K) the electrons are produced by first ionizations of abundant metals while at high temperatures (T > 5000K) the electrons are provided by partial ionization of hydrogen (Ayres 1979). I adopt a model chromospheric structure which consists of two linear segments about an inflection point. The base of the chromosphere is located at (m_{min}, T_{min}) and the top of the chromosphere (or the base of the transition region) is located at (m_o, T_o = 9000K). The inflection point is located at $m_6 \equiv m|_{T\ =\ 6000K}$. The upper chromospheric (T > 6000K) temperature gradient is steeper than the lower chromospheric (T < 6000K) temperature gradient in the model chromospheres considered here. I divide the chromosphere into two linear segments because I find that the K_2 flux is very sensitive to the location of m_6 while it is insensitive to the thermal structure above m_6. Furthermore I do not possess the requisite data to develop accurate models of the thermal structure above m_6. Hence adjustment of the thermal model in order to obtain agreement between the theoretical and observed K-line profiles proceeds through adjustment of the lower chromospheric temperature gradient. Kelch et al. (1978) and Kelch (1978) find a similar approach necessary to calculate semi-empirical chromospheric models based upon the Ca II K line. I simulate the beginning of a transition region by including a rapid temperature increase above m_o to 20,000K. At the depth point

corresponding to T_o = 9000K, a steep temperature rise in a stellar chromosphere is expected because the Lyman continuum is no longer an efficient radiator above this temperature (Thomas and Athay 1961). However, according to Ayres (1979), the origin of the thermal instability is that the principal source of electrons, neutral hydrogen, becomes severely depleted by ionization. In addition, the atoms and ions which provide radiative cooling (Hα, Mg II h and k, Ca II H and K, etc.) have ionization potentials comparable to that of hydrogen (Allen 1976). Hence they also ionize when hydrogen becomes ionized. As a result n_e = $n_p \simeq n_H$ and the electron pressure becomes subject to the constraint of hydrostatic equilibrium. Thus n_e decreases with decreasing mass column density m. Now if the nonradiative heating decreases outward more slowly than m (i.e., d F_{mech}/dh$|_h$ < dm/dh = $\rho(h)$) then the chromospheric plasma becomes thermally unstable at a height m_o, where T $\gtrsim$ 9000K. This is the physical basis for the existence of a transition region (Ayres 1979). A new thermal equilibrium is achieved near coronal temperatures where heat conduction and stellar wind losses begin to dominate the plasma energy balance (Ayres 1979). As expected, I find that the calculated K-line flux and profile is insensitive to the transition region thermal structure. This is, of course, due to the fact that Ca II is completely ionized at these temperatures. After specifying a thermal structure, T_e (m), ξ_t(m), in terms of the aforementioned inflection points, a linear interpolation in log m is made between each of these points with the desired grid spacing. The result is a model atmosphere consisting of linear segments within each of which dT/d log m and d ξ_t/d log m are constant.

I illustrate in Figures 24-38 the (1) inferred semi-empirical stellar model chromosphere, (2) the emergent theoretical K-line profile, and (3) the theoretical profile convolved with the instrumental profile, and the observed profile for each of the five stars listed in Table 9. A rotation measure of V sin i $\simeq$ 10 km s^{-1} is given by Smith (1980) for the dK5e star EQ Vir. I therefore convolve the theoretical profile computed for EQ Vir with a rotational profile. The rotational profile is (Gray 1976)

$$G(\Delta\lambda) = \frac{2(1-\epsilon)[1-(\Delta\lambda/\Delta\lambda_L)^2]^{1/2} + 1/2\pi\epsilon[1-(\Delta\lambda/\Delta\lambda_L)^2]}{\pi\Delta\lambda_L(1-\epsilon/3)} \qquad (4.8)$$

where $\Delta\lambda_L = (\lambda \text{ V sin i})/c$ and ϵ is a constant for an assumed limb darkening law (for which ϵ < 1). I neglect limb darkening in the K-line ($\epsilon \equiv 0$) since (1) the limb darkening is small (which is also true for the solar K-line; Zirin 1966) and (2) uncertainties in ϵ numerically mimic uncertainties in V sin i. Since the observed K-line profiles are symmetric I show only one-half of the observed and theoretical line profiles in Figures 24-38. The model properties of dM and dMe stellar chromospheres are summarized in Table 10 and a more detailed tabulation of the model chromospheres is given in Appendix A.

I note that the K_1 feature is not readily apparent in either the observed or theoretical K-line profiles. This may be a result of the shallow temperature gradient in the upper photosphere and temperature minimum region, as seen in Figures 24-38. In addition, the computed line wings are brighter than the observed K-line wings for the stars in the sample considered here. The adoption of a photospheric model with a value of T_{eff} higher than the actual effective temperature of the star

Figure 24.   Model chromosphere: EQ Vir.

Figure 25.   Theoretical K-line profile: EQ Vir.

Figure 26. The observed K-line profile and the theoretical K-line profile convolved with both the instrumental profile and a rotational profile: EQ Vir.
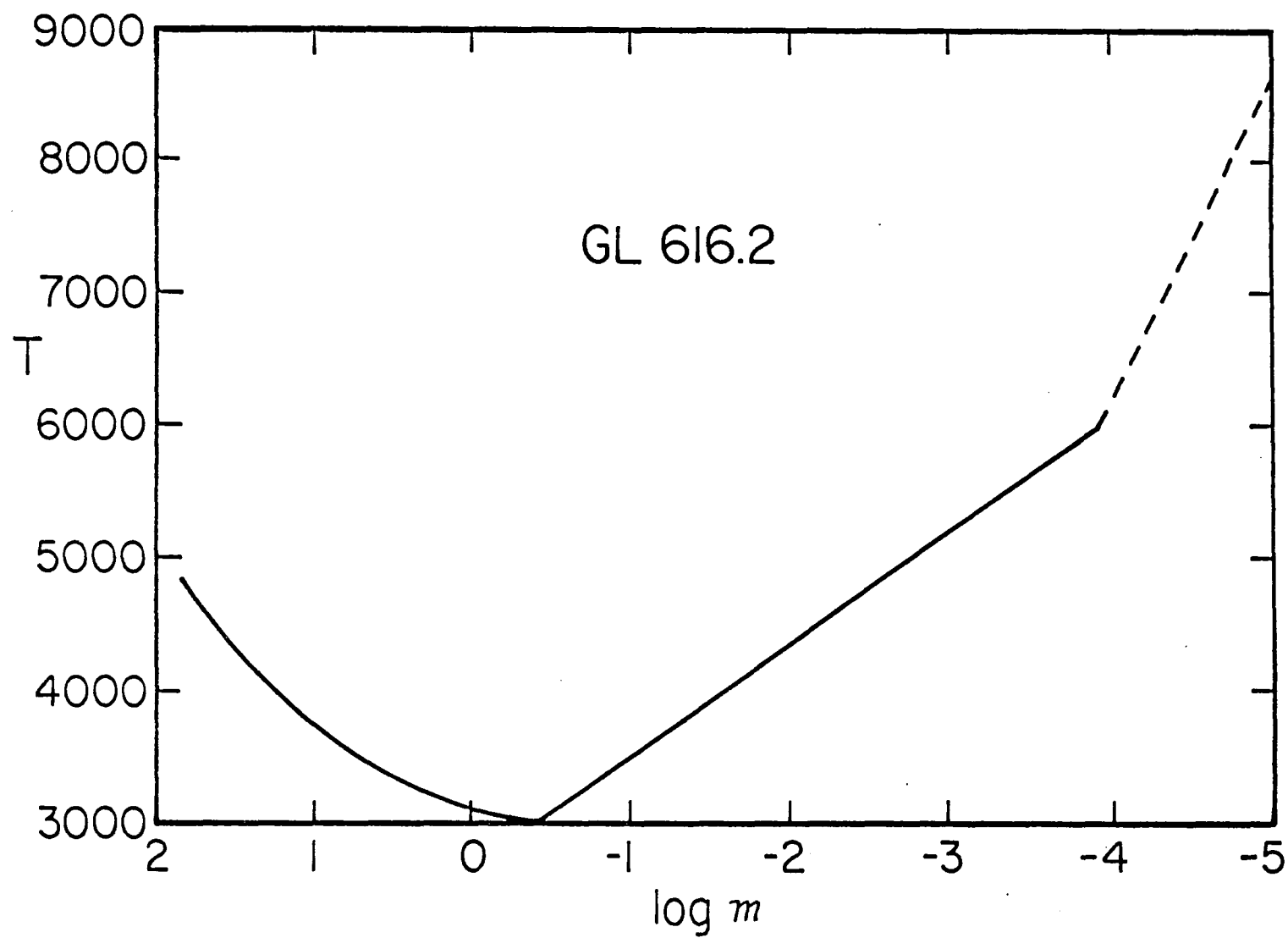
Figure 27.   Model chromosphere: GL 616.2.
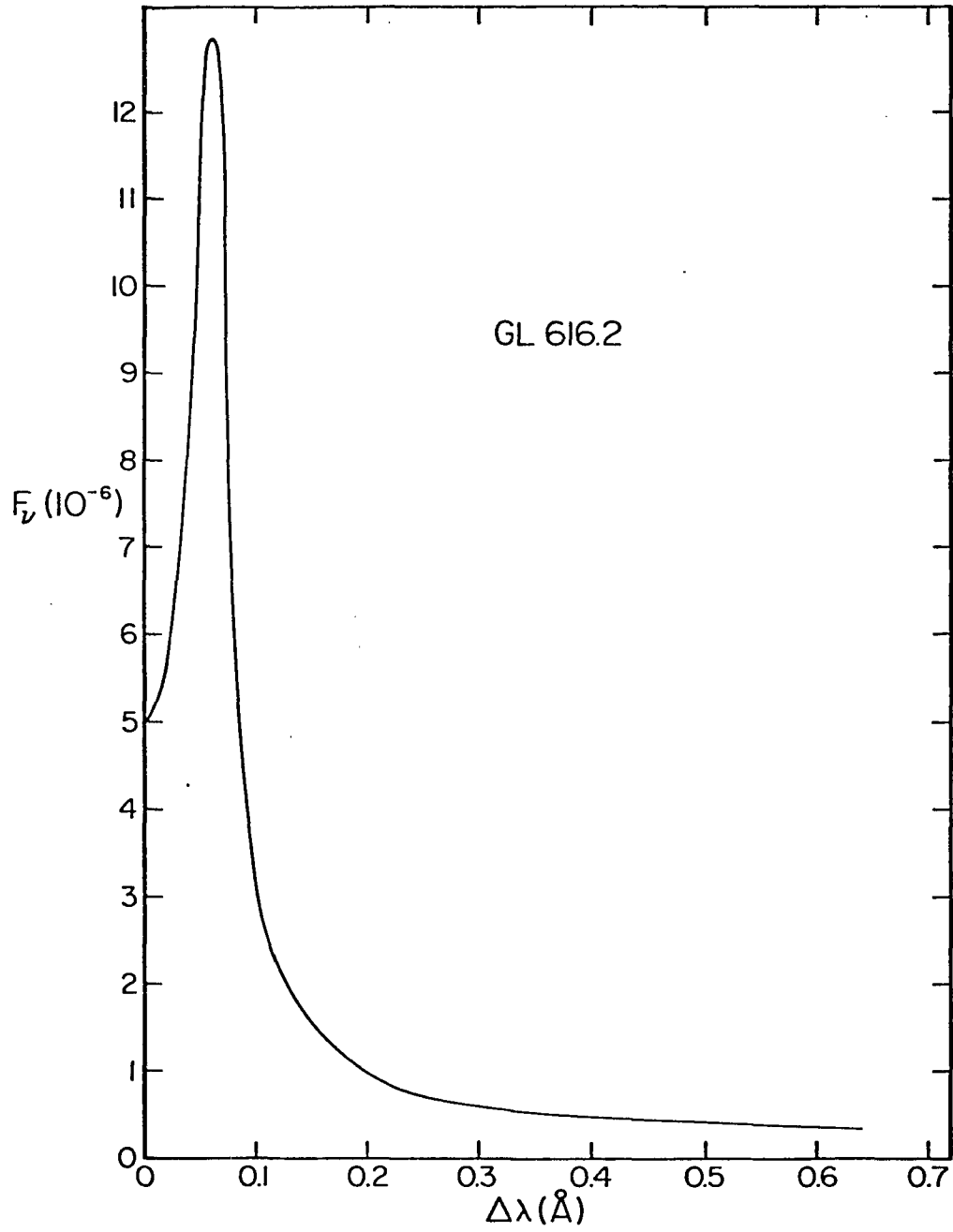
Figure 28.   Theoretical K-line profile: GL 616.2.
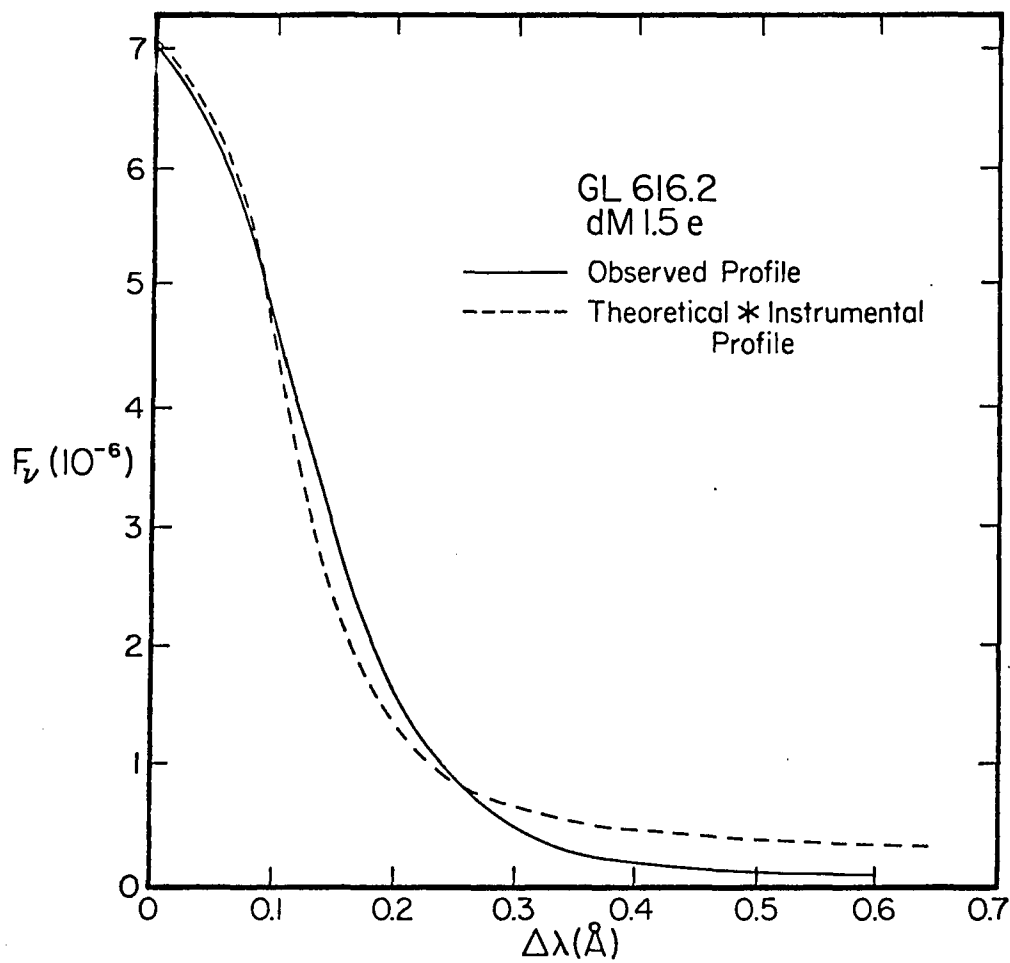
Figure 29. The observed K-line profile and the theoretical K-line
profile convolved with the instrumental profile: GL 616.2.
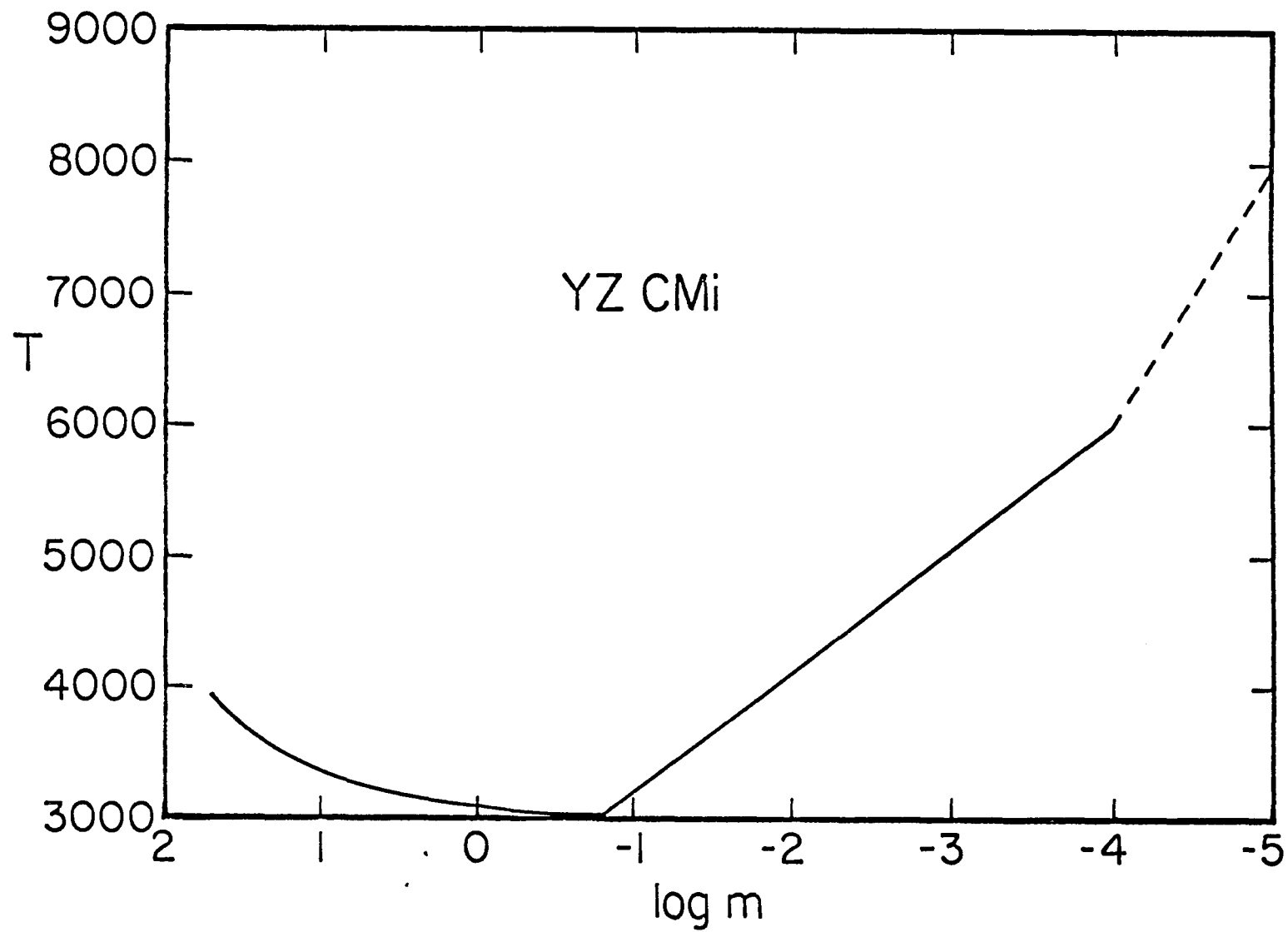
Figure 30. Model chromosphere: YZ CMi.
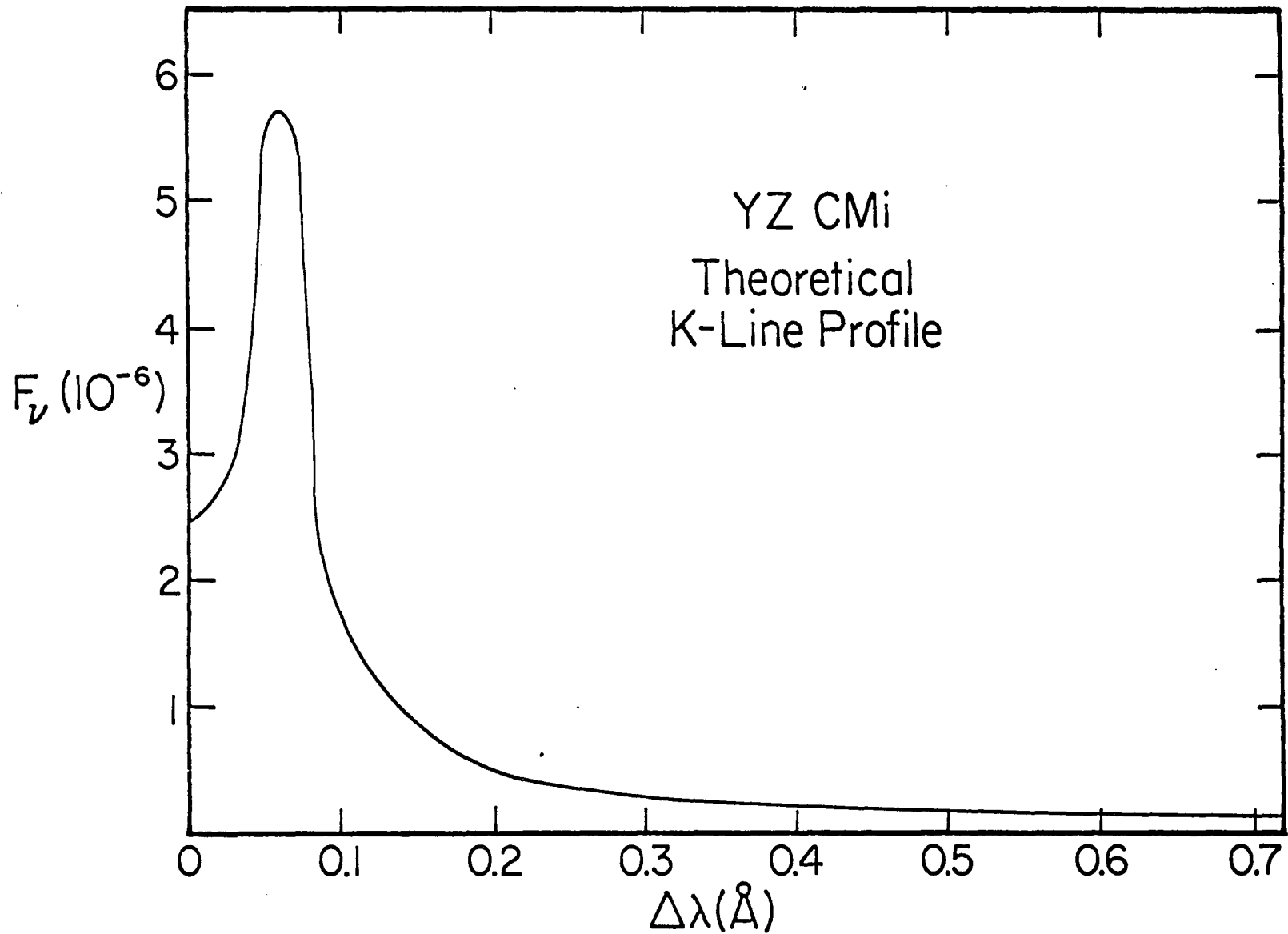
Figure 31. Theoretical K-line profile; YZ CMi.
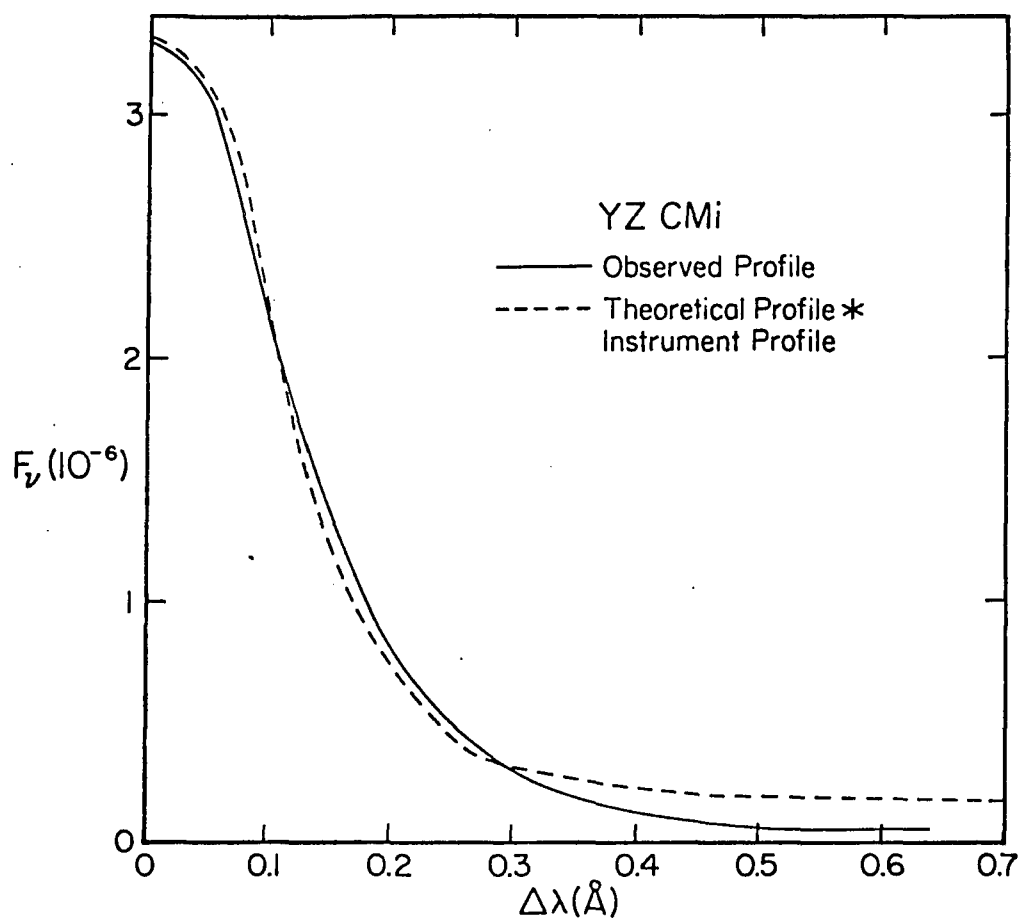
Figure 32. The observed K-line profile and the theoretical K-line
profile convolved with the instrumental profile: YZ CMi.
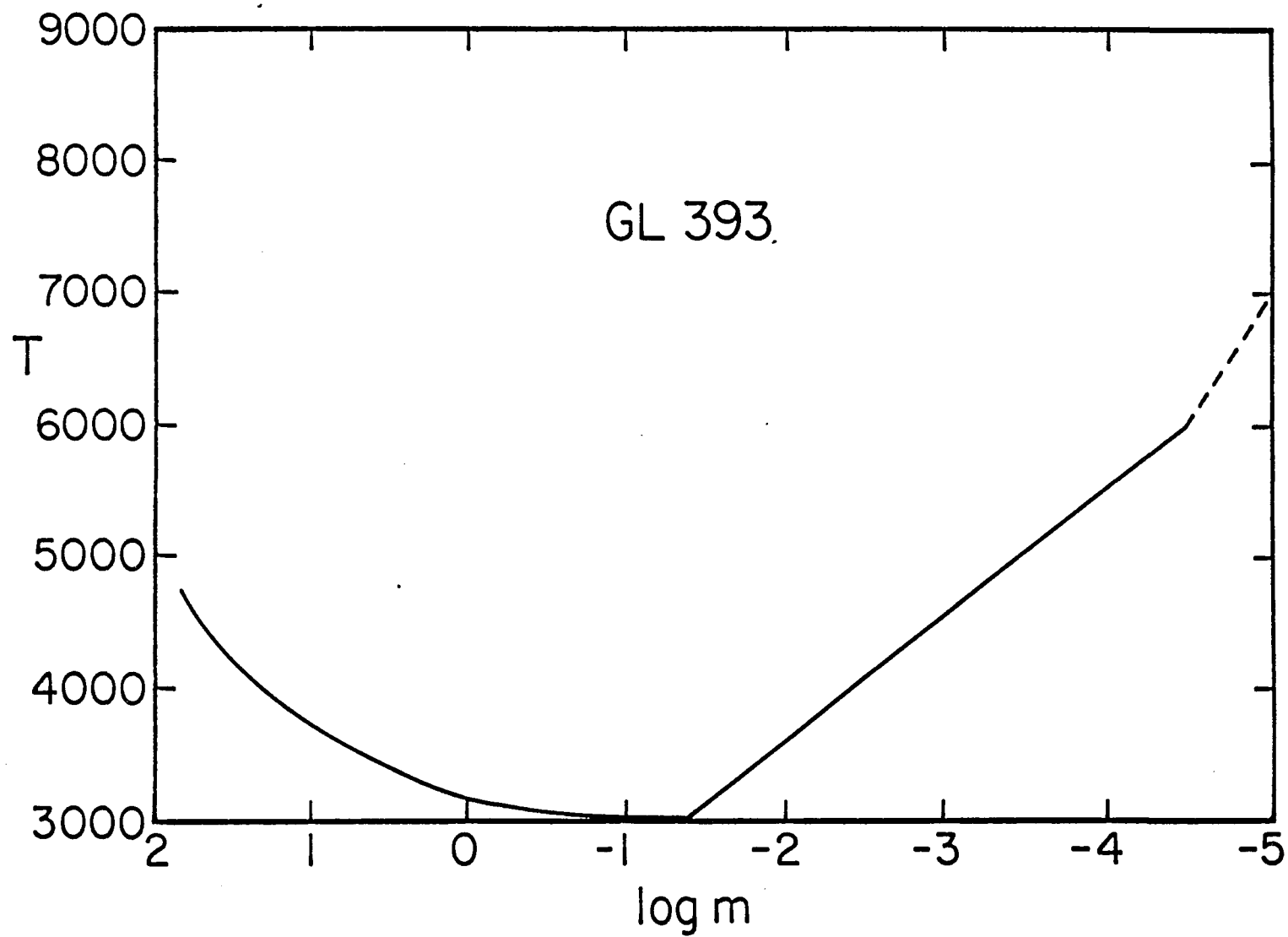
Figure 33. Model chromosphere: GL 393.
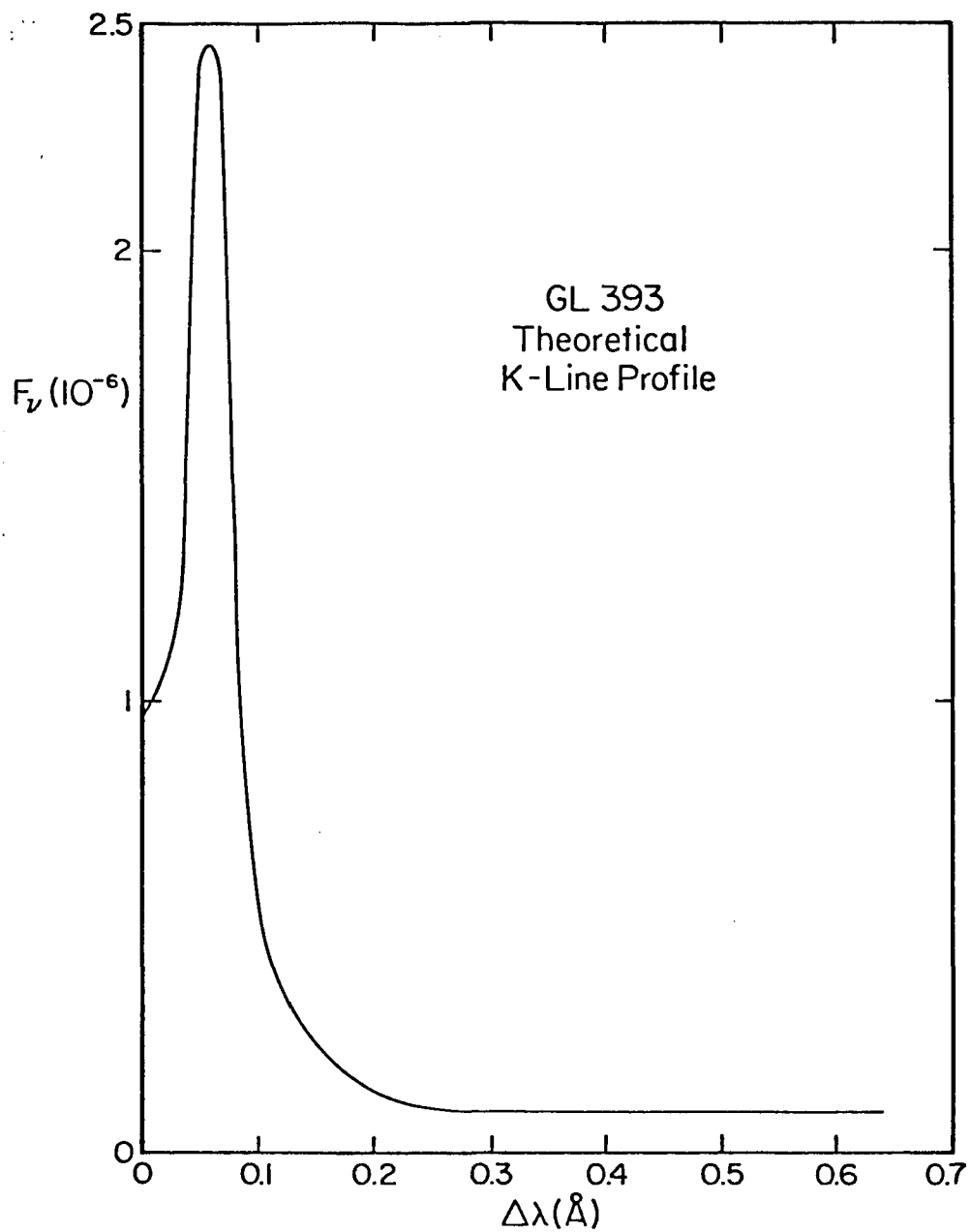
Figure 34. Theoretical K-line profile: GL 393.
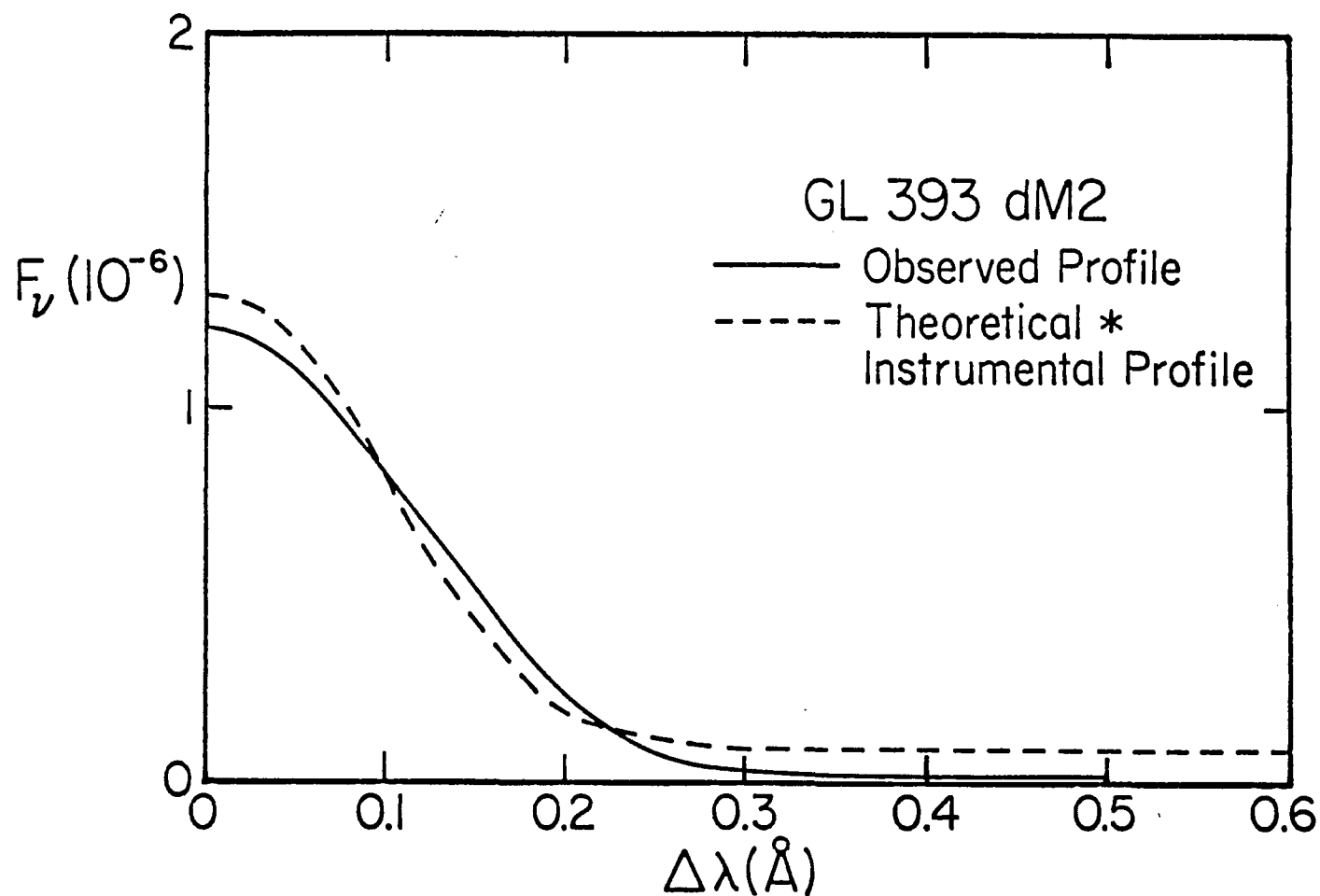
Figure 35. The observed K-line profile and the theoretical K-line profile convolved with the instrumental profile: GL 393.
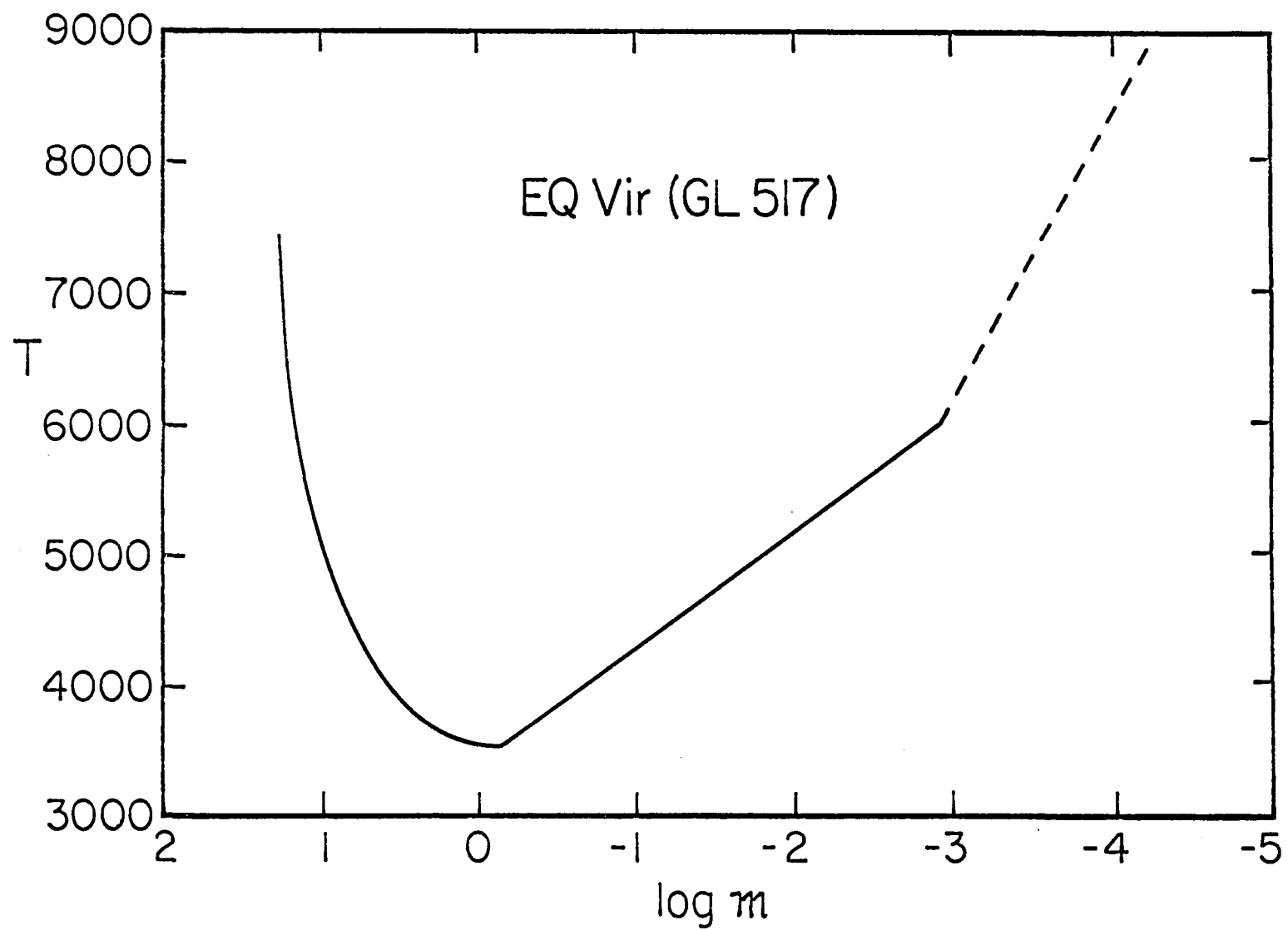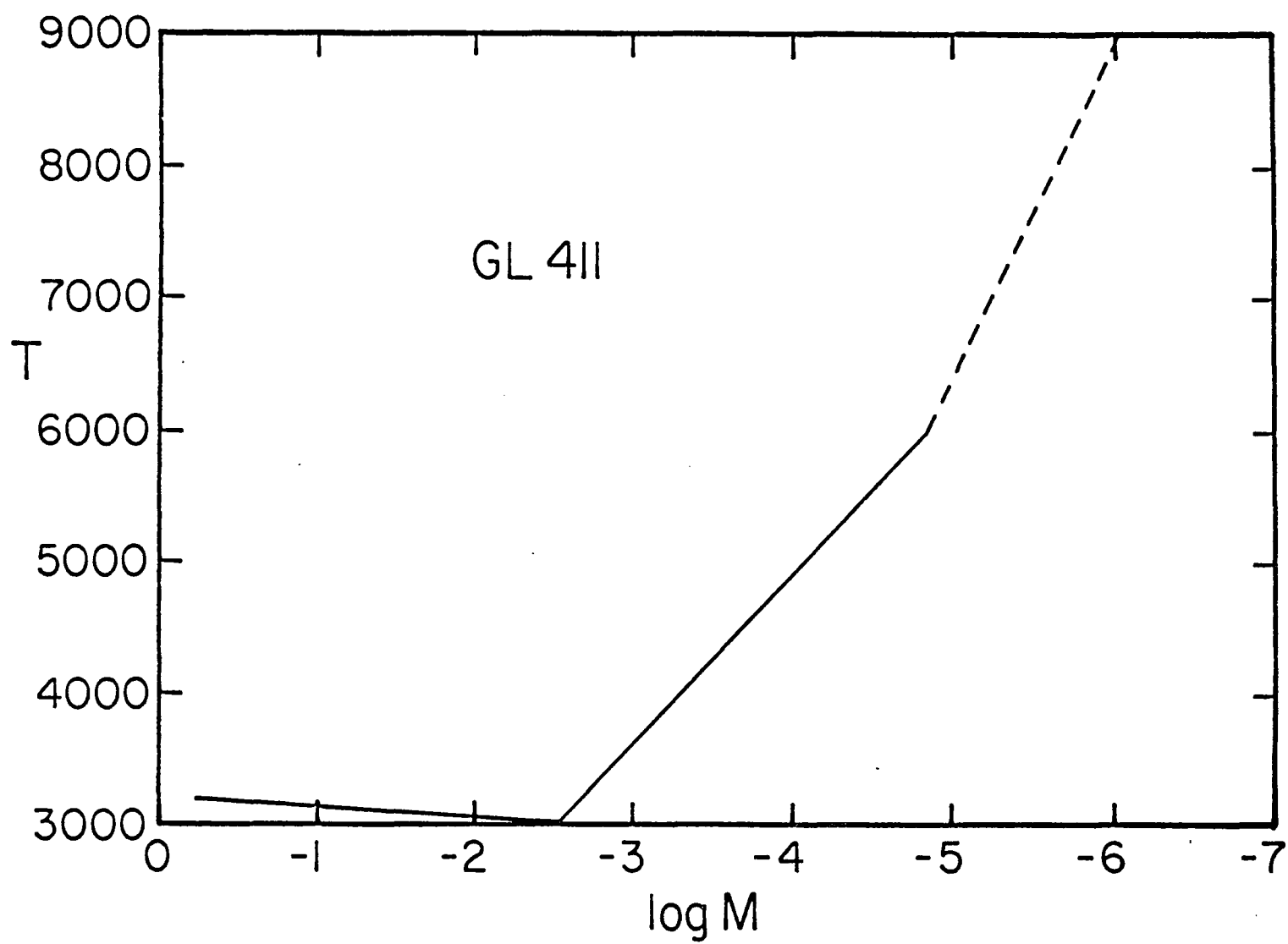
Figure 36.   Model chromosphere: GL 411.
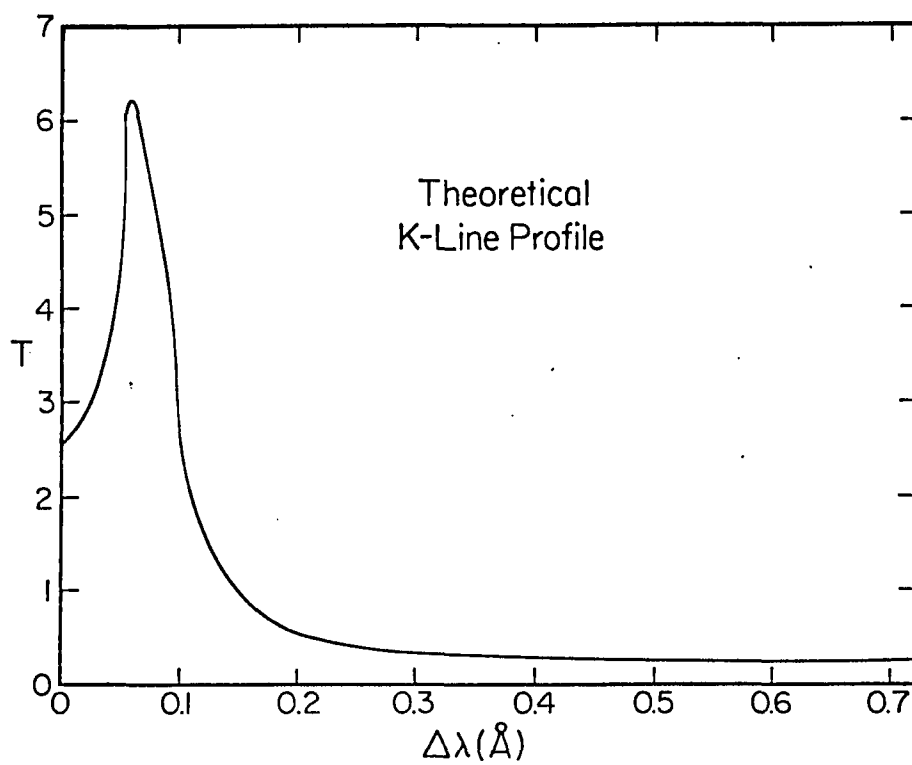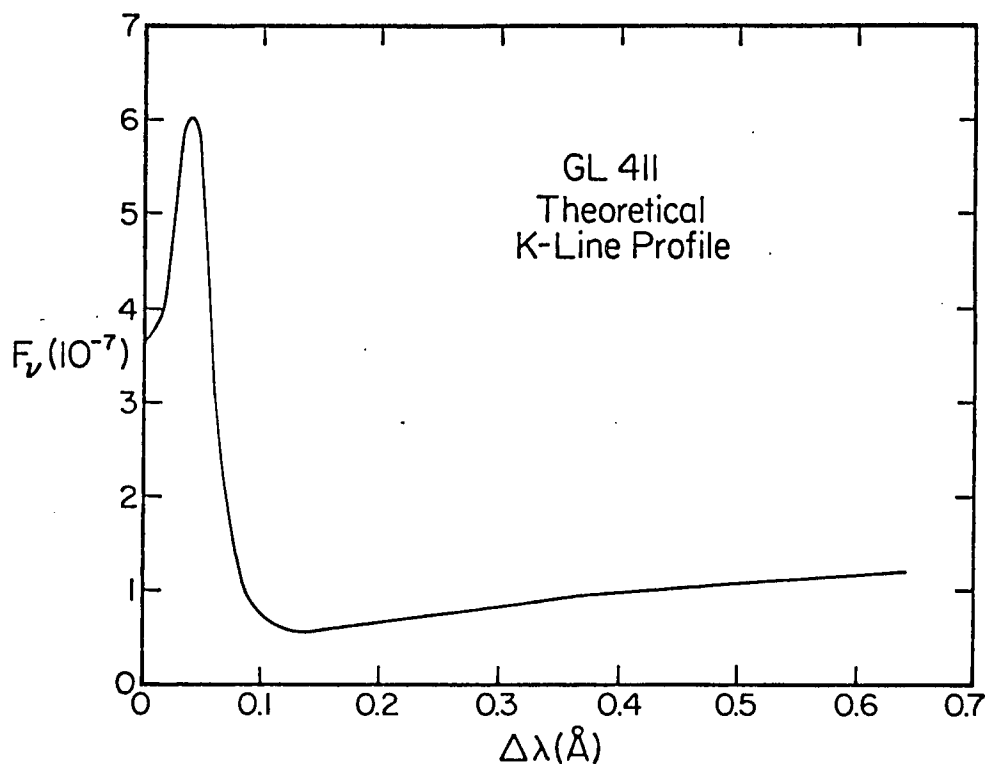
Figure 37. Theoretical K-line profile: GL 411.
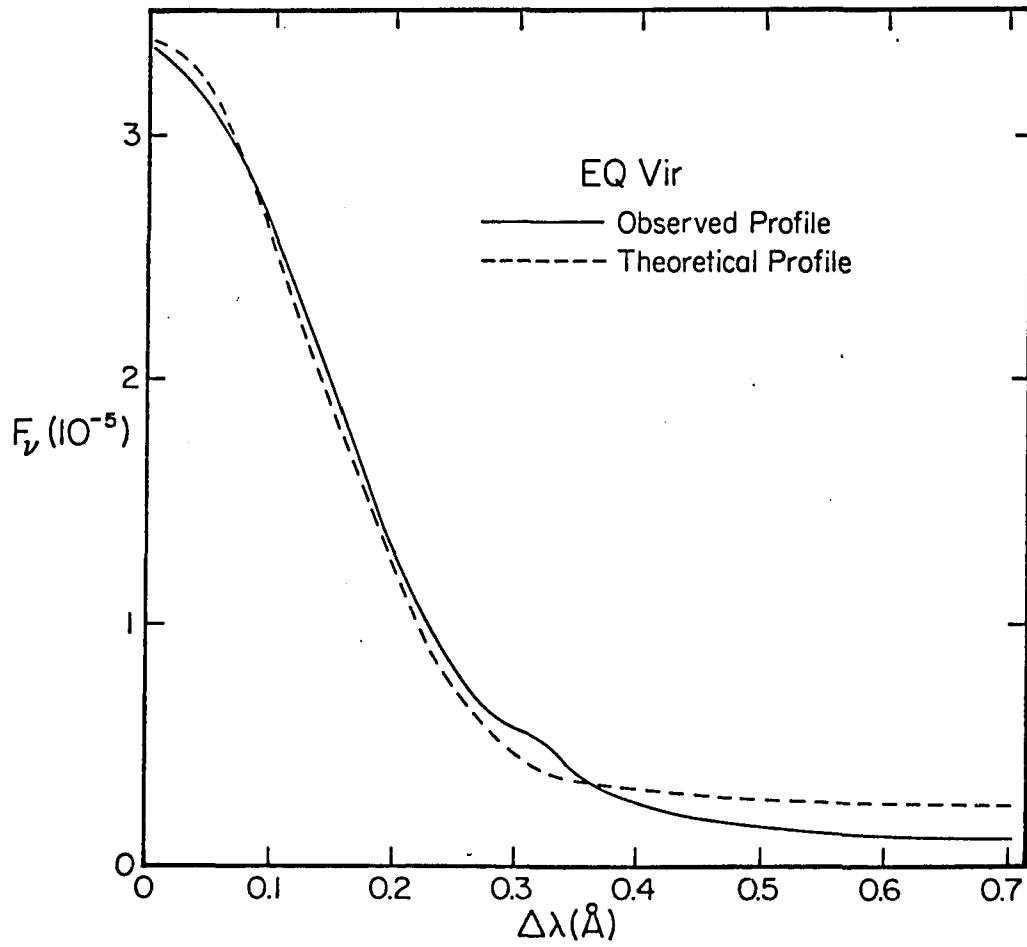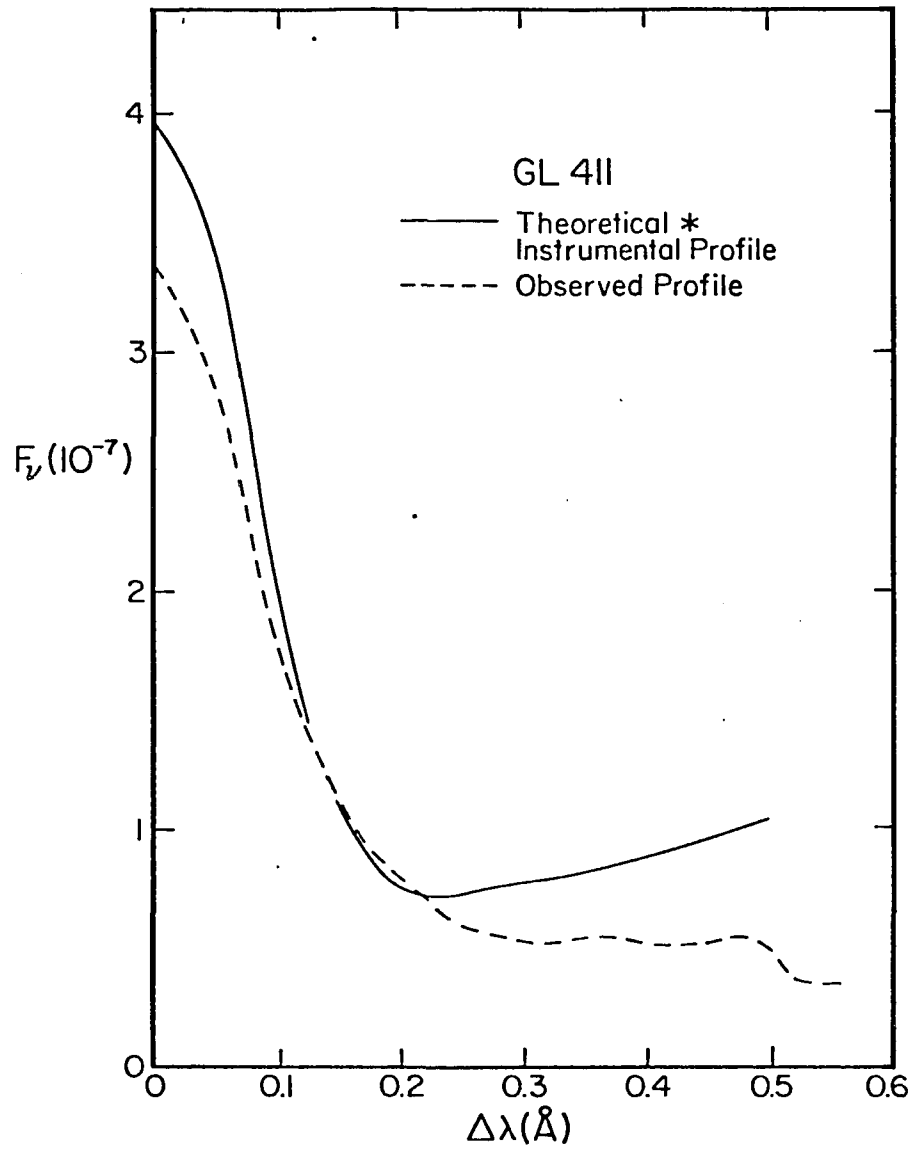
Figure 38. The observed K-line profile and the theoretical K-line profile convolved with the instrumental profile: GL 411.

Table 10. Model Properties for dMe and dM Stellar Chromospheres.

Star	T_{min}/T_{eff} [a]	m_{min} [b]	m_6 [b]	m_0 [b]	m_{20} [b]	log n_e (6000K)	log n_e (9000K)	ξ_o [c]
EQ Vir	0.82 (0.80)	7.00(-1)	125(-5)	50.0(-6)	32.0(-7)	11.8	12.0	2
GL 616.2	0.86 (0.86)	3.50(-1)	12.8(-5)	7.50(-6)	8.00(-7)	11.3	11.2	2
YZ CMi	0.94 (0.97)	1.55(-1)	9.75(-5)	3.16(-6)	3.20(-7)	11.2	10.9	2
GL 393	0.88 (0.88)	0.45(-1)	3.25(-5)	1.00(-6)	1.00(-7)	10.9	10.4	2
GL 411	0.88(0.88)	0.03(-1)	1.50(-5)	1.00(-6)	0.10(-7)	10.8	10.3	0.1

[a]The second number in parentheses is the ratio of T_{min} to the <u>actual</u> effective temperature. The preceding number is with respect to the <u>model</u> value of T_{eff}.

[b]Units: $g-cm^{-2}$.

[c]Microturbulent velocity in $km-s^{-1}$ at T = 9000K.

would overpredict the K-line wing intensities. However, the consistent appearance of the discrepancy between the observed and computed line wings implies another underlying physical cause. In particular, the M dwarf model photospheres given by Mould (1976), upon which I base the model chromospheres, do not include CO opacity, despite the fact that this may be the dominant source of opacity in the upper photospheres of cool dwarfs (Johnson 1973). I therefore conclude that more accurate M dwarf photospheric models which include the opacity due to CO will be required to resolve the discrepancy between the observed and theoretical K-line wing intensities. An additional feature exhibited by the theoretical emission profiles is a central reversal. The central reversal is a consequence of the non-LTE effect of the optical boundary through which line photons eventually escape (Jefferies and Thomas 1958). The central reversal is absent in the observed profiles. I conclude from the theoretical profiles, and the figures which show the result of the convolution of the theoretical profiles with the instrumental profile, that the instrumental resolution is insufficient to detect any central reversal in the observed Ca II K-line profiles (see also Chapters 2 and 7).

An inspection of the model chromospheric properties listed in Table 10 reveals a number of systematic trends. The value of the ratio T_{min}/T_{eff} is high for the dMe and dM stars in this sample as compared to other active chromosphere dwarfs (Chapter 2; Figure 17) and giants (Linsky et al. 1979). This is the result of the shallow temperature gradient exhibited by the thermal models in the upper photosphere-temperature minimum region. Interestingly, Kelch et al. (1979) conclude

that a high T_{min}/T_{eff} ratio is indicative of unusually high nonradiative heating in the upper photosphere of a star. I therefore conclude that the dissipation of mechanical energy is an important parameter in the control of the energy balance in the upper photospheres of M dwarf stars. The next four columns of Table 10 show the mass column densities at the temperature minimum, m_{min}; m_6 $(m|_{T=6000K})$; m_0 $(m|_{T=9000K})$; and m_{20} $(m|_{T=20,000K})$. The value of m_{min} clearly decreases (the temperature minimum moves outward) as R_{HK} decreases. Moreover, the value of the mass column density at the other inflection points declines as the importance of nonradiative heating decreases in the atmospheres of the M dwarf stars considered in this investigation. Since the computed K-line flux is most sensitive to the lower chromospheric temperature structure, I list the values of the temperature gradient in this region in Table 11. The similar values of dT/d log m among the stars considered here lead to the following important conclusion: the chromo-spheric K-line emission strength is most sensitive to the total amount of chromospheric material within the approximate temperature range T_{min} - 6000K. Thus increased emission strength is not simply due to an increased temperature gradient. Furthermore, the rise in T_e over the region in which the K-line emission core is formed is non-trivial regardless of the emission flux. These results are similar to the conclusion reached by Cram and Mullan (1979) who find that Balmer-line emission strength in nonspecific model M dwarf chromospheres is sensitive to the total amount of material in the temperature range $5500 \leq T_e \leq 50,000K$. The results I find, however, differ from the conclusion reached by Kelch (1978) and Kelch et al. (1979). These investigators find

Table 11. Lower Chromospheric Temperature Gradient

Star	dT/d log m
EQ Vir	−9.1(2)
GL 616.2	−8.7(2)
YZ CMi	−9.4(2)
GL 393	−9.6(2)
GL 411	−13 (2)

that the degree of chromospheric line emission is correlated with the

lower chromospheric temperature gradient, with the "active chromo-

sphere" stars having steeper chromospheric temperature gradients than

the "quiet chromosphere" stars. The range in spectral type studied by

Kelch et al. (1979) is FOV - MOV. Of course, I confine this investiga-

tion to a much narrower range in effective temperature, namely, K5V -

M4.5V. Nevertheless, I do not consider the disagreement between the

results I find and those given by Kelch et al. (1979) to be a serious

discrepancy. For example, a steep temperature gradient essentially

places more chromospheric material within a given temperature range

thus leading to enhanced chromospheric line emission. However, the

parameterization of stellar chromospheres according to temperature

gradient is beset by problems of uniqueness since a variety of tempera-

ture gradients can yield the same chromospheric emission line flux. I

avoid this difficulty through the specification of stellar chromo-

spheric models solely according to the chromospheric mass density

(within a temperature regime) required to yield the observed chromospheric emission line flux.

Linsky and Avrett (1970) propose a microturbulent velocity model for the solar chromosphere which consists of ξ_t = constant = 2 km-s^{-1} in the solar photosphere, and ξ_t increasing linearly in log m from ξ_t = 2 km-s^{-1} at T_{min} to $\xi_t = \xi_0 \approx$ 10 km-s^{-1} at T_6 in the chromosphere. Moreover, Kelch et al. (1978) report that this microvelocity model was found to fit best the Ca II resonance-line profiles of α CMi and α Cen A. However, I find that a solar-like microturbulent velocity distribution fails to reproduce the observed Ca II K-line profiles in this sample of dMe and dM stars (see Figure 39). Instead I find that a microturbulent velocity model with ξ_t = 1 km-s^{-1} in the stellar photosphere, and ξ_t increasing linearly in log m from ξ_t = 1 km-s^{-1} to ξ_0 = 2 km-s^{-1} in the chromosphere is the most appropriate microvelocity model. I therefore conclude that the microturbulent velocities in the chromospheres of M dwarf stars are small as compared to solar-like chromospheric micro-velocity fields. Furthermore, I suggest that chromospheric mass motions are inhibited by magnetic fields which pervade the stellar chromosphere and therefore lead to small microturbulent velocities. This suggestion is corroborated by Shaviv (1980). This investigator finds that in order to obtain a convergent interior model for the dM4.5e star, Kruger 60B (M/M_0 = 0.15; Mullan 1976), he must use a very small value of ℓ/H_p, where ℓ is the mixing-length and H_p is the pressure scale height. Shaviv (1980) also hypothesizes that strong interior magnetic fields inhibit convective mass motions, which in turn lead to the small ℓ/H_p value he finds for interior models of Kruger 60B. Finally, I suggest
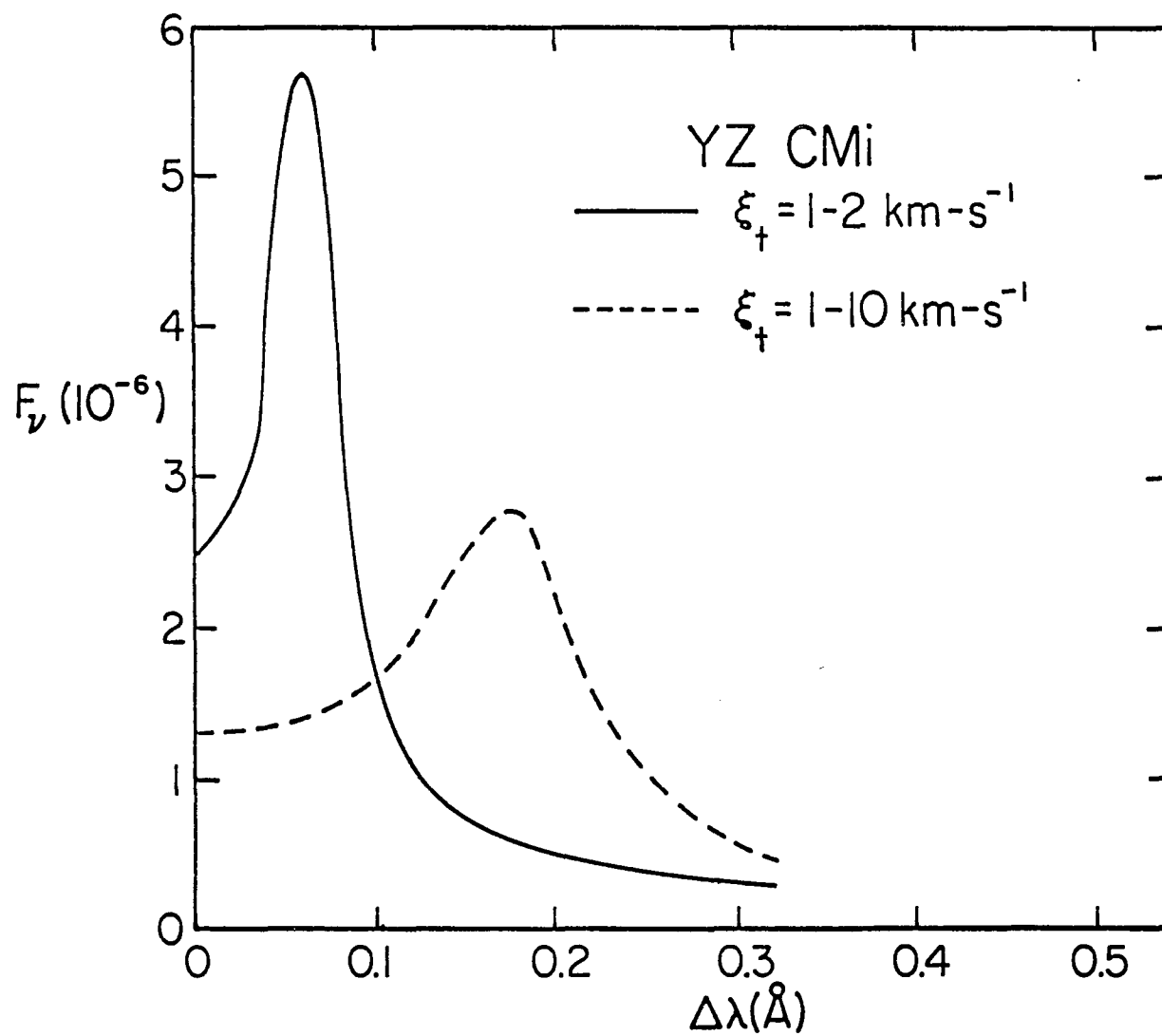
Figure 39.   Theoretical K-line profile using a solar-like microturbulent velocity distribution.

from these results that nonthermal velocity fields are <u>not directly</u> <u>correlated</u> with the degree of nonradiative heating in the M dwarf chromosphere. In fact, microturbulent velocities may generally be inversely correlated with the degree of mechanical energy dissipation in stellar chromospheres, in contrast to Athay (1976). In the following I will discuss the underlying physical processes which may give rise to these results.

Discussion

The dM4.5e star YZ CMi is a typical single, dMe star of intermediate importance in terms of the degree of nonradiative heating present in the atmosphere. The dM2 star GL 411 possesses the lowest degree of nonradiative heating, as reflected in its R_{HK} value (Chapter 2). I therefore display in Figures 40, 41, 42, and 43 the detailed atmospheric structure for YZ CMi and GL 411, respectively. Figures 41 and 43 show the depth dependence of the parameters of the Ca II K-line formation process for each star.

Inspection of Figures 40 and 42 reveals that both $\tau_{K_2} \sim 1$ and the maximum value of the source function at the K_2 peak, S_{K_2}, occur near $T \approx 6000K$. Hence the K-line flux is particularly sensitive to the location of the inflection point, m_6 (i.e., the lower chromospheric thermal structure) and insensitive to the thermal structure for $m < m_6$, as found in the previous section. From Figures 40 and 42 I note that $S_{K_3} \approx S_{K_2}$ while S_{K_1}, the source function at the base of the K-line emission (see Figure 44), is completely dissimilar. I recall that the line source function is frequency independent in the complete
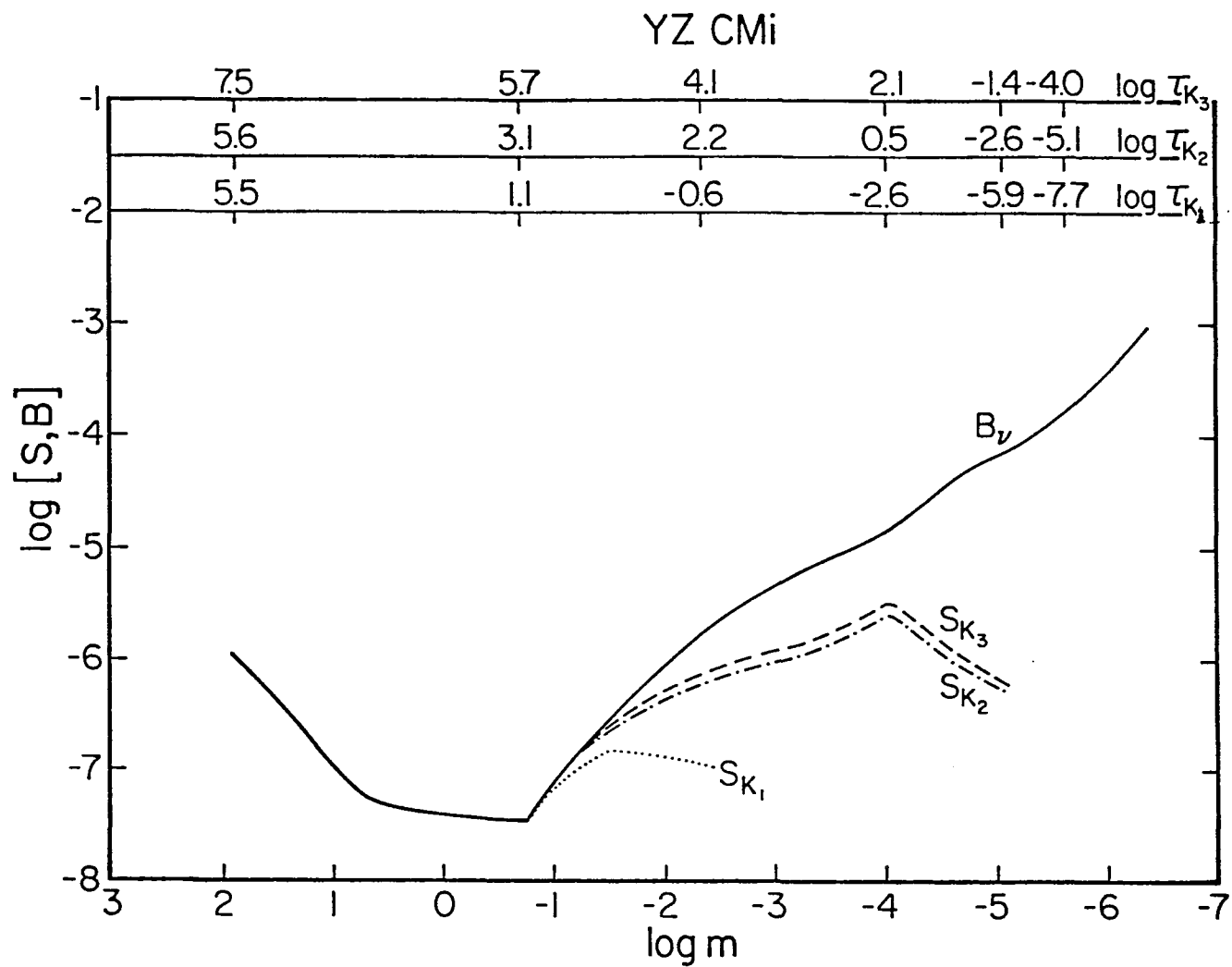
Figure 40.   The depth dependence of the frequency-dependent source function: YZ CMi.
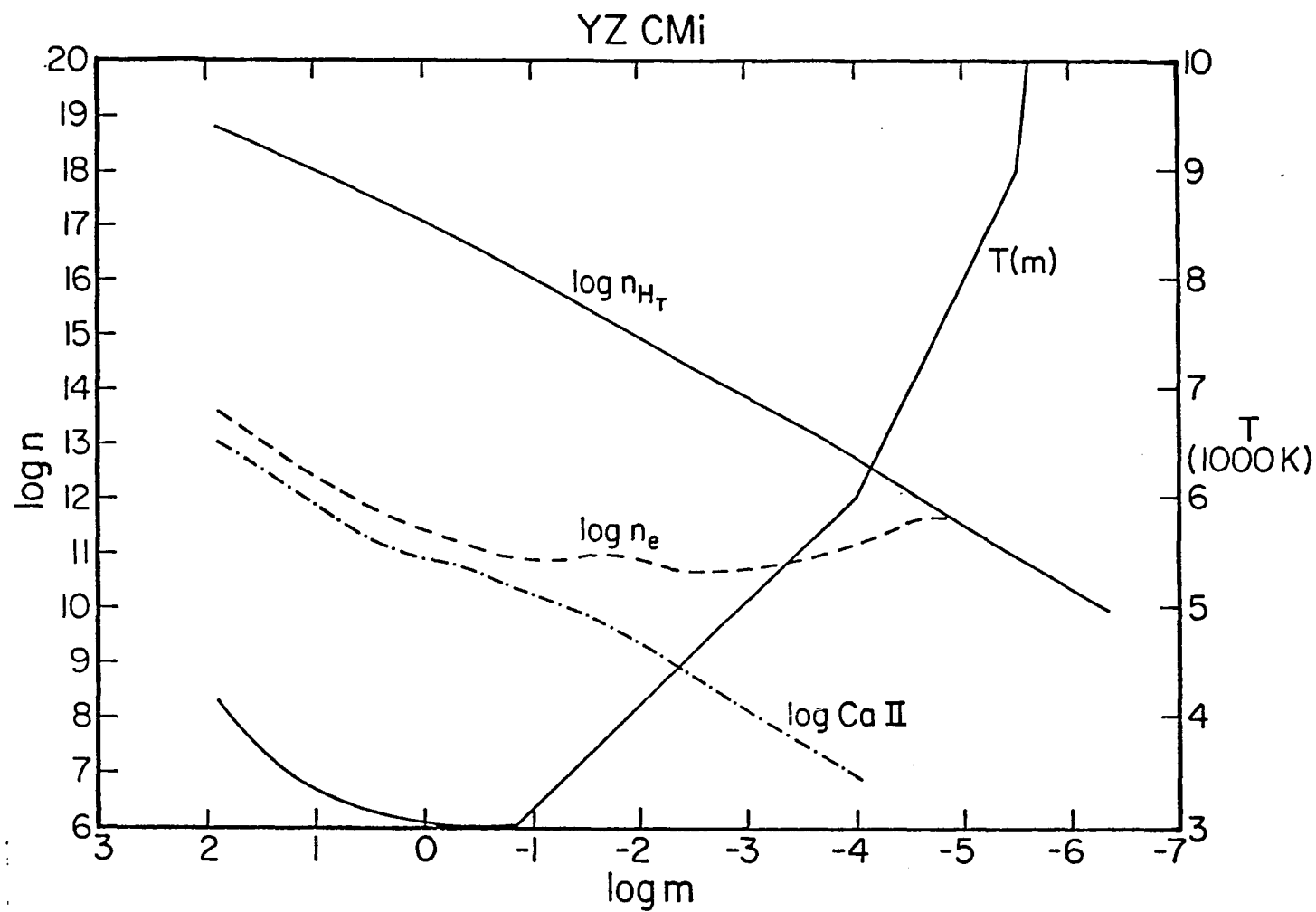
Figure 41. Depth dependence of the parameters of the Ca II K-line formation process: YZ CMi.
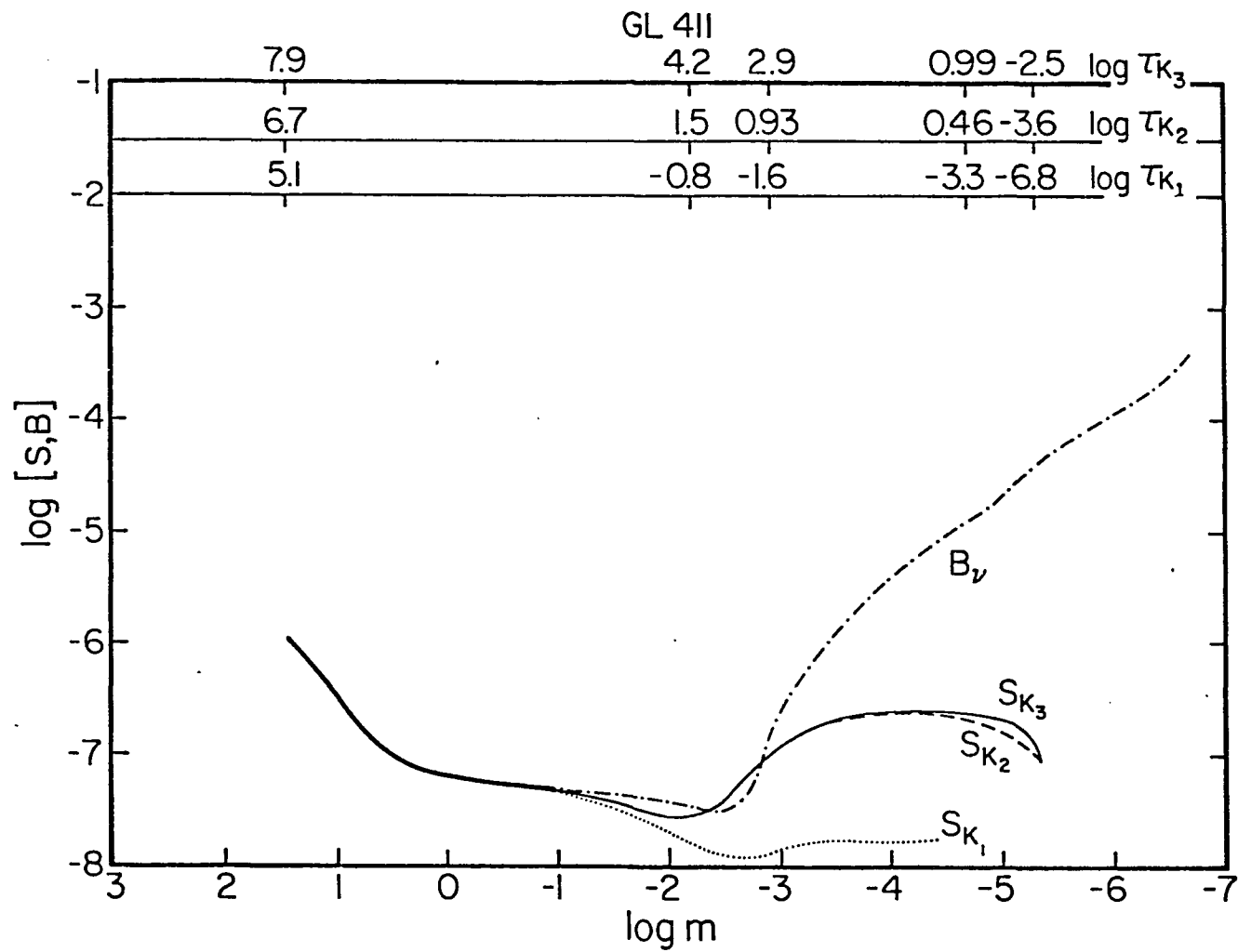
Figure 42. The depth dependence of the frequency-dependent source function: GL 411.
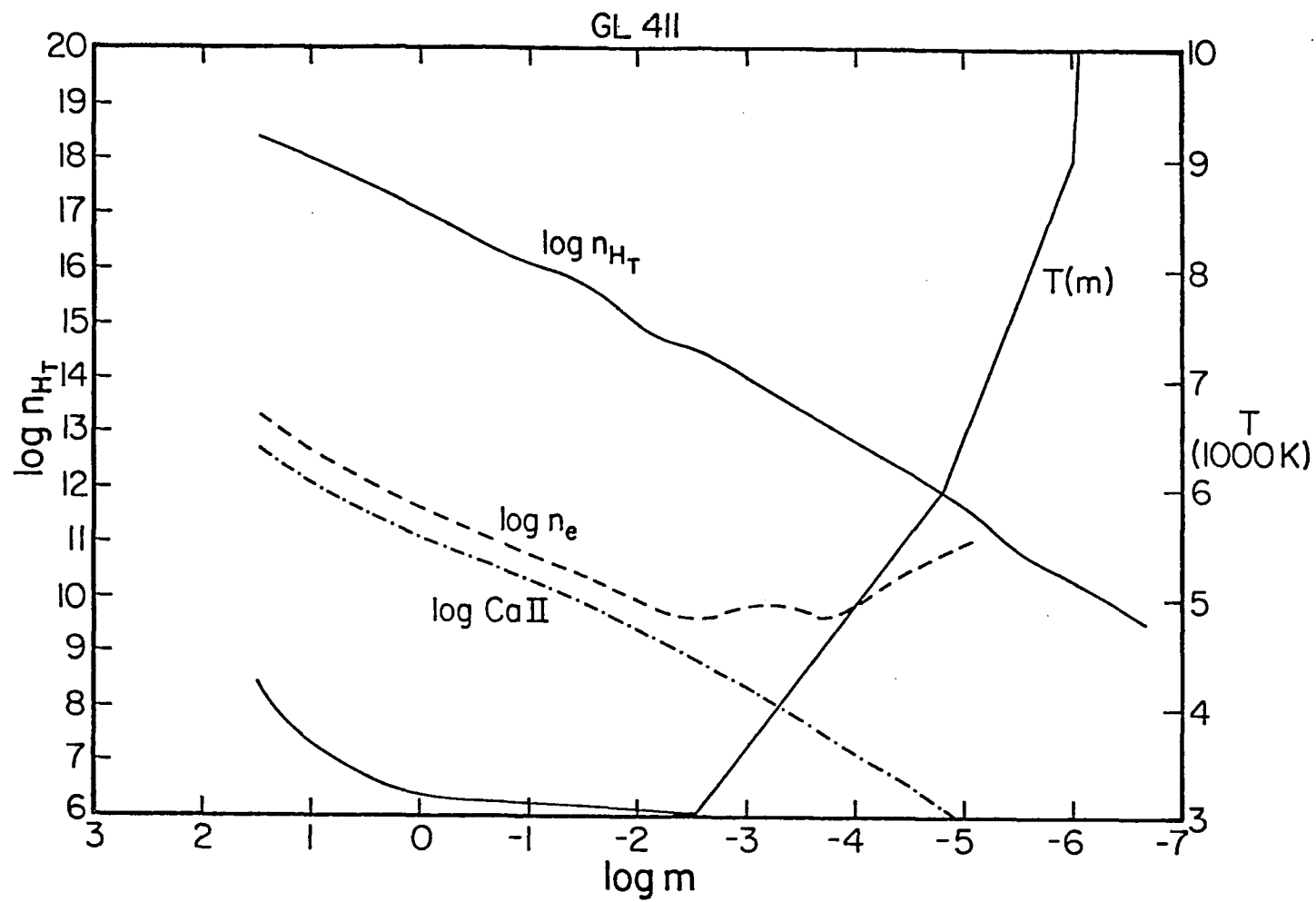
Figure 43. Depth dependence of the parameters of the Ca II K-line formation process: GL 411.
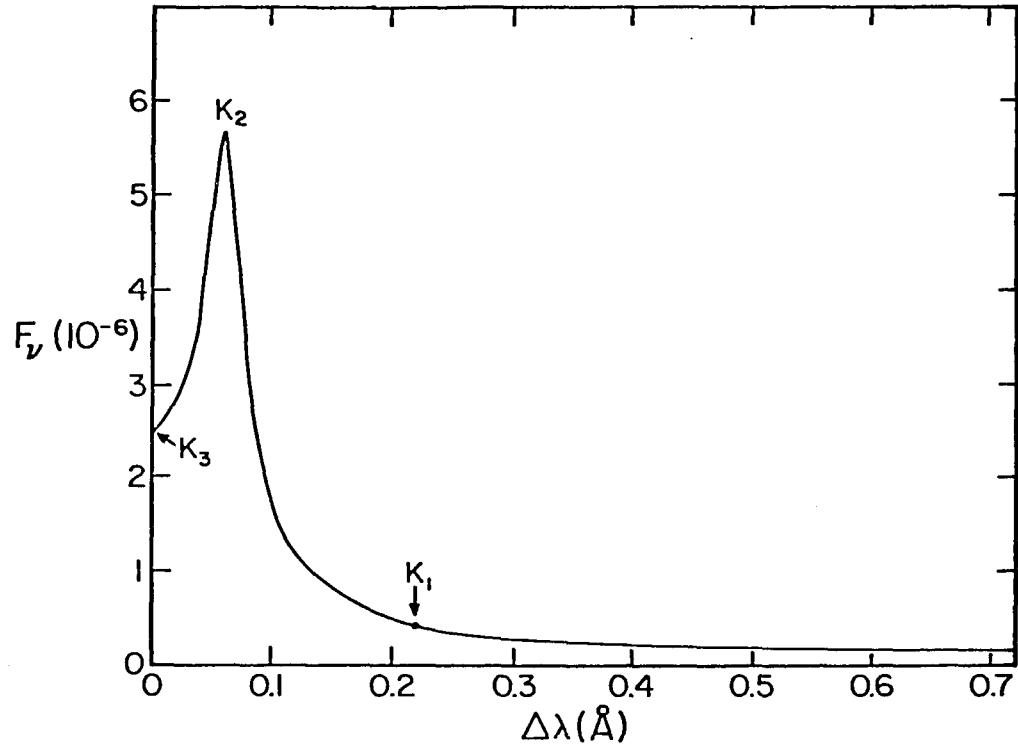
Figure 44.   Important features in the Ca II K-line.

redistribution (CRD) approximation. Therefore Figures 40 and 42 provide

post hoc verification of the a priori assumption of partial redistribu-

tion (PRD) in the method of treatment of the radiative transfer.

Corroborative evidence is seen in Figures 24-38, in which the theo-

retical line profiles exhibit a sharp decline in intensity just outside

the K_2 peaks. This is a typical characteristic which distinguishes

PRD profiles from CRD profiles (cf. Wilson 1973). However, $S_{K_3} \approx S_{K_2}$

implies, but does not prove, that the emission between K_3 and K_2 is

controlled by the Doppler core through Doppler redistribution. There-

fore CRD theory can be applied in order to understand line formation in

this region of the emission core of the K line profile.

An understanding of the relative values of the theoretical line

fluxes at K_3, K_2, and K_1 (Figure 44) may be gained through consideration

of the Eddington-Barbier relation. The Eddington-Barbier relation

essentially describes the mapping of a sufficiently monochromatic source

function to a monochromatic flux. The Eddington-Barbier approximation

is

$$F_{\Delta\lambda} = \pi S_{\Delta\lambda}(\tau_{\Delta\lambda} = t_o), \tag{4.9}$$

where I have neglected the limb darkening and $t_o \approx 1$. In fact, for a

source function which is linear, parabolic, or cubic in $\tau_{\Delta\lambda}$, the value

of t_o is t_o = 2/3, 1, and 1.34, respectively (Athay 1972). Moreover,

the Eddington-Barbier relation is quantitatively obeyed by the solar Ca

II K_1 feature with t_o = 2/3 (Cram and Ulmschneider 1978). I find for

$\tau_{\Delta\lambda} \approx 1$ and YZ CMi (Figure 28) that $F_{K_2}/F_{K_1} \approx 13$ and $F_{K_3}/F_{K_1} \approx 6$, while

$\pi S_{K_2}/\pi S_{K_1} \approx 15$ and $\pi S_{K_3}/\pi S_{K_1} \approx 5$, respectively. I therefore conclude

that the relative flux for features in the computed K-line profiles

for dMe and dM stars are basically consistent with an Eddington-Barbier relation.

The anomalous (with respect to the observed K-line profile) K-line profile corresponding to a solar microturbulent velocity distribution (Figure 39) can be understood through consideration of the line profile function. In particular, the profile function in the Doppler core is $\phi_{\Delta\lambda} \sim \exp[-(\Delta\lambda/\Delta\lambda_D)^2]$. Therefore

$$\tau_{\Delta\lambda} = \tau_{\ell c} \; e^{-(\Delta\lambda/\Delta\lambda_D)^2} , \qquad (4.10)$$

where $\tau_{\ell c}$ is the line-center optical depth and

$$\Delta\lambda_D = \frac{\lambda}{c} [2kT_e/M_{Ca} + \xi_t^2]^{1/2} . \qquad (4.11)$$

The $\xi_t = 1\text{-}10 \text{ km-s}^{-1}$ solar-like microturbulent velocity distribution leads to a high value of $\Delta\lambda_D$ resluting in an excessive line width. Within the Doppler core $\Delta\lambda/\Delta\lambda_D$ is small for high values of ξ_t. Hence

$$\tau_{\Delta\lambda} \approx \tau_{\ell c} [1-(\Delta\lambda/\Delta\lambda_D)^2] \qquad (4.12)$$

for $(\Delta\lambda/\Delta\lambda_D)^2 \ll 1$. In the high ξ_t case $\tau_{\Delta\lambda} < \Delta\lambda_D \approx \tau_{\ell c}$ by Eq. (4.12). Thus $\tau_{\Delta\lambda} \sim 1$ and $\tau_{\ell c} \sim 1$ at the same physical depth in the chromosphere and the validity of CRD in the Doppler core implies that $S_{\Delta\lambda}(\tau_{\Delta\lambda} \sim 1) \approx S_{\ell c}(\tau_{\ell c} \approx 1)$. Hence the emergent fluxes, $F_{\Delta\lambda} \leq \Delta\lambda_D$, are similar by the Eddington-Barbier approximation and lead to enhanced total flux in the line, as seen in Figure 39. Furthermore, this accounts for the relatively flat $F_{\Delta\lambda}$ distribution within the Doppler core of the K-line profile corresponding to the $\xi_t = 1\text{-}10 \text{ km-s}^{-1}$ distribution. Finally, the K_2 peak separation in the $\xi_t = 1\text{-}10 \text{ km-s}^{-1}$

profile is now dominated by the chromospheric velocity field and $\Delta\lambda_{K_2}$ is several times greater than the K_2 peak separation for the line profile with the $\xi_t = 1-2$ km-s^{-1} distribution. The position of the K_2 peak can be understood by realizing that in CRD photons can diffuse to the outer Doppler core and escape, lowering the intensity at line center and increasing it near $\Delta\lambda \simeq \Delta\lambda_D$, thus giving rise to a self-reversal.[4] In the high ξ_t case $\tau_{\Delta\lambda}$ begins to decrease significantly only near $\Delta\lambda \simeq \Delta\lambda_D$ and this is in fact approximately where K_2 is located in the theoretical line profiles displayed in Figure 39 and Figures 24 to 38. In more quantitative terms I find that

$$\Delta\lambda = \Delta\lambda_D \ (\ell n \ \tau_{\ell c}/\tau_{\Delta\lambda})^{1/2}, \qquad (4.13)$$

following Eq. (4.10). According to Cram and Mullan (1979)

$$\Delta\lambda_{max} = \Delta\lambda_D \ (\ell n\tau_c)^{1/2} \ , \qquad (4.14)$$

where $\Delta\lambda_{max}$ is the maximum K_2 peak separation and τ_c is the line center optical depth to the center of the stellar chromosphere. For YZ CMi, $\Delta\lambda_D \simeq 0.063$Å and $\tau_{\ell c} \sim 10^4$ so $\Delta\lambda_{max} = 0.19$Å. The theoretical profile has $\Delta\lambda_{K_2} = 0.12$Å. Hence there is fair agreement with Eq. (4.14). Moreover, the computed values of $\Delta\lambda_{K_2}$ for the M dwarfs considered here are similar (0.08Å to 0.12Å). This is likely due to the fact that $(\ell n\tau_c)^{1/2}$ varies only slowly with τ_c.

Additional physical insight into the parameters which enter into the formulation of the temperature gradient in the region of the

---

4. It is interesting to note that a self-reversal is eliminated entirely in high pressure transition region model chromospheres (Baliunas et al. 1979).

Ca II K-line formation can be obtained through consideration of the monochromatic optical depths to the base of the emission-line core and to the chromospheric maximum in the line-center source function, respectively. The departure from CRD beyond the K_2 feature (see Figures 40 and 42) suggests that the radiation transfer beyond K_2 is controlled by coherent scattering and therefore by the Lorentzian wings (Milkey 1976). The wavelength dependence of the Lorentz profile function is $\phi_{\Delta\lambda} \sim \Delta\lambda^{-2}$. Therefore the monochromatic optical depth to m_*, the base of the emission core, in the Lorentzian wings of Ca II K is (Ayres, Linsky, and Shine 1974)

$$\tau_{\Delta\lambda *} \approx K_\ell \, \tilde{A}_{e\ell} \, m_* \Delta\lambda_*^{-2} \,, \tag{4.15}$$

where $\tilde{A}_{e\ell}$ is the stellar chemical abundance normalized to the solar value and

$$K_\ell \equiv (\pi e^2 f/m_e c) \, (\lambda_\ell^4/c^2) \, (\Gamma_R/4\pi^2) \, (A_{e\ell}^\theta/1.4 \, m_H) \,, \tag{4.16}$$

according to Shine (1973). The value of K_ℓ for Ca II K is $K_\ell = 1.6$ $cm^2\text{-}g^{-1}\text{-}\mathring{A}^2$. According to Figures 40 and 42 the line source function between line center and K_2 is approximately frequency-independent. The chromospheric maximum in the frequency-independent line source function S_ℓ occurs at approximately a thermalization length Λ below the top $(\tau_{\ell c} \ll 1)$ of the chromosphere (Jefferies and Thomas 1959). In PRD the photon exchange between the line core and the damping wings is strongly reduced relative to the CRD case. Thus the thermalization of S_ℓ is principally controlled by the Doppler core. The thermalization length in the Doppler core is $\Lambda \approx \epsilon^{-1}$, where $\epsilon \equiv C_{u\ell}/A_{u\ell}$ is the probability of photon destruction by collisional de-excitation (Hummer and Stewart

1966). Here C_{ul} is the collisional de-excitation rate and A_{ul} is the spontaneous decay rate. The line center optical depth corresponding to a thermalization length is (Ayres 1979)

$$\tau_{lc}^{\Lambda} \simeq \Lambda \simeq K_{lc} \, \overline{A}_{el} \, \xi^{-1} \, m_{\Lambda} \, , \tag{4.17}$$

where ξ is the chromospheric Doppler width in velocity units, m_{Λ} is the mass column density to $\tau_{lc} \simeq \Lambda$ and $K_{lc} \equiv (\pi e^2 f/mc) \, (\lambda_l/\sqrt{\pi})$ $(A_{el}^{\Theta}/1.4 \, m_H)$, which has the value $K_{lc} = 3.6 \times 10^6 \, cm^2-g^{-1}-(km-s)^{-1}$ for the Ca II K-line (Shine 1973). Solving for m_* and m_{Λ} eventually leads to

$$\log \frac{m_{\Lambda}}{m_*} = -\log \, [\frac{K_{lc}}{K_l} \frac{\Delta\lambda_*^2}{\xi} \frac{\tau_{\Delta\lambda*}}{\Lambda}]. \tag{4.18}$$

The temperature gradient is

$$dT/d \log m \simeq \delta T/\delta \log m, \tag{4.19}$$

where

$$\delta T/\delta \log m = -\delta T \, \{\log \, [\frac{K_{lc}}{K_l} \frac{\Delta\lambda_*^2}{\xi} \frac{\tau_{\Delta\lambda*}}{\Lambda} \,]^{-1} \, , \tag{4.20}$$

and $\delta T = T_{\Lambda} - T_*$. From the Eddington-Barbier relation I adopt $\tau_{\Delta\lambda*} \sim 1$. The other parameters in Eq. (4.20) are listed in Table 12 for each star. The similarity of the values for these parameters among the stars considered here (with the exception of GL 411) combined with the fact that the logarithmic function varies slowly, results in similar values of the temperature gradient which are also close to the inferred model chromosphere values given in Table 11 for each star (again with the exception of GL 411). Since analytical expressions for δT are unavailable, I cannot offer a complete physical explanation for the values of the temperature gradients deduced from the model chromospheres

Table 12. Parameters Relating to Model Values of the Temperature Gradient

Star	$\Lambda \approx 1/6$	$\Delta\lambda_*$	ξ	δT	Eq. (4,20)
EQ Vir	7.94(1)	0.33Å	6.3	3047	1.13(3)
GL 616.2	5.26(2)	0.32	5.8	2700	1.44(3)
YZ CMi	9.97(2)	0.24	5.8	2424	1.80(3)
GL 393	3.15(3)	0.24	5.4	2400	2.70(3)
GL 411	1.00(4)	0.14	3.8	2408	3.70(3)

computation. However I can conclude that the values of the chromospheric Doppler width, ξ_t, the thermalization length, Λ, and the base emission width, $\Delta\lambda_*$, all inferred from the model chromspheres computation, are generally consistent with the value of the temperature gradient in the region of the K-line formation.

Further physical insight into the chromospheric Ca II K-line formation can be obtained through consideration of a model atom with two bound levels and a continuum. Since $S_{K_2} \approx S_{K_3}$ we may treat the K-line emission core in the CRD approximation. In this case the line source function may be written as (Mihalas 1978)

$$S_\ell = \frac{\int \phi_\nu J_\nu d\nu + \epsilon B_\nu + \eta B^*}{1 + \epsilon + \eta} \tag{4.21}$$

According to Gebbie and Steinitz (1974), the first term in the numerator represents the rate of radiative excitations in the line, the second term is a thermal source term representing the creation of line

photons by collisional excitation, and the third term represents the creation of line photons by indirect collisional and radiative transitions (e.g., recombination to the upper state followed by spontaneous emission). The first term in the denominator represents the rate of direct spontaneous emission in the line; the second, ε, the destruction of line photons by collisional de-excitation; and the third, η, the destruction of line photons by all indirect transitions (e.g., ionization from the upper state followed by recombination to the ground state). This formulation of the line source function was first derived by Thomas (1957). According to Thomas (1957, 1965), a line is collision dominated if $\varepsilon > \eta$ and $\varepsilon B_\nu > \eta B^*$ and the line therefore couples to the local value of T_e. If $\eta > \varepsilon$ and $\eta B^* > \varepsilon B_\nu$ then the line is photoionization dominated and controlled by $T_{rad} \neq T_e$. The line is of mixed domination if $\varepsilon > \eta$ but $\eta B^* > \varepsilon B_\nu$, or vice versa. The analytical expressions for these various source and sink terms are (Mihalas 1978)

$$\eta \equiv \frac{(R_{uk}+C_{uk})n_\ell^* (R_{k\ell}+C_{\ell k}) - g_\ell(R_{\ell k}+C_{\ell k})n_u^* (R_{ku}+C_{uk})/g_u}{A_u [n^* (R_{k\ell}+C_{\ell k}) + n_u^* (R_{ku}+C_{uk})]} , \qquad (4.22)$$

$$\eta B^* \equiv (\frac{2h\nu^3}{c^2})(\frac{g_\ell}{g_u A_{u\ell}}) \frac{(R_{\ell k}+C_{\ell k})n_u^* (R_{ku}+C_{uk})}{[n^* (R_{k\ell}+C_{\ell k})+n_u^* (R_{ku}+C_{uk})]} , \qquad (4.23)$$

$$\varepsilon \equiv \frac{C_{u\ell}/A_{u\ell}}{1+C_{u\ell}/A_{u\ell}} , \qquad (4.24)$$

$$\varepsilon B_\nu = \varepsilon \frac{2h\nu^3/c^2}{e^{h\nu/kT}-1} , \qquad (4.25)$$

where u, ℓ, and k refer to the upper, lower, and continuum levels in the K-line transition, respectively. The depth dependence of the above

source-sink terms are shown in Figures 45 and 46 for YZ CMi and GL 411, respectively. By inspection of Figures 45 and 46 I find that $\varepsilon > \eta$ and $\varepsilon B_\nu > \eta B^*$. Thus the Ca II K-line is collisionally controlled. In fact the functional form of the source term, ηB_ν, is very similar to the run of electron density, n_e, in the stellare chromosphere. In addition, I display in Figure 47 Ca II K-line profiles computed under the assumption of radiative equilibrium. More specifically, I adopted an atmospheric structure such that $T = T_{min}$ above the model photosphere. The resulting K-line absorption features offer additional corroborative evidence for the chromospheric origin of the K-line emission. Further-more, the collisional control of the Ca II K-line implies that the total chromospheric K-line radiation loss is essentially equal to the number of line photons created by collisional excitations. In particu-lar, the net chromospheric radiative loss rate in the K-line is due to the number of line photons created by collisional excitations within one thermalization length of the top of the chromosphere (Athay 1976). In a two-level atom approximation the net radiative cooling is (Ayres 1979)

$$\frac{dF_\ell}{dm} = 1/2 \frac{n_\ell C_{\ell u}}{\rho} (\frac{hc}{\lambda_{\ell u}}) \text{ ergs-s}^{-1}\text{-g}^{-1}, \qquad (4.26)$$

where n_ℓ is the number density in the lower level and the Ca II K-line collisional excitation rate is (Williams 1980)

$$C_{\ell u} = 8.63 \times 10^{-6} n_e \Omega(^2S-^2P)\omega_1^{-1} T_e^{-1/2} e^{-hc/\lambda_{\ell u} kT_e}. \qquad (4.27)$$

Equation (4.26) is valid in the effectively thin approximation. Now if the ion is a majority species then $n_\ell \approx A_{el} n_H$, where A_{el} is the abundance. I also have that $\rho \approx n_H m_H$. Substituting these expressions
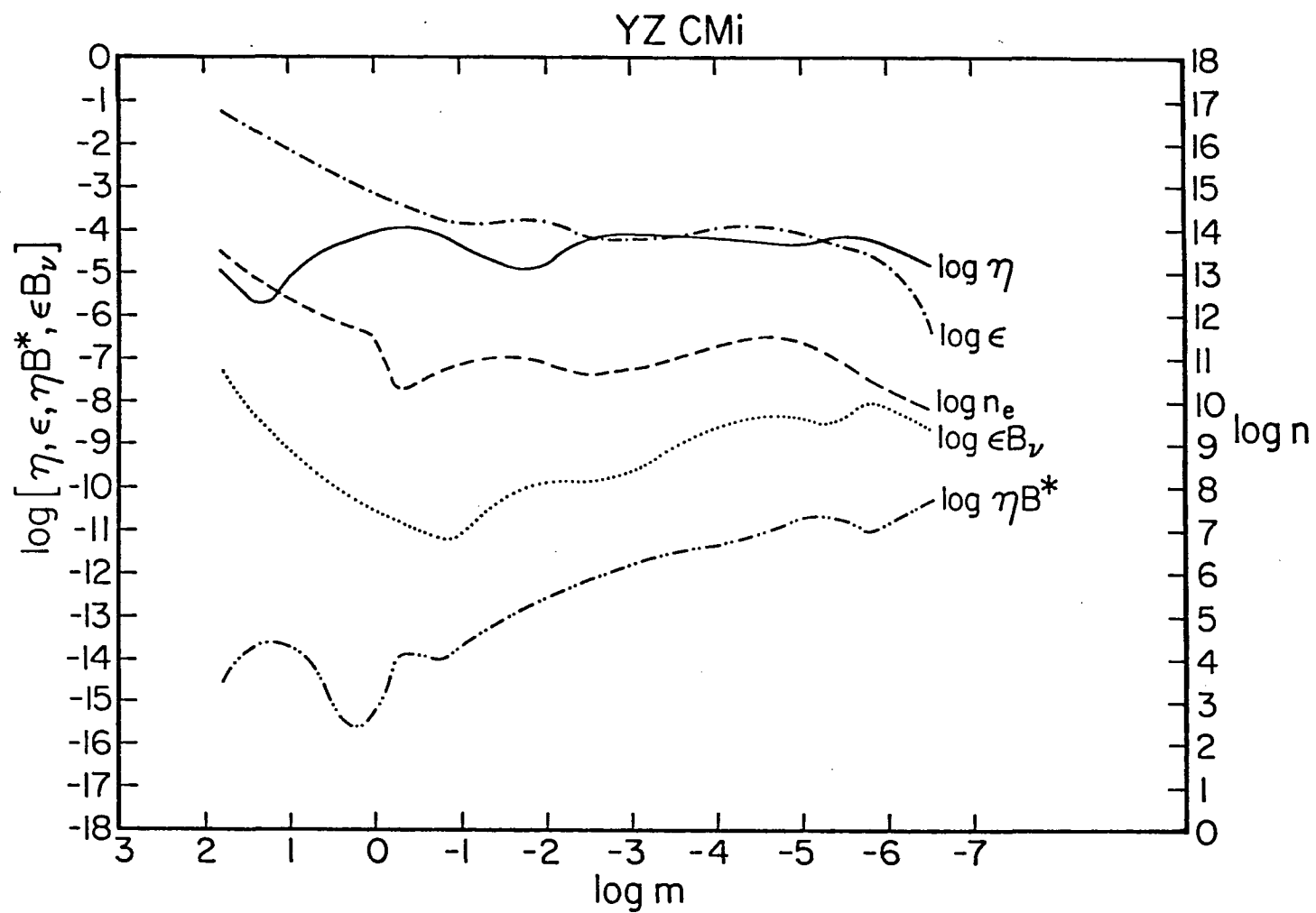
Figure 45. Depth dependence of the K-line source-sink terms: YZ CMi.
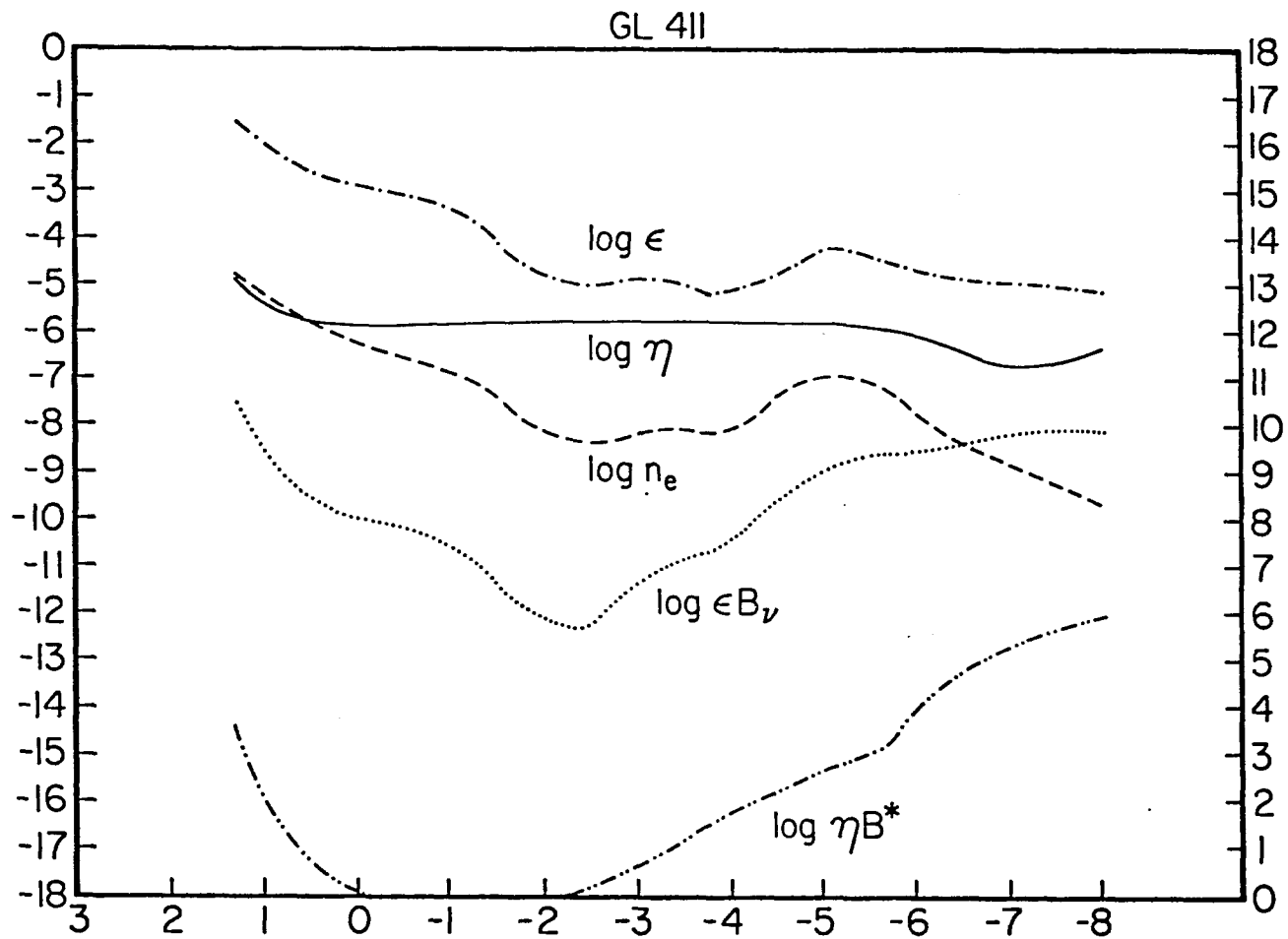
Figure 46. Depth dependence of the K-line source-sink terms: GL 411.
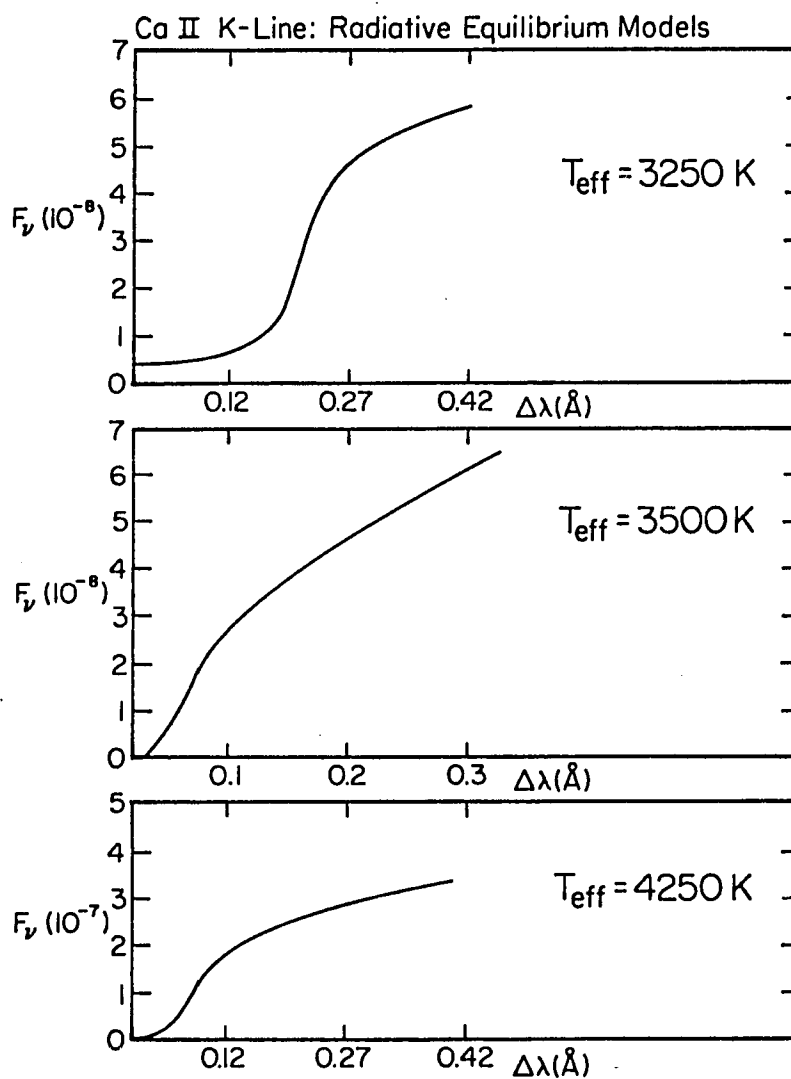
Figure 47. Ca II K-line profiles for an atmosphere in radiative
            equilibrium.

along with numerical values for constants for the K-line transition finally gives

$$\frac{dF_K}{dm} = 2.2 \times 10^2 \, n_e T_e^{-1/2} \, e^{-35900/T_e} \quad \text{ergs-s}^{-1}\text{-g}^{-1}, \qquad (4.28)$$

where I have assumed solar abundances. The peak in the line source function, S_ℓ, occurs approximately a thermalization length Λ below the top ($\tau_{\ell c} \ll 1$) of the chromosphere (Jefferies and Thomas 1959). Taking the values of n_e and T_e at $\tau_{\ell c} = \Lambda$ for each of the model stellar chromospheres considered here yields the results in Table 13. The fifth column is the calculated value of dF_K/dm normalized to that of GL 411 while the sixth column simply shows the net chromospheric K-line surface flux for each star normalized to that of GL 411 (Chapter 2, Table 1).

The results in Table 13 clearly show a trend of decreasing n_e, T_e, and dF_K/dm with decreasing K-line chromospheric emission. <u>I therefore conclude that the K-line collisional excitation rate within</u> <u>Λ of $\tau_{\ell c} \ll 0$ is greater for the dMe stars than for the non-dMe stars.</u> <u>More specifically, the electron density and electron temperature at a</u> <u>thermalization length below the top of the chromosphere are each</u> <u>greater for the dMe stars than for the dM stars</u>. As a result, the chromospheric line emission in collisionally controlled lines is enhanced in dMe stars relative to the non-dMe stars. This conclusion is equivalent to stating that the chromospheric thermal structure is shifted upward in mass column density in dMe stars relative to the non-dMe stars.

Table 13. Net Radiative Cooling Rate Evaluated at One Thermalization Length Into the Chromosphere

Star	n_e	T_e	dF_K/dm	$\dfrac{dF_K/dm}{(dF_K/dm)_{GL\ 411}}$	$F'(K)/-[F'(K)]_{GL\ 411}$
EQ Vir	2.9(12)	7737	7.0(10)	7.0(2)	1.7(2)
GL 616.2	4.2(11)	6600	4.9(9)	4.9(1)	2.6(1)
YZ CMi	2.1(11)	6214	1.8(9)	1.8(1)	1.3(1)
GL 393	6.5(10)	5700	3.5(8)	3.5(0)	4.4(0)
GL 411	2.5(10)	5438	1.0(8)	1	1

CHAPTER 5

SPECTRAL SYNTHESIS OF THE Hα LINE AND THE Mg II
k-LINE IN dMe and dM STARS

The Balmer lines are distinctive spectral features in dMe stars
and the appearance of Hα in emission observationally distinguishes the
dMe stars from the dM stars (Joy and Abt 1974; Chapter 1). Worden and
Peterson (1976) demonstrate the chromospheric origin of the Hα emission
in dMe stars while Cram and Mullan (1979) find that the Balmer lines are
particularly sensitive diagnostics of the thermal structure of the upper
chromosphere and transition region, respectively, in the dMe stars.
Furthermore, Cram and Mullan (1979) find that Hα absorption as well as
Hα emission indicates the presence of a chromosphere in M dwarf stars.
These investigators demonstrate that as the temperature and electron
density in the M dwarf chromosphere increases in response to an increase
in non-radiative heating, the n = 2 level population (or, alternatively,
the Hα line opacity) increases due to increased collisional excitation
from the ground state. However, the electron density and Hα line
opacity is not sufficient to collisionally control the Hα line source
function at this point. Thus the line is radiatively controlled by the
background photosphere. Hence the upper limit to the line source
function is $S_{\ell} = B_{\nu}(T_{eff})$ and the line appears in absorption. As the
degree of non-radiative energy dissipation increases, the electron
density increases and collisional control of the Hα line source function

146

eventually occurs. In this case the line source function becomes coupled to the local chromospheric temperature, T_e. Therefore the upper limit to the Hα line source function is now $S_\ell = B_\nu(T_e)$. Since $T_e > T_{eff}$ the Hα line appears in emission. The essentially chromospheric origin of the Balmer lines, combined with the sensitivity of these spectral diagnostics to upper chromosphere and transition region thermal structure in M dwarf stars offers compelling reasons to briefly discuss Hα line formation in the stars considered in this investigation. More specifically, I wish to discover if the semi-empirical model chromospheres developed in Chapter 4 on the basis of the Ca II K-line will successfully predict Hα emission versus absorption for the stars discussed in this chapter. This study differs from the investigation by Cram and Mullan (1979) in that I use accurate models for the lower chromospheres of _specific_ dMe and dM stars. The models by Cram and Mullan (1979) are _nonspecific_ and consist simply of an _ad hoc_ temperature rise adjoined to the very top of a M dwarf photospheric model taken from Mould (1976). Thus their adopted values of T_{min} are approximately 1000K cooler than the values I find on the basis of observed Ca II K-lines, while their values of m_{min} are typically an order of magnitude too small. I do not attempt to fit theoretical profiles to observed Hα line profiles since calibrated Hα profiles were not available for this particular study. Instead I discuss chromospheric models which successfully predict the Hα profile at a plausible relative flux level (see Worden et al. 1980) for a given dMe or dM star.

Method of Solution for Hα

I adopt the model hydrogen atom and the relevant cross-sections given in Chapter 3 with the following modification: in order to accurately solve for the Hα line profile I must include important transitions which affect the $n = 2$ level population. I therefore explicitly solve the coupled equations of radiative transfer and statistical equilibrium for Hβ and Hγ as well as Hα and the Lyman continuum. The emergent profiles are determined by the depth dependent Doppler broadening and natural, resonance, and Stark broadening parameters. Therefore the depth dependent Voigt profile is characterized by a damping parameter (the Voigt $\underline{a}$ parameter; Swihart 1968) which combines the aforementioned broadening mechanisms. In quantitative terms (Chapter 4)

$$a = \frac{\gamma_N + \gamma_R + \gamma_S}{\Delta\nu_D} , \tag{5.1}$$

where γ_N, γ_R, and γ_S refer to natural, resonance, and Stark broadening, respectively. The Stark broadening is, following Sutton (1978)

$$\gamma_S = 0.255 \, a_1 (n_u^2 - n_\ell^2) \, n_e^{2/3} , \tag{5.2}$$

where $a_1 = 0.642$ for Hα and $a_1 = 1$ for Hβ and Hγ (I warn the reader that this expression for γ_S is incorrectly quoted in the paper by Cram and Mullan 1979). The resonance broadening is, following Mihalas (1978)

$$\gamma_R = 4/3 \, \frac{e^2 f_{1n}}{3m\nu_{1n}} \, n_{HI} , \tag{5.3}$$

where the oscillator strengths, f_{1n}, are given by Green, Rush, and Chandler (1957). Finally, I have that $\gamma_N = A_{u\ell}$, where $A_{u\ell}$ is the

Einstein coefficient for the transition. I find that at $T_e \sim$ 6000K in the chromosphere, the Hα line broadening is dominated by Doppler broadening and natural damping for the M dwarf stars considered in this investigation. I solve the coupled equations of radiative transfer and statistical equilibrium under the assumption of complete redistribution (CRD) in the scattering process. Cram and Mullan (1979) use the same approach since the problem of partial redistribution (PRD) within subordinate lines such as Hα has not yet been treated adequately. Hence the appropriate redistribution functions are currently unavailable. However, CRD is an adequate approximation since the thermal Doppler effect will completely redistribute photons scattering in the line core (Thomas 1957) and the Hα lines in dMe stars do not exhibit well developed line wings (Worden et al. 1980).

Results and Discussion for Hα

The model chromospheric structure inferred for the dM2 star GL 411 on the basis of the observed Ca II K-line profile (Chapter 4) correctly predicts an Hα absorption line for this star. The Hα line profile is displayed in Figure 48 while the depth dependence of the line source function and the Hα Planck function are each shown in Figure 49. Inspection of Figure 49 reveals that the line source function is relatively constant through much of the chromosphere, as may be expected for a line which is controlled by the background continuum. In the region of the temperature minimum and low chromosphere, $S_{H\alpha} > B_\nu(T_e)$. Therefore the Hα line source function in this region of the stellar chromosphere is controlled by radiation from the deeper layers
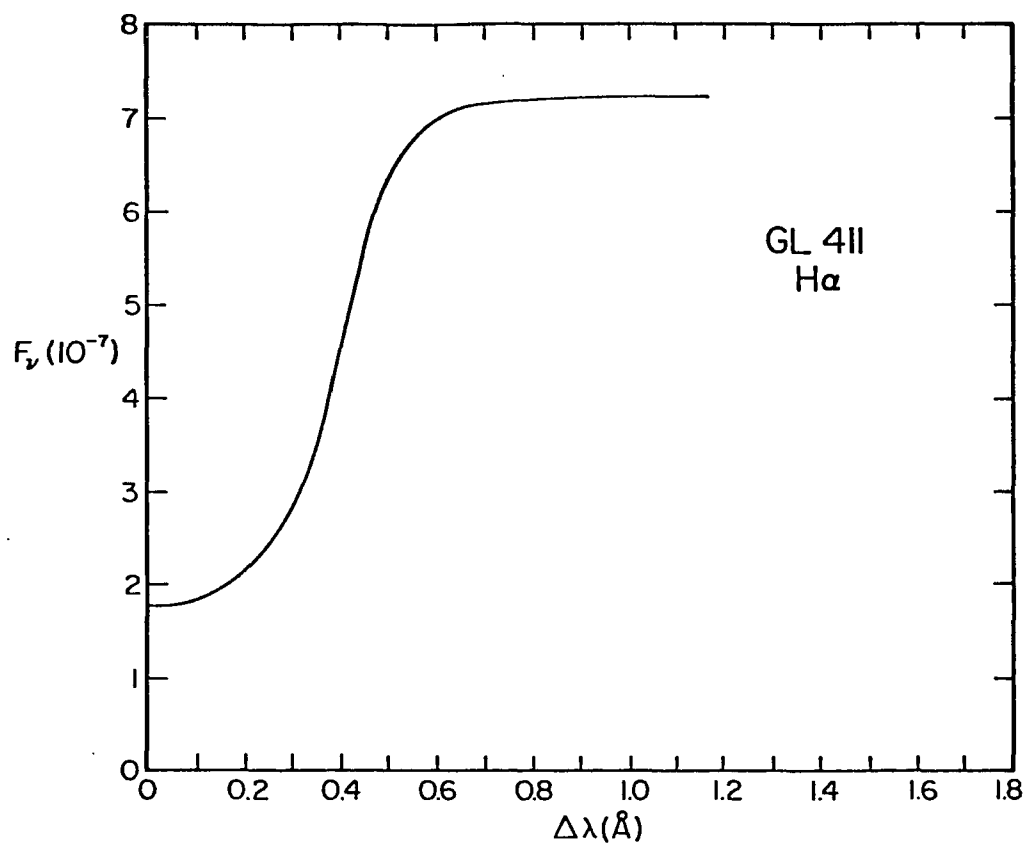
Figure 48. Theoretical Hα absorption line profile computed for GL 411.
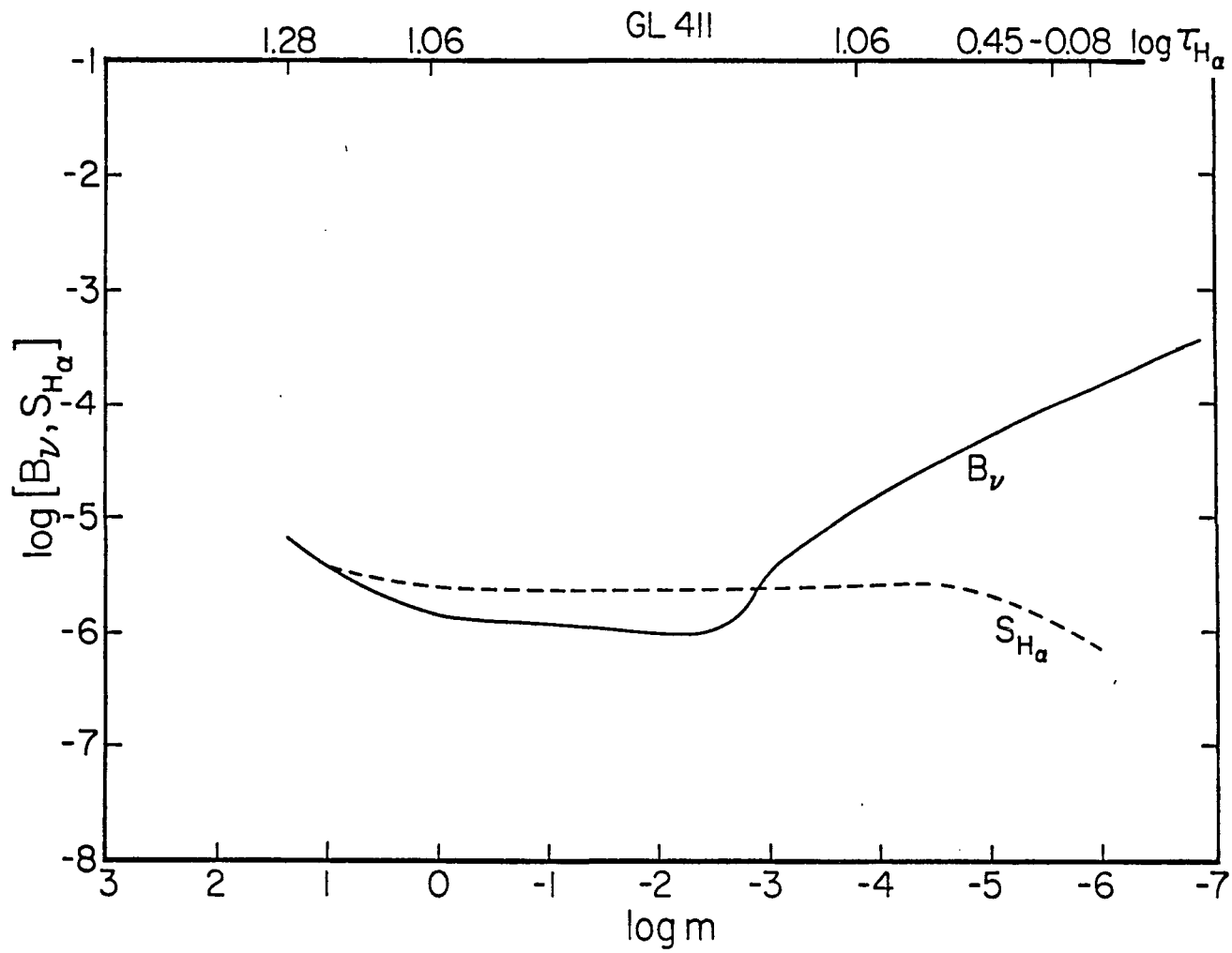
Figure 49. The behavior of the Hα source function in GL 411.

in the photosphere and the higher layers in the chromosphere. Thus the

Hα line cannot be used as a diagnostic of the temperature minimum

region in M dwarf chromospheres. This result is also confirmed by Cram

and Mullan (1979). The model chromospheric structure inferred for the

dK5e star EQ Vir on the basis of the observed Ca II K-line profile

(Chapter 4) incorrectly predicts an Hα absorption line. Of course the

observed Hα feature is variable in this particular active chromosphere

star (Worden et al. 1980) but the Hα line is often observed in emission

(Hartmann and Anderson 1977) at a relative flux level of approximately

twice the continuum level. I therefore adjusted and extended the

transition region thermal structure such that $\log m = -4.40$ at $T =$

$1 \times 10^5 K$. Recall that $\log m = -4.30$ at $T = 9000K$ but $\log m = -5.5$ at

$T = 20000K$ in the semi-empirical model chromosphere inferred for EQ Vir

in Chapter 4 (see Table 10). I did not change the value of m at the

base of the transition region [i.e., $m(T = 9000K)$] in this new model.

This new model chromosphere yields the Hα emission line displayed in

Figure 50. The depth dependence of the line source function and the Hα

Planck function are each shown in Figure 51. The theoretical Hα

emission-line profile shown in Figure 50 also has a central reversal

resulting from the non-LTE effect of the optical boundary (Worden and

Peterson 1976). Inspection of Figure 51 reveals that the behavior of

the Hα line source function in the temperature minimum region is similar

to that found for GL 411 (Figure 49). However, unlike GL 411, the line

source function is close to the Hα Planck function in the chromosphere.

Thus the Hα source function is collision dominated and $S_{H_\alpha} \approx B_\nu(T_e)$.

Hence the line appears in emission. Given a new thermal structure for
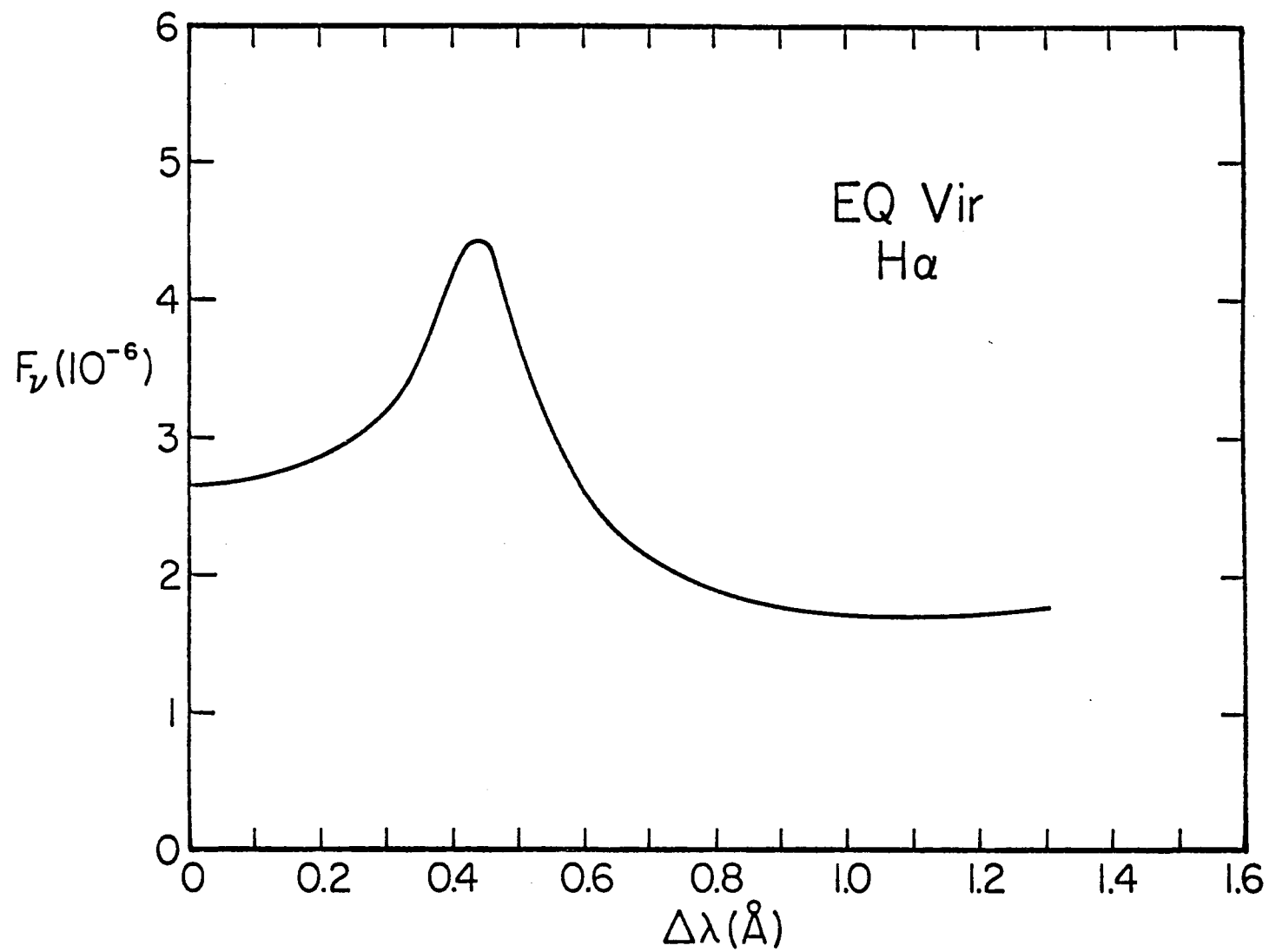
Figure 50.   Theoretical Hα emission line profile computed for EQ Vir.
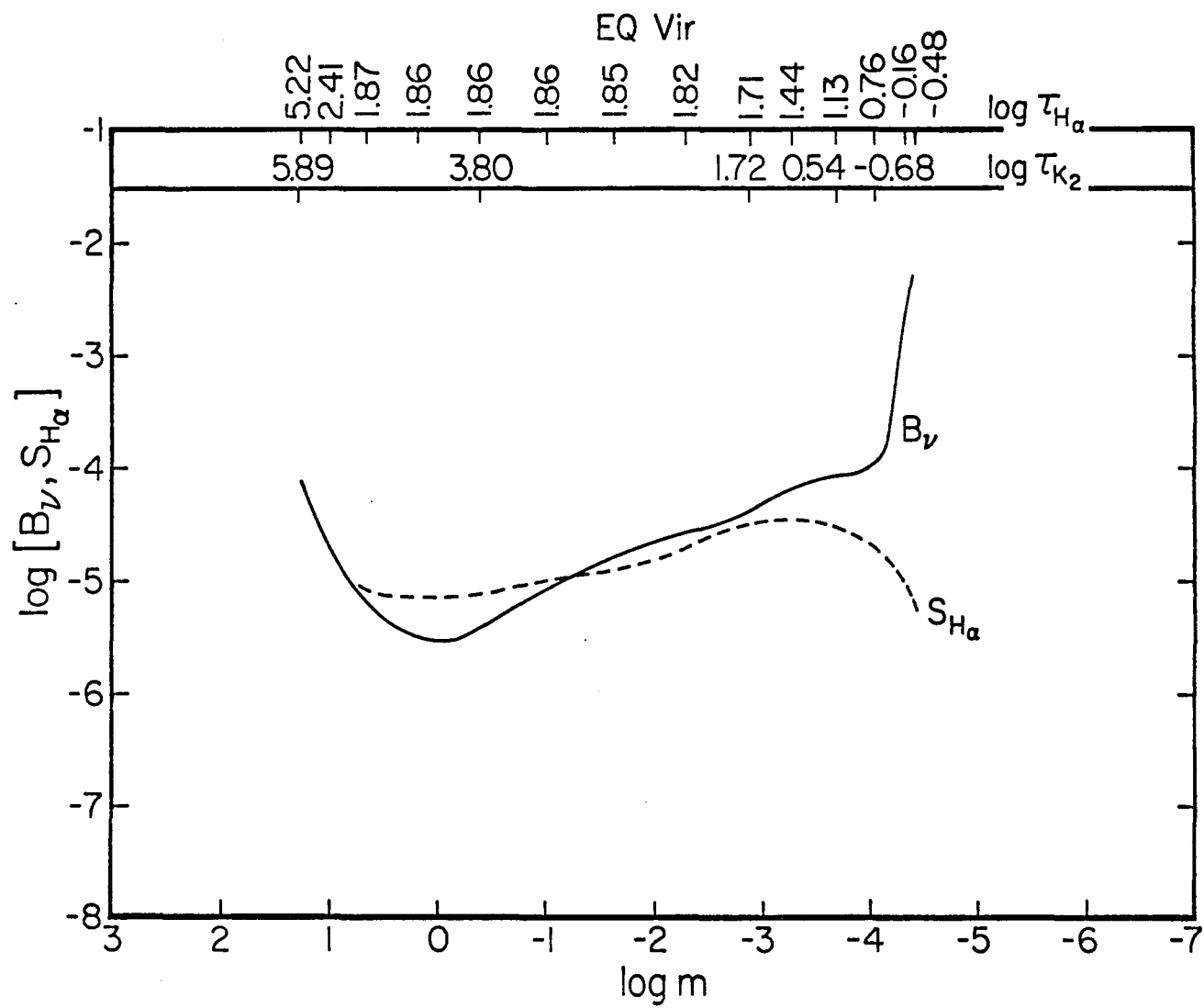
Figure 51.   The depth dependence of the Hα source function in EQ Vir.

EQ Vir (which only differs from the previous thermal structure given in Chapter 4 by the adoption of a steeper transition region temperature gradient), I recompute the Ca II K-line assuming PRD. The resulting theoretical K-line profile is shown in Figure 52, along with the theoretical K-line profile found in Chapter 4 for EQ Vir. Clearly, there is virtually no difference between these line profiles. Inspection of the optical depth scales for the K_2 peak and the Hα line (see Figure 51) reveals that $\tau_{K_2} \sim 1$ in the 6500-7500K temperature range while $\tau_{H\alpha} \sim 1$ in the 9000-10000K temperature regime. As noted in Chapter 4, Ca II becomes depleted by ionization and the K-line becomes optically thin in the region where Hα is still optically thick (Figure 51). I am therefore led by these results to conclude that <u>it is possible to construct single-component, semi-empirical model chromospheres for M dwarf stars which simultaneously satisfy both the Ca II K-line and the Hα line</u> (see also Kelch et al. 1979). The agreement that can be achieved is consistent since these two spectral diagnostics really address two different regions of the M dwarf chromosphere; the Ca II K-line is a lower chromospheric diagnostic ($T_e \lesssim 6000$K) while the Hα line is more sensitive to the upper chromospheric-transition region ($T_e \gtrsim 9000$K) thermal structure. It would therefore be interesting to compare models based upon the cores of the Balmer lines with transition region models inferred from transition region spectral diagnostics such C II or C IV.

Finally, I note that the mass column density at the top of the transition region is less than the mass column density at the base of the transition region $[m_o(T \approx 9000)]$ by only ~ 0.1 dex for the
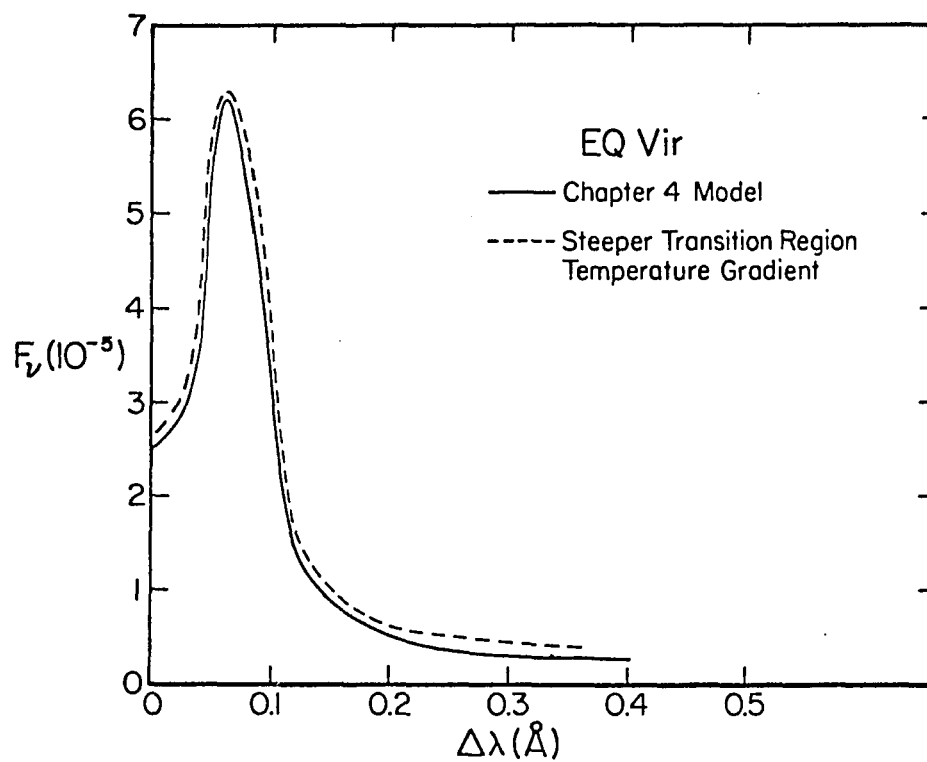
Figure 52. The theoretical Ca II K-line profiles deduced from the thermal structures for EQ Vir presented in Chapters 4 and 5, respectively.

chromospheric model which predicts Hα emission in EQ Vir. This is con-
sistent with the results obtained by Cram and Mullan (1979, their Table
1). These investigators also typically find that log $[m(10^5K)]$ - log
$[m_o(9000K)]$ = -0.1, for M dwarf model chromospheres which exhibit an Hα
emission line profile.

The final set of prominent chromospheric spectral diagnostics
which appear in the spectra of dM and dMe stars, and which I will now
consider, are the Mg II h and k resonance lines at λ2802.7Å and
λ2795.5Å, respectively. The advent of the International Ultraviolet
Explorer (IUE) satellite has made the resonance lines of Mg II available
for observation and subsequent theoretical analysis. The height of
formation of the h and k line cores is somewhat greater than the height
of formation of the Ca II H and K resonance line cores, but there is
also a large region of overlap (Linsky and Avrett 1970). Thus the Mg II
and Ca II resonance lines sample similar regions of the stellar
chromosphere. In the following I will offer a brief quantitative
assessment of Mg II h and k line observations obtained with the IUE
satellite for a sample of 6 dMe and 3 dM stars.

Results and Discussion for the Mg II
Observations

The Mg II h and k line fluxes were obtained with the IUE
satellite in the long wavelength, low dispersion mode resulting in a
spectral resolution of 7Å (Boggess, Carr, and Evans 1978). The stars
observed, their spectral types, and the Mg II (h+k) line fluxes at the

earth are given in the first three columns of Table 14.[5] The spectral

types are taken from Kunkel (1975) or Veeder (1974), except for 61 Cyg B.

The spectral type for this star is given by Kelch et al. (1979). The

relations between stellar angular diameter and (V-R) color convert the

observed flux to surface flux (Barnes and Evans 1976, Barnes et al.

1976). The (V-R) color index for each star follows from Veeder (1974)

or Pettersen (1976) [the (V-R) color for AT Mic is not available). The

ratio of the Mg II (h+k) stellar surface flux to the same quantity for

the mean Sun is listed in column for of Table 14. This ratio is based

upon the mean solar value of the Mg II (h+k) line flux given by Linsky

and Ayres (1978). The importance of chromospheric non-radiative heating

in this sample of M dwarf stars considered here can be readily inter-

compared through the ratio

$$R_{hk} = F(\text{Mg II } h+k)/\sigma \, T_{eff}^4 \, , \qquad (5.4)$$

where R_{hk} represents the chromospheric radiative losses in the h and k

lines normalized to the total stellar surface flux. I assume that the

radiative equilibrium contribution to the h and k line fluxes is

negligible in these cool dwarfs (Linsky and Ayres 1978). The values of

R_{hk} are listed in column 5 of Table 14. The effective temperatures for

GL 380 and GL 411 are taken from Chapter 2. The values of T_{eff} for

EQ Vir and YZ CMi are taken from Pettersen (1980). The effective

temperature of 61 Cyg B is taken from Linsky et al. (1979) while those

for UV Ceti, BD+43.44, and Prox Cen are estimated from their spectral

---

5. The observed Mg II fluxes for YZ CMi and UV Ceti have been
kindly provided by K. G. Carpenter and R. F. Wing in advance of
publication.

Table 14. Summary of IUE Mg II (h+k) Observations

Star	Spectral Type	$f(\text{Mg II})$[a]	$F(\text{Mg II})$[a]	$\frac{F}{F_\odot}(\text{Mg II})$	R_{hk}	R_{HK}	$F(\text{Mg II})/F(\text{Ca II})$
EQ Vir	dK5e	1.3 (−12)	2.6 (6)	2.00	1.71 (−4)	1.2 (−4)	1.41
61 Cyg B	dM0	6.5 (−12)	3.1 (5)	0.24	2.92 (−5)	8.2 (−6)	2.67
GL 380	dM0	8.7 (−13)	5.3 (4)	0.04	4.25 (−6)	1.0 (−5)	0.41
GL 411	dM2	5.8 (−13)	3.3 (4)	0.03	4.39 (−6)	1.4 (−6)	3.03
BD+43.44	dM2.5e	4.0 (−12)	5.4 (5)	0.42	9.77 (−5)	−−	−−
AT Mic	dM4.5e	3.9 (−12)	−−	−−	−−	−−	−−
YZ CMi	dM4.5e	1.3 (−12)	9.7 (5)	0.75	1.74 (−4)	2.5 (−5)	6.98
Prox Cen	dM5e	8.6 (−13)	9.8 (4)	0.08	1.88 (−5)	−−	−−
UV Ceti	dM6e	6.4 (−13)	1.8 (5)	0.14	5.37 (−5)	−−	−−

[a]Units: $\text{ergs-cm}^{-2}\text{-s}^{-1}$.

types and Allen (1976). Values of R_{HK}, the analogous quantity for the Ca II H and K lines, are taken from Chapter 2 and listed in column 6 of Table 14 [the R_{HK} value for 61 Cyg B follows from Linsky et al. (1979) while the R_{HK} values for EQ Vir and YZ CMi given in Chapter 2 have been slightly modified to reflect the new T_{eff} measurements presented by Pettersen (1980)]. Finally, I list in column 7 of Table 14 the ratio of the Mg II (h+k) line fluxes to the Ca II (H+K) line fluxes. Omitted entries in Table 14 indicate that the particular value is not available.

The values of the ratio F(Mg II h+k)$/F_{\odot}$(Mg II h+k) are less than unity, with the exception of the most active star (as defined by the R_{hk} values), EQ Vir. The values of R_{hk} for the dMe stars are basically an order of magnitude greater than for the dM stars. Furthermore, F(Mg II h+k)$/F_{\odot}$(Mg II h+k) increases with increasing R_{hk}. In addition, the ratio F(Mg II h+k)$/F$(Ca II H+K) is greater than unity (with the exception of GL 380) for the sample considered here. Thus the Mg II resonance lines generally play a more important role in the overall chromospheric energy balance in dMe and dM stars than do the Ca II H and K resonance lines (see also Linsky and Ayres 1978). However, there is an important caveat that must be noted: the Mg II data and the Ca II data discussed in this investigation were not acquired simultaneously. Thus the emergence and decay of stellar surface activity combined with the rotational modulation of these features are likely to cause variations in the observed net chromospheric radiative losses. Therefore data sets obtained at widely separated times of observation cannot be confidently compared on a star-by-star basis (with the possible exceptions of the "most active" and the "least active" stars). I can,

however, partially circumvent this difficulty by comparing the mean values of physical quantities for a particular sample of stars. Since the degree of chromospheric activity among stars in a given sample is uncorrelated, the mean values of physical quantities will remain relatively constant. I thus find the mean value of the ratio F(Mg II)/ F(Ca II) to be 2.90. This is similar to the mean solar value of 2.5 (Linsky et al. 1979). The mean values of R_{hk} and R_{HK} are $\overline{R_{HK}}$ = 6.91(-5) and $\overline{R_{HK}}$ = 3.3(-5) respectively. The ratio $\overline{R_{hk}}/\overline{R_{HK}}$ is 2.1 which is close to the solar value of 2.5. Thus I conclude that the mechanism which determines the relative contributions of certain spectral lines to the energy balance in the chromosphere must be similar in the late-type, main sequence dwarf stars. This conclusion is also supported by Linsky and Ayres (1978).

As in the case of Hα, I now wish to discover if the semi-empirical model chromospheres developed in Chapter 4 on the basis of the Ca II K-line will successfully predict the Mg II k-line flux at a level greater than or equal to the Ca II K-line flux, which is the requirement implied by the results given in Table 14. The spectral resolution of the IUE observations is not adequate to allow a detailed comparison of an observed Mg II k-line profile with a k-line profile computed theoretically. Therefore, I compare only the observed and computed values of the flux where I assume F(Mg II k) ≈ 1/2 F(Mg II h+k) in order to deduce the observed value of F(Mg II k).

Method of Solution for Mg II

The method of solution of the coupled equations of radiative transfer and statistical equilibrium is identical to the method employed for the Ca II K-line (Chapter 4). The appropriate atomic parameters (assumed solar abundance; oscillator strengths; and radiative, Stark, and van der Waals damping parameters) are taken from Shine and Linsky (1974) and Shine (1973). The Mg II collisional rate coefficients and photoionization cross-sections are given in Shine (1973). In the CRD computation, I adopt a representation of Mg II consisting of three bound levels and the continuum. I include the ground state, $3s\ ^2S_{1/2}$, and two radiating states, $3p\ ^2P_{1/2}$ and $3p\ ^2P_{3/2}$, respectively. The permitted radiative transitions are $3p\ ^2P_{3/2} - 3s^2S_{1/2}$ (the 2796Å k line) and $3p\ ^2P_{1/2} - 3s\ ^2S_{1/2}$ (the 2803Å h line), while collisions couple all bound levels and the continuum. The PRD refinement of the CRD computation utilizes a two-level representation of Mg II, explicitly calculating the k-line profile. This approximation is even more necessary for the Mg II system since it lacks intermediate metastable states analogous to the Ca II infrared triplet levels.

Results and Discussion for Mg II

The results of the spectral synthesis of the Mg II k-line flux based upon the model chromospheres given in Chapter 4 are presented in Table 15. The stars are listed in order of decreasing importance of non-radiative heating in the particular stellar atmosphere (i.e., decreasing R_{HK} value; Chapter 2). The second column gives the theoretically computed value of the Mg II k-line flux. The third column

Table 15. Comparison of Theoretical and Observed Mg II k Line Fluxes

Star	$F(Mg\ II\ k)_{theo}$	$F(Mg\ II\ k)_{obs}$	$F'(K_1)$	$F(Mg\ II\ k)_{theo}/F'(K_1)$
EQ Vir	2.08(6)	1.34(6)	8.5(5)	2.4
GL 616.2	1.10(5)	--	1.3(5)	0.8
YZ CMi	3.21(4)	4.69(5)	6.6(4)	0.5
GL 393	2.20(3)	--	2.2(4)	0.1
GL 411	1.03(4)	1.70(4)	5.0(3)	2.1

shows the observed value of the k-line flux (if available) while the fourth column contains the observed chromospheric Ca II K-line emission (Chapter 2). The fourth column lists the ratio of the theoretical k-line flux to the observed Ca II K-line chromospheric emission flux. Inspection of this column reveals that the "most active" and "least active" chromosphere stars, EQ Vir and GL 411, each have values of the ratio $F(Mg\ II\ k)_{theo}/F'(K_1)$ close to the observed mean value of 2.4 [where I have assumed in this comparison that $F(Mg\ II\ k) \approx 1/2$ $F(Mg\ II\ h+k)$ and $F'(K_1) \approx 1/2\ F'(K_1+H_1)$]. Interestingly, these two particular stars may possess the most homogeneous chromospheres of the stars listed in Table 15. In fact the observed and theoretically inferred values of $F(Mg\ II\ k)$ for EQ Vir and GL 411, respectively, are comparable. Thus the level of surface activity exhibited by these stars may remain relatively constant. However, the stars with intermediate degrees of nonradiative heating, GL 616.2, YZ CMi, and GL 393, each exhibit an anomalously low value of the ratio $F(Mg\ II\ k)_{theo}/$ $F'(K_1)$. Furthermore, the observed value of $F(Mg\ II\ k)$ for YZ CMi is approximately a factor of 15 greater than the theoretically computed value, $F(Mg\ II\ k)_{theo}$. An adjustment of the chromospheric thermal structure of YZ CMi which yields a value of $F(Mg\ II\ k)_{theo}$ such that $F(Mg\ II\ k)_{theo} \approx F(Mg\ II\ k)_{obsv}$, overpredicts the value of the Ca II K-line flux by a factor of ~ 50. I therefore conclude that single-component, homogeneous model atmospheres may not be adequate representations of the chromospheres of M dwarf stars.

CHAPTER 6

THE APPLICABILITY OF SINGLE-COMPONENT
MODEL CHROMOSPHERES

A principal simplification I utilize in the construction of semi-empirical model chromospheres is the assumption of lateral homogeneity (Chapter 3). However, the inability of single-component model chromospheres to reconcile the Ca II K-line and the Mg II k-line (Chapter 5) implies that the assumption of a homogeneous chromosphere is suspect. Corroborative evidence for this conclusion is offered by Heasley et al. (1978). These investigators find that models of the lower chromosphere and upper photosphere of Arcturus, as inferred from high spectral resolution observations of the fundamental vibration-rotation bands of CO, differ radically from models developed by Ayres and Linsky (1975) of the same atmospheric region, but based upon the Ca II K-line wings. Thus Heasley et al. (1978) conclude that it is not possible to reproduce the Ca II K-line wings and the CO fundamental lines in the spectrum of Arcturus with a single-component model chromosphere. I therefore will attempt to quantitatively ascertain the degree of surface inhomogeneity present in the dMe and dM stars as well as offer a hypothesis which may explain the inability of single-component model chromospheres to reconcile various chromospheric spectral diagnostics.

An alternative approach to account for the degree of chromo-spheric emission in M dwarf stars is to assume that the dM and dMe

165

stars fundamentally differ from each other in terms of the fractional area of their surface which is covered by active regions (Mullan 1976, Worden 1975). Such an approach is especially suggested by the inhomogeneous nature of the solar atmosphere and photosphere. Furthermore, flare stars often exhibit quasi-periodic variability which has been attributed to the probable presence of magnetic surface activity that is similar in character to such solar phenomena as sunspots and plages (Bopp and Evans 1973, Torres and Mello 1973, Kunkel 1975, Vogt 1975, Worden 1975, Fix and Spangler 1976, Chapter 1).

In order to estimate the active region filling factor for each of the M dwarf stars given in Table 16, I make the following assumptions: (1) the star with the largest R_{HK} (R_{hk}) values, EQ Vir, has a filling factor of A $\equiv$ 1 and the star with the smallest R_{HK} (R_{hk}) value, GL 411, has a filling factor of A $\equiv$ 0; (2) the character of an active region is the same for all the stars; and (3) the center-to-limb behavior of the chromospheric emission line intensity can be neglected. The expression for the total chromospheric emission line flux is

$$F = 2\pi \int_0^\infty \int_0^{+1} I_\nu \mu \, d\mu \, d\nu \ , \tag{6.1}$$

or,

$$F = 2\pi \int_0^\infty d\nu \{ \int_0^{\mu_A} I_A \mu \, d\mu + \int_{\mu_A}^{+1} I_Q \mu \, d\mu \} \ , \tag{6.2}$$

where I_A and I_Q are the intensities of the line emission in the active region and quiet region, respectively, and μ_A represents the geometrical extent of the active region. Figure 53 is an illustration of the geometry adopted for the calculation of Eq. (6.2). The aforementioned crude assumptions and Eq. (6.2) lead to the following

Table 16. Active Region Filling Factors

Star	Sp. Type	A(Ca II)	A(Mg II)
EQ Vir	dK5e	$\equiv$ 1.0	$\equiv$ 1.00
61 Cyg B	dM0	0.065	0.10
GL 380	dM0	0.07	0.01
GL 616.2	dM1.5e	0.14	--
GL 411	dM2	$\equiv$ 0.00	0.00
GL 393	dM2	0.016	--
BD+43.44	dM2.5e	--	0.21
GL 526	dM4	0.013	--
YZ CMi	dM4.5e	0.07	0.34
Prox Cen	dM5e	--	0.03
UV Ceti	dM6e	--	0.14
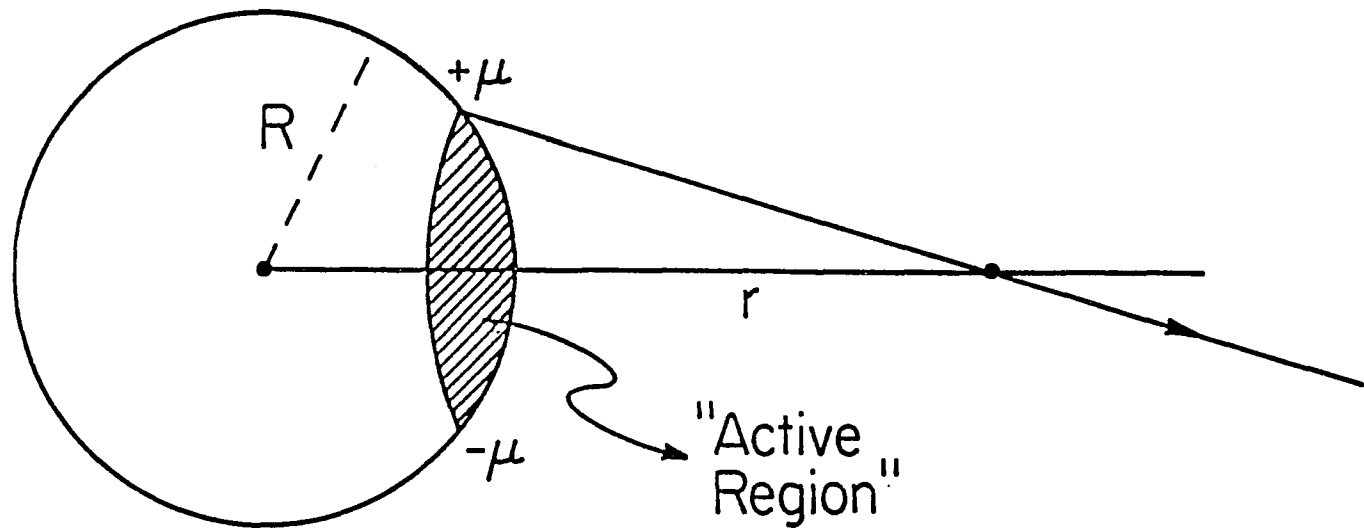
Figure 53. Geometry utilized for the estimation of active region filling factors.

expression for the chromospheric radiative losses in the Ca II H and K

lines (or the Mg II h and k lines) for a star

$$F = A\,F_a + (1 - A)\,F_q \; , \tag{6.3}$$

where A is the dimensionless ratio of the area of the active region to

the area of the visible quiet stellar surface. The symbols F_a and F_q

represent a chromospheric line surface flux for an active and quiet

region, respectively. The values of A deduced from the observed values

of F'(Ca II H+K) and F(Mg II h+k) are given in Table 16 for a sample of

dMe and dM stars. The relative active region filling factors for the

dMe stars are generally greater than for the dM stars. If I exclude

the assumed extreme values of A for EQ Vir and GL 411, I find the mean

values $\langle A(\text{Mg II})\rangle = 0.14$ while $\langle A(\text{Ca II})\rangle = 0.06$. In summary, the

apparently discrepant mean active region filling factors derived from

the Ca II H and K and the Mg II h and k lines combined with the failure

of model chromospheres to reconcile two overlapping chromospheric

spectral features suggest that single-component, homogeneous model

atmospheres are not physically realistic representations of M dwarf

stars.

The stellar chromospheric emission features probably arise from

plage regions which are, in turn, composed of magnetic flux tubes. A

schematic model of a magnetic flux tube is presented in Figure 54. The

levels h_1 and h_2 represent the heights of formation of the Ca II K-line

core and the Mg II k-line core, respectively. I consider a flux tube in

hydrostatic equilibrium. Therefore

$$P_{ext}(h) = P_g(h) + [B(h)]^2/8\pi \tag{6.4}$$
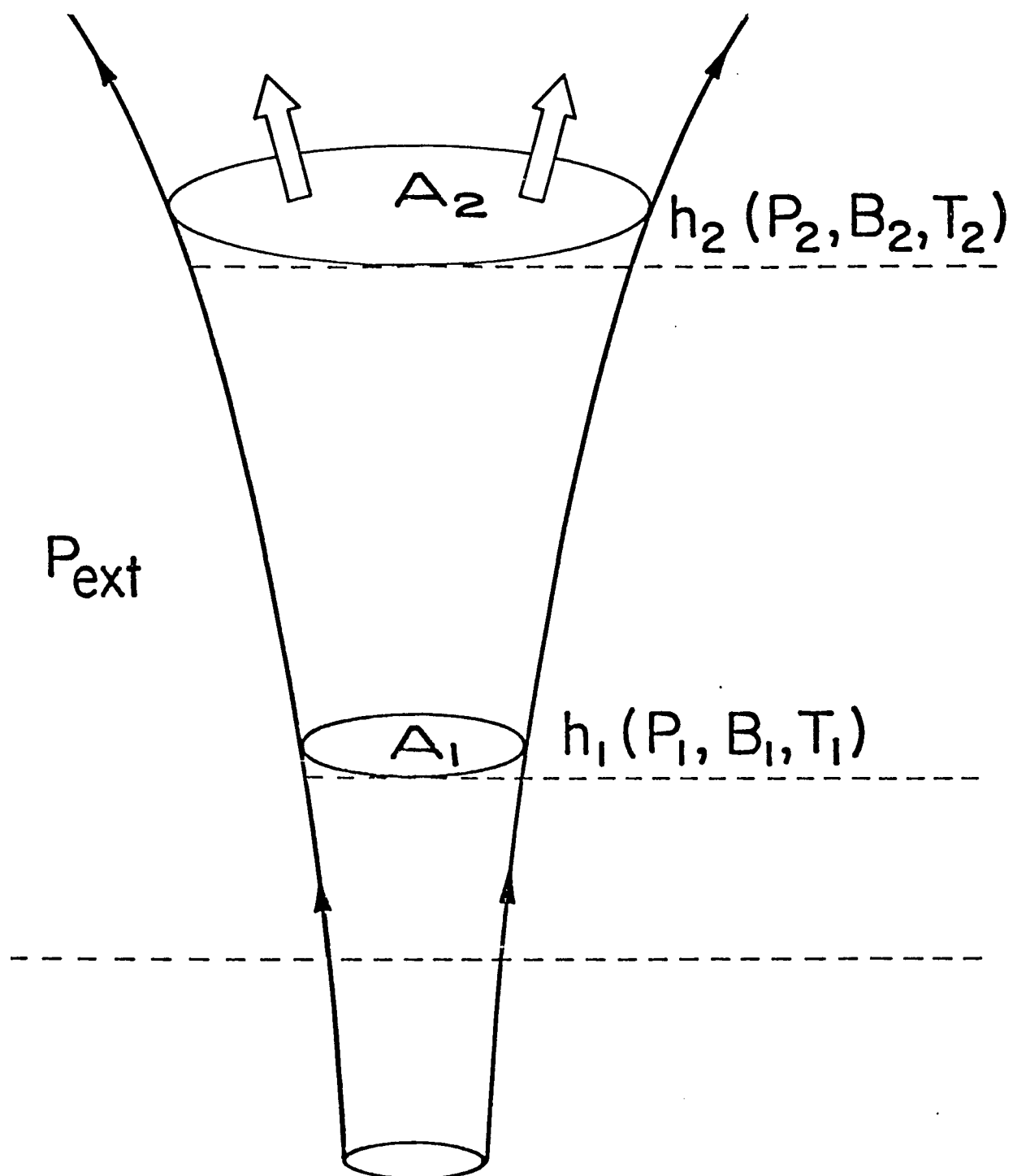
Figure 54.   Schematic model of a magnetic flux tube.

where $P_{ext}(h)$ is the external (field-free) gas pressure at height h, $P_g(h)$ is the internal gas pressure, and $B(h)$ is the internal magnetic field strength, also at height h. I ignore turbulent pressure in this preliminary analysis. At the levels h_1 and h_2 I have

$$P_1^{ext} = P_1^g + B_1^2/8\pi , \qquad (6.5)$$

$$P_2^{ext} = P_2^g + B_2^2/8\pi . \qquad (6.6)$$

Now $P_2^{ext} < P_1^{ext}$ by the constraint of hydrostatic equilibrium. But $B_2 < B_1$ in a flux tube characterized by diverging field lines (see Figure 54). Thus it is possible for $P_2^g > P_1^g$, which would lead to enhanced Mg II k-line emission. The condition $P_2^g > P_1^g$ occurs if the inequality

$$B_1^2 - B_2^2 > 8\pi \ (P_1^{ext} - P_2^{ext}), \qquad (6.7)$$

is fulfilled. An alternative way to conceptualize the problem is to note that the emission area (filling factor) for the k line, A_2, is greater than the emission area for the Ca II K line, A_1, as shown schematically in Figure 54. Giovanelli (1980) finds diverging magnetic field structure, similar to Figure 55, in the solar chromosphere as deduced from Mg I b_2 magnetogram observations near the solar limb. A schematic diagram of this field structure is taken from Giovanelli (1980) and shown in Figure 54. I use Figure 54 (Giovanelli 1980) not as a proof, but as a plausibility argument for the existence of similar magnetic field structures in the chromospheres of late-type dwarf stars. Of course a proper analysis of the chromospheric line spectrum in a magnetic flux tube requires a two-dimensional radiative transfer
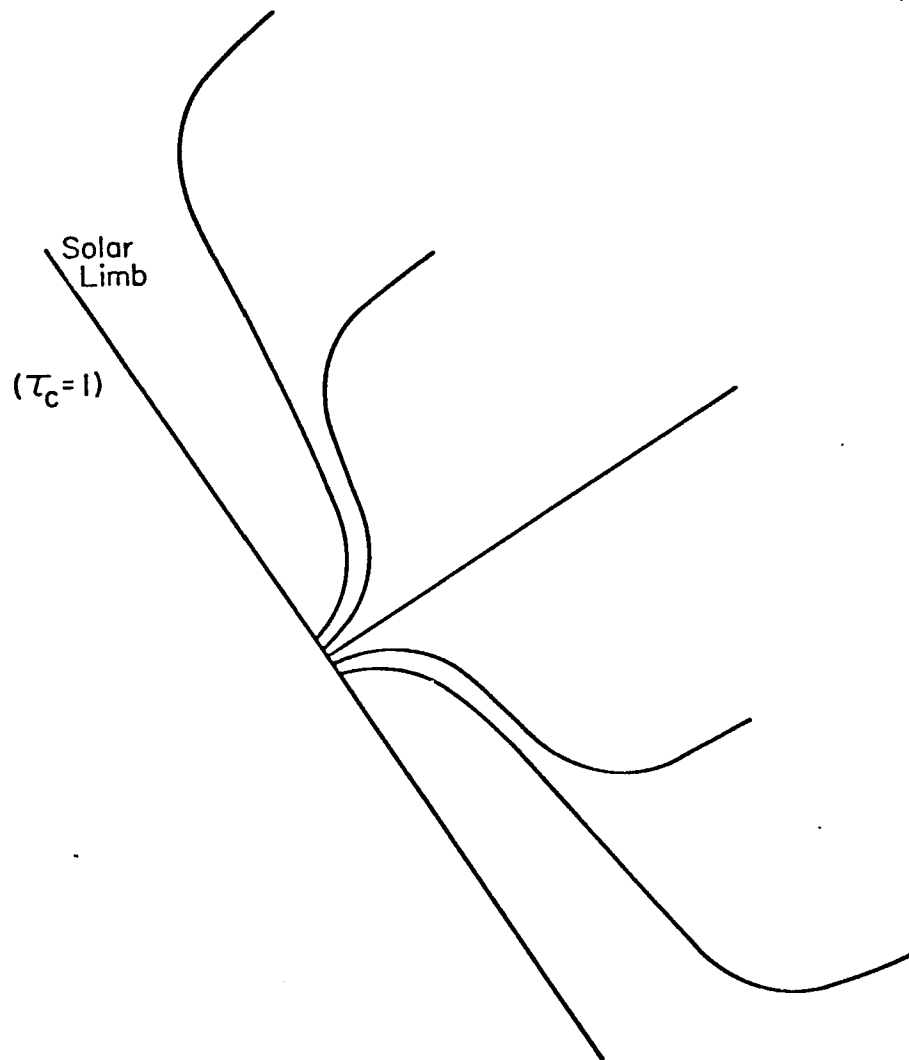
Figure 55. Magnetic field structure observed in the Sun.

calculation since the flux tube is in radiative exchange with its surroundings. Moreover, the importance of lateral turbulent heat exchange will change along a flux tube as the field decreases with height (Zwaan 1977, 1978). I do not perform these calculations here because (1) it is beyond the scope of the present investigation, and (2) observations of the emergent line spectrum from a single magnetic flux tube are currently unavailable, even for the Sun.

In conclusion, I suggest that multi-component model atmospheres are more realistic physical representations of stellar chromospheres. In particular, I hypothesize that a detailed consideration of the line spectrum arising from magnetic flux tubes is required in order to reconcile various chromospheric spectral line diagnostics.

CHAPTER 7

SUMMARY

The estimated chromospheric radiative loss rates in the Ca II H and K lines (Chapter 2) for the dMe stars are larger than for the dM stars by a factor of 2.5 or more. The dM stars have chromospheric radiative loss rates which are comparable to that of the mean Sun. Thus nonradiative heating is systematically larger in dMe than dM stars as may be expected in analogy with the relative nonradiative heating rate in solar plages and quiet regions. However, the degree of mechanical energy dissipation in the chromospheres of the M dwarf stars is inconsistent with the predictions of the acoustic wave heating theory. Hence magnetic heating processes, such as the dissipation of MHD waves as originally proposed by Osterbrock (1961), may play the dominant role in the energy balance of an M dwarf chromosphere and corona.

I also find that the chromospheric scaling law proposed by Ayres (1979) basically agrees with the trend of the observed K_1 line widths exhibited by the dMe and dM stars considered in this investigation. Moreover, the M dwarfs generally follow the Wilson-Bappu relation.

The results which follow from the semi-empirical model chromospheres developed in Chapter 4 indicate that the central reversals present in the Ca II K-line profiles computed theoretically are not detectable with the instrumental resolution available for this investigation. However, future observations of the Ca II H and K lines at even

higher spectral resolutions may still not reveal the central reversals, suggested by the theoretical profiles, because of the presence of such macroscopic velocity fields as rotation (Kelch et al. 1979). Another result given in Chapter 4 is that both the observed ratio $T_R(K_1)/T_{eff}$ and the theoretically inferred value of T_{min}/T_{eff} for the M dwarfs discussed in this investigation indicate an unusually large degree of non-radiative heating in the upper photospheres of M dwarf stars. Moreover, the location of the temperature minimum, m_{min}, moves outward as R_{HK} decreases, thus confirming the result given by Kelch et al. (1979) for a sample of solar-type stars. Of course, these particular conclusions are subject to the constraints of certain assumptions, especially the assumption of solar abundances and the treatment of the metals in an LTE approximation. An accurate model of the upper photospheres and temperature minimum regions in late-type dwarf stars may well require a more rigorous radiative transfer analysis for the metals and an accurate measure of the metal abundance for a given star. I also find that the chromospheric K-line emission strength is most sensitive to the total amount of chromospheric material within the approximate temperature range T_{min} - 6000K. Thus increased emission strength is not simply due to an increased temperature gradient. In addition, the rise in T_e (i.e., $dT_e/d\log m$) over the region in which the K-line emission core is formed is steep, regardless of the total chromospheric emission line flux. Furthermore, an analysis of the atomic processes which control the net radiative cooling in the chromospheres of M dwarf stars yields the following result: the electron density, n_e, and electron temperature, T_e, at a thermalization length below the top of the chromosphere

are each greater for the dMe stars than for the dM stars. Thus the chromospheric line emission in collisionally controlled lines is enhanced in dMe stars relative to the dM stars. Finally, the model chromospheres developed in Chapter 4 reveal that the microturbulent velocities in the chromospheres of M dwarf stars are small as compared to solar-like chromospheric microvelocity fields. I suggest that chromospheric mass motions are inhibited by magnetic fields which pervade the stellar chromosphere and therefore lead to small microturbulent velocities. If this is true then the microturbulent velocities I infer must be <u>upper limits</u> to the actual microturbulent velocities which exist in M dwarf chromospheres since I do not include the effects of magnetic line broadening in this investigation.

The model chromospheres analysis presented in Chapter 5 suggests that the Hα line emission flux is most sensitive to the upper chromospheric-transition region thermal structure, in agreement with the results of Cram and Mullan (1979). In addition, I find that it is possible to construct single-component, semi-empirical model chromospheres for M dwarf stars which simultaneously satisfy both the Ca II K-line and the Hα line However, the agreement is logically consistent as the Ca II K-line is a lower chromospheric diagnostic while the Hα line is especially sensitive to the transition region thermal structure. By comparison, I find that single-component, homogeneous model chromospheres fail to reconcile the Ca II K and the Mg II k lines in those dMe and dM stars with intermediate degrees of nonradiative heating. I therefore conclude that the assumption of lateral homogeneity is suspect and I pursue the implications of this conclusion in Chapter 6. In

particular, I estimate from observations of the Ca II H and K lines and the Mg II h and k lines relative active region filling factors which likely give rise to the chromospheric emission observed in the M dwarf stars. I find that the relative active region filling factors for the dMe stars are generally greater than for the dM stars. Thus the inhomogeneous nature of the solar chromosphere, the quasi-periodic variability exhibited in flare stars, and the active region filling factor estimates presented in this dissertation suggest that it may be more realistic to define "active" and "quiet" chromosphere stars in terms of that fraction of their surface area that is covered by active regions. In addition, the apparently discrepant mean active region filling factors derived from the Ca II and Mg II resonance lines combined with the failure of model chromospheres to reconcile two overlapping chromospheric spectral features suggest (but do not prove) that single component, homogeneous model atmospheres are not physically realistic representations of M dwarf stars. Furthermore, I suggest that a detailed consideration of the line spectrum arising from magnetic flux tubes is required in order to reconcile various chromospheric spectral diagnostics. However, in order to more firmly establish this hypothesis it would be necessary to obtain a completely general, simultaneous solution of the coupled equations of radiative transfer and statistical equilibrium involving all important line and continuum transitions, for all constituents of the stellar atmosphere.

The conclusions and hypotheses presented in this dissertation suggest several lines of future observational and theoretical research. For example, if the filling factor of active regions is representative

of the surface density of magnetic flux tubes, as it is on the Sun, then magnetic flux measurements using the techniques of Robinson et al. (1980) and Robinson (1980) would be particularly interesting. In addition, measurements of the net chromospheric radiative losses in the Ca II H and K lines versus magnetic _flux_ (as opposed to magnetic _field_) on the Sun, following the methods of Frazier (1978), would prove valuable.

The proposed magnetic field measurements combined with rotation measures, utilizing the techniques of Smith (1980) and/or Worden (1975), would demonstrate the importance of magnetic heating processes in the stellar chromosphere as well as test the dynamo theory espoused by Mullan (1974) and the battery mechanism developed by Worden (1974) for the dMe stars. Complementary theoretical investigations may include a rigorous treatment of the radiative transfer in a magnetic flux tube combined with the development of models which delineate the method of generation of magnetic flux in the stellar interior followed by its emergence on the stellar surface. The eventual aim of the program of observational and theoretical research which I have just outlined is to understand how magnetic flux is generated and then appears on the stellar surface where it, in turn, couples to the emergent chromospheric line spectrum. A detailed knowledge of this entire process may then allow astronomers to spectroscopically infer the physical conditions which characterize the very interiors of the stars.

COARSE TABULATION OF dMe AND dM MODEL
CHROMOSPHERES

I include in the following pages a tabulation of the model properties characterizing the region of the lower chromospheric temperature gradient for 3 dMe and 2 dM stars.

Temp (K)	Mass (g-cm^{-2})	n_e (cm^{-3})	n_{H_t} (cm^{-3})	ξ_t (km-s^{-1})
		YZ CMi (dM4.5e)		
6000	9.75(−5)	1.56(11)	5.76(12)	1.80
5684	2.12(−4)	1.13(11)	1.34(13)	1.76
5368	4.60(−4)	7.55(10)	3.10(13)	1.72
5053	9.99(−4)	4.84(10)	7.15(13)	1.67
4737	2.17(−3)	3.58(10)	1.66(14)	1.63
4421	4.72(−3)	4.88(10)	3.85(14)	1.59
4263	6.96(−3)	6.62(10)	5.89(14)	1.57
3947	1.51(−2)	9.74(10)	1.38(15)	1.53
3632	3.28(−2)	9.30(10)	3.26(15)	1.48
3316	7.13(−2)	7.24(10)	5.01(15)	1.44
3000	1.55(−1)	6.97(10)	1.85(16)	1.40
3013	2.49(−1)	1.02(11)	2.97(16)	1.37
3025	4.00(−1)	1.48(11)	4.76(16)	1.34
		GL 393 (dM2)		
6000	3.25(−5)	8.86(10)	1.91(12)	1.60
5700	6.70(−5)	6.53(10)	4.23(12)	1.58
5400	1.38(−4)	4.42(10)	9.28(12)	1.56
5100	2.85(−4)	2.81(10)	2.03(13)	1.54
4800	5.87(−4)	1.79(10)	4.44(13)	1.52
4500	1.21(−3)	1.56(10)	9.75(13)	1.50
4200	2.49(−3)	2.56(10)	2.15(14)	1.48
3900	5.13(−3)	3.99(10)	4.76(14)	1.46
3600	1.06(−2)	4.11(10)	1.06(15)	1.44
3300	2.18(−2)	3.09(10)	2.38(15)	1.42
3000	4.50(−2)	2.75(10)	5.38(15)	1.40
3075	1.70(−1)	8.61(10)	1.99(16)	1.33
3149	6.42(−1)	2.65(11)	7.39(16)	1.27

Temp (K)	Mass (g-cm^{-2})	n_e (cm^{-3})	n_{H_t} (cm^{-3})	ξ_t (km-s^{-1})
		GL 411 (dM2)		
6000	1.50(-5)	5.98(10)	8.86(11)	0.1
5625	2.91(-5)	3.60(10)	1.91(12)	0.1
5250	5.64(-5)	1.88(10)	4.03(12)	0.1
4875	1.09(-4)	8.85(9)	8.44(12)	0.1
4500	2.12(-4)	4.41(9)	1.77(13)	0.1
4125	4.11(-4)	4.81(9)	3.75(13)	0.1
3750	7.98(-4)	7.67(9)	8.01(13)	0.1
3375	1.55(-3)	6.82(9)	1.73(14)	0.1
3000	3.00(-3)	3.72(9)	3.76(14)	0.1
3025	6.31(-3)	6.81(9)	7.85(14)	0.1
3050	1.33(-2)	1.25(10)	1.64(15)	0.1
				0.1
		EQ Vir (dK5e)		
6000	1.25(-3)	5.78(11)	7.50(13)	1.80
5762	2.28(-3)	4.60(11)	1.43(14)	1.76
5524	4.17(-3)	3.56(11)	2.73(14)	1.72
5286	7.62(-3)	2.76(11)	5.22(14)	1.69
5048	1.39(-2)	2.35(11)	9.98(14)	1.65
4810	2.54(-2)	2.70(11)	1.91(15)	1.61
4571	4.65(-2)	4.06(11)	3.68(15)	1.57
4333	8.49(-2)	5.70(11)	7.09(15)	1.53
4095	1.55(-1)	6.55(11)	1.37(16)	1.50
3857	2.83(-1)	6.16(11)	2.66(16)	1.46
3619	5.18(-1)	5.44(11)	5.17(16)	1.42
3536	8.23(-1)	6.36(11)	8.50(16)	1.20
3609	1.36(0)	1.04(12)	1.38(17)	1.10
3737	2.21(0)	1.85(12)	2.18(17)	1.10
		GL 616.2 (dM1.5e)		
6000	1.28(-4)	1.81(11)	7.67(12)	1.60
5700	2.82(-4)	1.37(11)	1.80(13)	1.58
5400	6.23(-4)	9.64(10)	4.20(13)	1.56
5100	1.37(-3)	6.59(10)	9.81(13)	1.54
4800	3.03(-3)	5.15(10)	2.30(14)	1.52
4500	6.69(-3)	6.95(10)	5.40(14)	1.50
4200	1.48(-2)	1.23(11)	1.27(15)	1.48
3900	3.26(-2)	1.60(11)	3.02(15)	1.46
3600	7.19(-2)	1.43(11)	7.21(15)	1.44
3300	1.59(-1)	1.24(11)	1.73(16)	1.42
3000	3.50(-1)	1.27(11)	4.19(16)	1.40
3075	6.67(-1)	2.37(11)	7.83(16)	1.33
3149	1.27(0)	4.36(11)	1.46(17)	1.27
				1.20

REFERENCES

Adams, T. F., D. G. Hummer, and G. B. Rybicki. 1971. J.Q.S.R.T., 11, 1365.

Allen, C. W. 1976. Astrophysical Quantities, 3rd ed. (London: Athlone).

Anderson, C. M., and B. W. Bopp. 1975. B.A.A.S., 7, 235.

Athay, R. G. 1972. Radiation Transport in Spectral Lines (Dordrecht: Reidel).

Athay, R. G. 1976. The Solar Chromosphere and Corona: Quiet Sun (Dordrecht: Reidel).

Athay, R. G., and O. R. White. 1978. Ap. J., 226, 1135.

Auer, L. H. 1973. Ap. J., 180, 469.

Auer, L. H., J. N. Heasley, and R. W. Milkey. 1972. Kitt Peak National Obsv. Contrib. No. 555.

Auer, L. H., and D. Mihalas. 1969. Ap. J., 158, 641.

Ayres, T. R. 1975. Unpublished Ph.D. thesis, University of Colorado, Boulder.

Ayres, T. R. 1979. Ap. J., 228, 509.

Ayres, T. R., and J. L. Linsky. 1975. Ap. J., 200, 660.

Ayres, T. R., J. L. Linsky, A. W. Rodgers, and R. L. Kurucz. 1976. Ap. J., 210, 199.

Ayres, T. R., J. L. Linsky, and R. A. Shine. 1974. Ap. J., 192, 93.

Baliunas, S. L., E. H. Avrett, L. Hartmann, and A. K. Dupree. 1979. Ap. J. (Letters), 233, L129.

Barnes, T. G., and D. S. Evans. 1976. M.N.R.A.S., 174, 489.

Barnes, T. G., D. S. Evans, and S. B. Parsons. 1976. M.N.R.A.S., 174, 503.

Barry, D. C., S. Schoolman, and E. K. Hege. 1980. Unpublished manuscript, University of Southern California, Los Angeles.

Basri, G. S. 1979. Unpublished Ph.D. thesis, University of Colorado, Boulder.

Basri, G. S., and J. L. Linsky. 1979. *Ap. J.*, 234, 1023.

Beebe, H. A., and R. W. Milkey. 1972. *Ap. J. (Letters)*, 172, L111.

Biermann, L. 1946. *Naturwiss*, 33, 118.

Biermann, L. 1950. *Zs. f. Naturforsch*, 5a, 65.

Boggess, A., F. A. Carr, and D. C. Evans. 1978. *Nature*, 275, 372.

Bohm, K. H. 1960. In *Stellar Atmospheres*, ed. J. L. Greenstein (Chicago: University of Chicago Press).

Bopp, B. W. 1974. *M.N.R.A.S.*, 46, 108.

Bopp, B. W. 1980. In *Highlights of Astronomy*, 5, in press.

Bopp, B. W., and D. S. Evans. 1973. *M.N.R.A.S.*, 164, 343.

Carpenter, K. G., and R. F. Wing. 1979. *B.A.A.S.*, 11, 419.

Carpenter, K. G., R. F. Wing, P. L. Bornmann, J. L. Linsky, S. P. Worden, and M. S. Giampapa. 1980. *B.A.A.S.*, in press.

Carrasco, L., J. Franco, and M. Roth. 1980. *Astr. Ap.*, in press.

Chiu, L. G. 1978. Unpublished Ph.D. thesis, University of California, Berkeley.

Coleman, G. D., and S. P. Worden. 1976. *Ap. J.*, 205, 47.

Cram, L. E. 1977. *Astr. Ap.*, 59, 151.

Cram, L. E., and D. J. Mullan. 1979. *Ap. J.*, 234, 579.

Cram, L. E., and P. Ulmschneider. 1978. *Astr. Ap.*, 62, 239.

Crandall, D. H., G. H. Dunn, A. Gallagher, D. G. Hummer, C. V. Kunasz, D. Leep, and P. O. Taylor. 1974. *Ap. J.*, 191, 789.

Evans, D. S. 1975. In *Variable Stars and Stellar Evolution*, ed. V. E. Sherwood and L. Plaut (Dordrecht: Reidel).

Ezer, D., and A. G. W. Cameron. 1967. *Canadian J. Phys.*, 45, 3429.

Fix, J. D., and S. R. Spangler. 1976. *Ap. J. (Letters)*, 205, L163.

Fosbury, R. A. E. 1974. *M.N.R.A.S.*, 169, 147.

Frazier, E. N. 1978. Astr. Ap., 64, 351.

Gebbie, K. B., and R. Steinitz. 1974. Ap. J., 188, 399.

Geltman, S. 1962. Ap. J., 136, 935.

Giampapa, M. S., P. L. Bornmann, T. R. Ayres, J. L. Linsky, and S. P. Worden. 1980. NASA Symposium, The Universe in Ultraviolet Wavelength: The Second Year of IUE. In press.

Giampapa, M. S., J. L. Linsky, T. J. Schneeberger, and S. P. Worden. 1978. Ap. J., 226, 144.

Giampapa, M. S., and S. P. Worden. 1980. Unpublished manuscript, University of Arizona, Tucson.

Giampapa, M. S., S. P. Worden, and L. B. Gilliam. 1979. Ap. J., 229, 1143.

Gibson, E. G. 1973. The Quiet Sun (NASA: U. S. Government Printing Office).

Gingerich, O. 1964. SAO Spec. Rept. No. 167.

Gingerich, O., R. W. Noyes, W. Kalkofen, and Y. Cuny. 1971. Solar Phys., 18, 347.

Gingerich, O., and J. C. Rich. 1968. Solar Phys., 3, 82.

Giovanelli, R. G. 1980. Unpublished manuscript, C.S.I.R.O. Division of Applied Physics, New South Wales, Australia.

Gliese, W. 1969. Catalogue of Nearby Stars (Karlsruhe: Verlag G. Braun).

Golden, L. B., and D. H. Sampson. 1971. Ap. J., 163, 405.

Golub, L., C. Maxson, R. Rosner, S. Serio, and G. S. Vaiana. 1980. Unpublished manuscript, Center for Astrophysics, Cambridge.

Golub, L., R. Rosner, G. S. Vaiana, and N. O. Weiss. 1980. Unpublished manuscript, Center for Astrophysics, Cambridge.

Gray, D. F. 1976. The Observation and Analysis of Stellar Photospheres (John Wiley & Sons).

Green, L. C., P. P. Rush, and C. D. Chandler. 1957. Ap. J. Supplement, 3, 37.

Greenstein, J. L., and H. Arp. 1969. Ap. J. (Letters), 149, L3.

Grossman, A. S., and H. C. Graboski, Jr. 1971. _Ap. J._, 164, 475.

Haisch, B. M., J. L. Linsky, O. B. Slee, I. Nikoloff, P. J. Quinn, B. Hidayat, and F. D. Seward. 1980. _Ap. J._, in press.

Hartmann, L., and C. M. Anderson. 1977. _Ap. J. (Letters)_, 213, L67.

Hartmann, L., R. Davis, A. K. Dupree, J. Raymond, P. C. Schmidtke, and R. F. Wing. 1979. _Ap. J. (Letters)_, 233, L69.

Hayashi, C. 1966. _Ann. Rev. Astr. Ap._, 4, 171.

Hayashi, C., R. Hoshi, and D. Sugimoto. 1962. _Progr. Theo. Phys. Suppl._, 22, 1.

Heasley, J. N., S. T. Ridgway, D. F. Carbon, R. W. Milkey, and D. N. B. Hall. 1978. _Ap. J._, 219, 970.

Hoxie, D. T. 1973. _Astron. Astrophys._, 26, 437.

Hummer, D. G. 1962. _M.N.R.A.S._, 125, 21.

Hummer, D. G., and J. C. Stewart. 1966. _Ap. J._, 146, 290.

Iben, I. 1965. _Ap. J._, 141, 993.

Iben, I. 1967. _Ann. Rev. Astr. Ap._, 5, 571.

Jefferies, J. T. 1968. _Spectral Line Formation_ (Blaisdell Publishing Co.).

Jefferies, J. T., and R. N. Thomas. 1958. _Ap. J._, 127, 667.

Jefferies, J. T., and R. N. Thomas. 1959. _Ap. J._, 129, 401.

John, T. L. 1964. _M.N.R.A.S._, 128, 93.

Johnson, H. L. 1966. _Ann. Rev. Astr. Ap._, 4, 193.

Johnson, H. L., R. I. Mitchell, B. Iriarte, and W. Z. Wisniewski. 1966. _Comm. Lunar Planet. Lab._, 4, 99.

Johnson, H. R. 1973. _Ap. J._, 180, 81.

Joy, A. H., and H. A. Abt. 1974. _Ap. J. Suppl._, 28, 1.

Kelch, W. L. 1978. _Ap. J._, 222, 931.

Kelch, W. L., J. L. Linsky, G. S. Basri, H. Y. Chiu, S. H. Chang, S. P. Maran, and I. Furenlid. 1978. _Ap. J._, 220, 962.

Kelch, W. L., J. L. Linsky, and S. P. Worden. 1979. Ap. J., 229, 700.

Krzeminski, W. 1969. In Low Luminosity Stars, ed. S. Kumar (London: Gordon and Breach).

Kumar, S. S. 1963. Ap. J., 137, 1121.

Kunkel, W. E. 1970. Ap. J., 161, 503.

Kunkel, W. E. 1973. Ap. J. (Supplement), 25, 1.

Kunkel, W. E. 1975. In Variable Stars and Stellar Evolution, ed. V. E. Sherwood and L. Plaut (Dordrecht: Reidel).

Lacy, C. H. 1977. Ap. J., 218, 444.

Lambert, D. L., and B. Warner. 1968. M.N.R.A.S., 140, 197.

Liebert, J., C. C. Dahn, M. Gresham, and P. A. Strittmatter. 1979. Ap. J., 233, 226.

Liebert, J. W., and R. F. Green. 1980. Unpublished manuscript, University of Arizona, Tucson.

Linsky, J. L. 1968. Ph.D. thesis, Harvard University, SAO Spec. Rept. No. 274.

Linsky, J. L. 1977. In The Solar Output and Its Variation, ed. O. R. White (Boulder: Colorado Associated University Press), Chap. 7.

Linsky, J. L. 1980a. Unpublished manuscript, University of Colorado, Boulder.

Linsky, J. L. 1980b. Ann. Rev. Astr. Astrophys., in press.

Linsky, J. L., and E. H. Avrett. 1970. Pub. A.S.P., 82, 169.

Linsky, J. L., and T. R. Ayres. 1978. Ap. J., 220, 619.

Linsky, J. L., S. P. Worden, W. McClintock, and R. M. Robertson. 1979. Ap. J. Suppl., 41, 47.

Lites, B. W. 1972. Unpublished Ph.D. thesis, University of Colorado, Boulder.

Lovell, B. 1971. Quart. J.R.A.S., 12, 98.

Lutz, T. E. 1970. A. J., 75, 1007.

Luyten, W. J. 1968. M.N.R.A.S., 139, 221.

Luyten, W. J. 1974. Highlights Astron. Ap., 3, 389.

Mestel, L., and I. W. Roxburgh. 1962. Ap. J., 136, 615.

Mihalas, D. 1967a. Methods in Computational Physics, 7, 1.

Mihalas, D. 1967b. Ap. J., 149, 169.

Mihalas, D. 1970. Stellar Atmospheres, 1st ed. (San Francisco: Freeman).

Mihalas, D. 1978. Stellar Atmospheres, 2nd ed. (San Francisco: Freeman).

Milkey, R. W. 1976. In Interpretation of Atmospheric Structure in the Presence of Inhomogeneities, ed. C. J. Cannon (Sydney: University of Sydney).

Milkey, R. W., and D. Mihalas. 1973. Ap. J., 185, 709.

Moffett, T. J., and B. W. Bopp. 1976. Ap. J. Suppl., 31, 61.

Mould, J. R. 1976. Astr. Ap., 48, 443.

Mullan, D. J. 1974. Ap. J., 192, 149.

Mullan, D. J. 1976. Irish A. J., 12, 161.

Noyes, R. W., and W. Kalkofen. 1970. Solar Phys., 15, 120.

Osterbrock, D. E. 1961. Ap. J., 134, 347.

Peach, G. 1967. Mem. R.A.S., 71, 1.

Petit, M. 1961. J. Observ., 44, 11.

Pettersen, B. R. 1976. Inst. Theo. Ap., Report #46, Oslo.

Pettersen, B. R. 1980. Astron. Astrophys., in press.

Photobulletin: Kodak Pamphlet No. 14. 1979.

Raymer, M. 1979. Unpublished Ph.D. thesis, University of Colorado, Boulder.

Renzini, A., C. Cacciari, P. Ulmschneider, and F. Schmitz. 1977. Astr. Ap., 61, 39.

Robinson, R. D. 1980. Ap. J., in press.

Robinson, R. D., S. P. Worden, and J. W. Harvey. 1980. Ap. J. (Letters), 236, L155.

Sampson, D. H., and L. B. Golden. 1970. Ap. J., 161, 321.

Schneeberger, T. J., E. De Luca, S. P. Worden, M. S. Giampapa, and L. E. Cram. 1980. Ap. J., submitted.

Schneeberger, T. J., J. L. Linsky, W. McClintock, and S. P. Worden. 1979. Ap. J., 231, 148.

Schwarzschild, M. 1948. Ap. J., 107, 1.

Schwarzschild, M. 1958. Structure and Evolution of the Stars (Princeton University Press).

Shaviv, G. 1980. Unpublished manuscript, Tel Aviv University, Israel.

Shine, R. A. 1973. Ph.D. thesis, University of Colorado, Boulder.

Shine, R. A., and J. L. Linsky. 1974. Solar Phys., 39, 49.

Shine, R. A., R. W. Milkey, and D. Mihalas. 1975a. Ap. J., 199, 724.

Shine, R. A., R. W. Milkey, and D. Mihalas. 1975b. Ap. J., 201, 222.

Skumanich, A. 1972. Ap. J., 171, 565.

Skumanich, A., C. Smythe, and E. N. Frazier. 1975. Ap. J., 200, 747.

Smith, M. A. 1980. Ap. J., in press.

Stein, R. F., and J. Leibacher. 1980. In Stellar Turbulence, eds. D. F. Gray and J. L. Linsky (New York: Springer-Verlag).

Stencel, R. E., D. J. Mullan, J. L. Linsky, G. S. Basri, and S. P. Worden. 1980. Ap. J. Suppl., in press.

Straka, W. C. 1971. Ap. J., 165, 109.

Sutton, K. 1978. J.Q.S.R.T., 20, 333.

Svestka, Z. 1972. Ann. Rev. Astron. Astrophys., 10, 1.

Swihart, T. L. 1968. Astrophysics and Stellar Astronomy (New York: John Wiley & Sons, Inc.).

Thomas, R. N. 1957. Ap. J., 125, 260.

Thomas, R. N. 1965. Some Aspects of Non-Equilibrium Thermodynamics in the Presence of a Radiatio Field (Boulder: University of Colorado Press).

Thomas, R. N., and R. G. Athay. 1961. Physics of the Solar Chromosphere (New York: Interscience).

Torres, C. A. O., and F. S. Mello. 1973. Astr. Ap., 27, 231.

Ulmschneider, P. 1979. Space Sci. Rev., in press.

Ulmschneider, P., F. Schmitz, A. Renzini, C. Cacciari, W. Kalkofen, and R. L. Kurucz. 1977. Astr. Ap., 61, 515.

Vaiana, G. S. 1980. Unpublished manuscript, Center for Astrophysics, Cambridge.

Veeder, G. J. 1974. A. J., 79, 1056.

Vernazza, J. E. 1972. Paper presented at 3rd OSO Workshop, Stanford University, September 5-8.

Vernazza, J. E., E. H. Avrett, and R. Loeser. 1973. Ap. J., 184, 605.

Vernazza, J. E., E. H. Avrett, and R. Loeser. 1976. Ap. J. Suppl., 30, 1.

Vogt, S. S. 1975. Ap. J., 199, 418.

Wielen, R. 1974. Highlights Astr., 3, 395.

Williams, R. E. 1980. Unpublished manuscript, University of Arizona, Tucson.

Willstrop, R. V. 1964. Mem. R. Astr. Soc. London, 69, 83.

Willstrop, R. V. 1972. Unpublished manuscript, Royal Greenwich Observatory, England.

Wilson, O. C. 1973. In Stellar Chromospheres, IAU Colloq. No. 19, eds. S. D. Jordan and E. H. Avrett (Washington: NASA SP-317), p. 305.

Wilson, O. C., and M. K. V. Bappu. 1957. Ap. J., 125, 661.

Worden, S. P. 1974. P.A.S.P., 86, 595.

Worden, S. P. 1975. Unpublished Ph.D. dissertation, University of Arizona, Tucson.

Worden, S. P., and B. M. Peterson. 1976. Ap. J. (Letters), 206, L145.

Worden, S. P., T. J. Schneeberger, E. De Luca, and M. S. Giampapa. 1979. B.A.A.S. 11, 628.

Worden, S. P., T. J. Schneeberger, and M. S. Giampapa. 1980. Ap. J. Suppl., in press.

Zirin, H. 1966. The Solar Atmosphere (Waltham: Blaisdell).

Zwaan, C. 1977. Mem. S.A.It., p. 525.

Zwaan, C. 1978. Solar Phys., 60, 213.